# ONE DIMENSIONAL TRANSPORT OF ULTRACOLD BOSONS

by

DAVID PETER SIMPSON


A thesis submitted to
The University of Birmingham
for the degree of
DOCTOR OF PHILOSOPHY

School of Physics and Astronomy
The University of Birmingham

September 2, 2014

## Abstract

This thesis concerns the transport of ultracold bosons in a one-dimensional geometry. I consider two three-dimensional reservoirs of Bose-Einstein condensed atoms that are connected via weak tunnel junctions to each end of a one-dimensional (Luttinger) channel. The particle current along the channel is driven only by a constant phase difference between the two reservoirs. I theoretically investigate the bosonic flow and demonstrate it has characteristics completely distinct from its superconducting counterpart. In fact, I show that a perturbative approach to describing the particle current completely fails for bosonic atoms in contrast to the superconducting current. Instead I develop a non-perturbative mean field description of the bosonic flow, showing the existence of metastable solutions for all values of tunnelling. I show there are two separate branches of the mean field solution and the lowest energy solution necessarily jumps discontinuously between these branches. I then demonstrate that such a mean field solution is robust against fluctuations for values of the Luttinger parameter pertinent to bosonic atoms. In particular, I demonstrate that fluctuations do not connect different branches of the mean field solution, meaning that the energy crossings between metastable configurations are not avoided. I provide a possible experimental realisation of such a geometry by utilising the versatility of atom chips and describe how one can experimentally observe both the phase profile in the channel and the flow of particles along the channel. Finally, I also explore the non-equilibrium dynamics following a quench in the tunnelling energy and demonstrate that such a quench can lead to switching between different branches of the mean field solution.

## Acknowledgements

A massive thank-you to my supervisors, Igor Lerner and Dima Gangardt for all of your input and guidance over the last four years. It's certainly true to say I learnt more through our times of discussion than at any other point of my study. Having stayed on in Birmingham after completing my undergraduate degree, I want to thank all the staff, particularly those from the theory department, who have contributed to my understanding and sparked the desire to continue my studies to this level. I'd also like to thank all of my fellow PhD students from the theory group for feedback on talks I've presented, discussions of ongoing research and making my time in Birmingham so enjoyable. Particular thanks to Jon Watkins for putting up with me in the office and having infinite patience when helping me solve computer issues! I want to thank the EPSRC for the funding to do this PhD. Also, thanks to Peter Krüger with whom we collaborated in publishing some of the work this thesis is based on and who has designed an experiment in which these results may hopefully one day be verified.

Finally, thanks to all my friends and family who have supported me throughout my studies. Thanks to all at Monyhull who have feigned interest when I've described my work, thanks to my parents for giving me the best possible start in life and most of all thanks to my amazing wife for being a source of patience and fun when I've struggled to see the light at the end of the tunnel.

*This thesis is dedicated*
*to my wonderful wife...*

*... even if she doesn't*
*understand a word of it!*

# Contents

# List of Figures

# Part I

# INTRODUCTION

Since the first experimental observation of a Bose-Einstein condensate almost 20 years ago, the field of ultracold atomic physics has been a hotbed of physical research. Experimentally, such systems offer an unparalleled degree of control over a wide range of different parameters. There has also been renewed theoretical interest as ultracold atomic systems offer the intriguing possibility to macroscopically investigate quantum effects.

In particular, this thesis concerns the transport of ultracold bosonic atoms in a one-dimensional geometry [1–7]. I consider two 3-dimensional reservoirs of Bose-condensed atoms, differing only by a constant phase difference and connected via weak tunnelling links to each end of a one-dimensional channel. Such a *geometry* has received much interest over the years for both electronic and superconducting systems of wires [8–24]. Recently, a parallel experiment has been carried out to observe similar phenomena in a system of ultracold fermions [25–27]. This opens up the possibility to also explore the *bosonic* transport through a similar geometry which has no direct analogy in condensed matter physics [28,29]. In this thesis I theoretically investigate such a bosonic flow and show that the resulting behaviour is drastically different to the parallel superconducting situation.

In the first section I provide a general introduction to the two main fields of research this thesis covers. Chapter 1 contains an introduction to ultracold atomic physics including Bose-Einstein condensation, experimental methods of trapping and cooling atoms, the main theoretical treatments of the condensed state and a summary of the Josephson effect. Chapter 2 focuses on one-dimensional physics, including the main peculiarities of 1D systems and a general introduction to the idea of a Luttinger liquid as a universal low energy description of a one-dimensional problem.

The second section provides more targeted overviews of some of the main theoretical techniques I shall utilize: Chapter 3 gives details about the functional integral formalism and provides an example of its use in calculating correlation functions, chapter 4 introduces the idea of renormalization and applies it to the Kane-Fisher problem of a single impurity in a Luttinger liquid, and chapter 5 introduces the idea of the Keldysh contour as a tool for investigating non-equilibrium dynamics.

Section III and IV represent my original work. Section III is based on material published in Physical Review Letters [30] for which I am the first author in collaboration with I.V.Lerner, D.M.Gangardt and P.Krüger. In chapter 6 I introduce the model of interest before demonstrating in chapter 7 that a perturbative approach to this model completely fails, in contrast with the superconducting situation. In chapter 8 I introduce a non-perturbative mean field solution and demonstrate its properties before considering the effects of fluctuations on this solution in chapter 9. Finally in chapter 10 I introduce the idea of an atom chip and outline a possible experimental realization of these results on such a device.

The final section is based on work to be submitted for publication for which I am the first author in collaboration with I.V.Lerner and D.M.Gangardt [31]. It concerns the dynamics of the mean field solution and in particular investigates the possibility of the solution switching between metastable branches. I first derive the non-equilibrium Keldysh action in chapter 11 before using this framework to study the non-equilibrium dynamics after a quantum quench in chapter 12. Some further technical details are also contained within the Appendices.

# Chapter 1

# ULTRACOLD BOSONS

The physics of ultracold atoms has a history dating back to the 1920s when Einstein built upon Bose's statistical theory of photons to predict the occurrence of a low temperature phase transition in a gas of non-interacting bosons - what's now referred to as Bose-Einstein condensation (BEC) [32, 33]. The 1930s-1950s was a time of theoretical effort to understand the link between Bose-Einstein condensation and superfluidity - first postulated by London in 1938 [34] and developed by the likes of Bogoliubov, Landau and Lifshitz and Penrose and Onsager [35–37]. In 1958, Hecht postulated that spin-polarized Hydrogen should form a BEC and methods of trapping and cooling atoms were developed in order to reach temperatures low enough to observe condensation [38]. As laser based methods of trapping and cooling were coming to the fore in the 1980s, the focus switched from spin-polarized hydrogen to alkali metallic atoms because they had optical transitions that could easily be exploited by these techniques. The first observation of Bose Einstein condensation was in a cloud of Rubidium atoms almost 20 years ago [39] and since then the field of ultracold atomic physics has rapidly expanded (see e.g. reviews [40–42]).

Ultracold atomic systems allow unparalleled control of the system, for in-

stance, properties of the trapping fields may be readily changed and even the interaction between atoms can be controlled via an external magnetic field utilizing the Feshbach resonance. What's more, because all atoms in a BEC occupy the same (lowest) quantum state, this allows access to information about the wave function on a macroscopic scale that can easily be accessed by experiments.

This thesis concerns transport in a system of ultracold bosonic atoms. In this chapter I introduce some of the main concepts of ultracold atomic physics which form the foundation of the work that follows. It is in no way intended to be a comprehensive review and will mainly follow [43, 44], although many other helpful reviews exist (see for example [41,45–48]). Instead, I will focus primarily on those topics built upon later in this thesis. I will first introduce the concept of Bose-Einstein condensation before considering some of the experimental techniques required to observe it. I will then outline a theoretical framework for treating weakly-interacting, trapped ultracold atoms - namely the Gross-Pitaevskii (mean field) theory. Finally, I will introduce the idea of a Josephson junction of ultracold atoms which is central to this thesis.

## 1.1 Bose-Einstein Condensation

An intuitive way of understanding the transition to a BEC is to consider the thermal de Broglie wavelength, $\Lambda = \frac{\sqrt{2\pi}\hbar}{\sqrt{mk_{\mathrm{B}}T}}$, where $m$ is the particle mass, $T$ is temperature and $k_{\mathrm{B}} = 1.38 \times 10^{-23}\mathrm{m}^2\mathrm{kgs}^{-2}\mathrm{K}^{-1}$ is the Boltzmann constant. The de Broglie wavelength can be thought of as a measure of the quantum uncertainty in the position of a particle due to the momentum it has at temperature $T$. As temperature decreases, the de Broglie wavelength increases so that at low temperatures the

uncertainty in the position can be of the order of the distance between particles. At these low temperatures the indistinguishability of particles becomes important and the quantum statistics of the particles dominates the classical (Maxwell-Boltzmann) statistics.

### 1.1.1 The Non-Interacting Bose Gas

The average occupation of an energy level $\varepsilon_i$ in a gas of non-interacting bosonic particles at thermodynamic equilibrium is given by the Bose distribution function,

$$n_{\mathrm{B}}(\varepsilon_i) = \frac{1}{e^{\beta(\varepsilon_i - \mu)} - 1}, \tag{1.1.1}$$

where $\beta = 1/k_{\mathrm{B}}T$ and $\mu(N,T)$ is the chemical potential which is fixed by the total number of particles, $N = \sum_i n_{\mathrm{B}}(\varepsilon_i)$. By introducing the density of states, $g(\epsilon) = \sum_i \delta(\epsilon - \varepsilon_i)$, the total particle number may be expressed as

$$N(T,\mu) = \int \mathrm{d}\epsilon g(\epsilon) n_{\mathrm{B}}(\epsilon). \tag{1.1.2}$$

At high temperatures, the gas is classical so that $n_{\mathrm{B}}(\epsilon) \sim e^{-\beta(\epsilon-\mu)} \ll 1$ and the chemical potential is large and negative. As the temperature decreases (for a fixed number of particles) the chemical potential increases up to a maximum value corresponding to the energy of the ground state, $\min[\varepsilon_i] = \varepsilon_0$. The chemical potential cannot increase beyond this point as it would lead to negative occupation numbers of states with energy lower than $\mu$. Instead, as the temperature continues to decrease a macroscopic number of particles begin to occupy the ground state.

To make this discussion more concrete, consider a 3-dimensional ideal Bose gas confined in a box of volume $V$. The density of states in the 3d box is given

by $g(\epsilon) = 2\pi V(2m/h^2)^{3/2}\epsilon^{1/2}$. The lowest energy level of the system is at $\varepsilon_0 = 0$ so that $\mu \leq 0$. At high temperatures, the occupation of the ground state is $N_0 \ll 1$. The number of particles in excited states is an increasing function of the chemical potential. At the critical temperature, $T_\mathrm{c}$, the chemical potential reaches its maximum value ($\mu = 0$) so that

$$\frac{N(T_\mathrm{c})}{V} = 2\pi(2m/h^2)^{3/2}\int_0^\infty \mathrm{d}\epsilon\, \frac{\epsilon^{1/2}}{e^{\beta\epsilon}-1} = \frac{g_{3/2}(1)}{\Lambda^3(T_\mathrm{c})}, \tag{1.1.3}$$

where $\Lambda(T_\mathrm{c})$ is the de Broglie wavelength calculated at the critical temperature and $g_p(z) = \frac{1}{\Gamma(p)}\int\limits_0^\infty \mathrm{d}x \frac{x^{p-1}}{z^{-1}e^x-1} = \sum\limits_{l=1}^{\infty}\frac{z^l}{l^p}$ is the Bose function, with $g_{3/2}(1) \approx 2.61$. Rearranging this equation gives the critical temperature to be $T_\mathrm{c} \approx \frac{\pi\hbar^2}{mk_\mathrm{B}}(N/V)^{2/3}$. The number of particles in excited states at any temperature (the thermally excited population) can then be expressed using $\frac{N(T)}{N(T_\mathrm{c})} = \frac{\Lambda^3(T_\mathrm{c})}{\Lambda^3(T)}$.

As the temperature is lowered beyond $T_\mathrm{c}$ the chemical potential remains constant and the ground state begins to become macroscopically occupied. The total particle number is given as the sum of the ground state population and the thermally excited population,

$$N = N_0 + \left(\frac{T}{T_\mathrm{c}}\right)^{3/2} N. \tag{1.1.4}$$

The condensate fraction is then defined as

$$\frac{N_0}{N} = \begin{cases} 0 & \text{if } T > T_\mathrm{c} \\ 1 - \left(\frac{T}{T_\mathrm{c}}\right)^{3/2} & \text{if } T < T_\mathrm{c}, \end{cases}$$

and is depicted in Fig. (1.1).

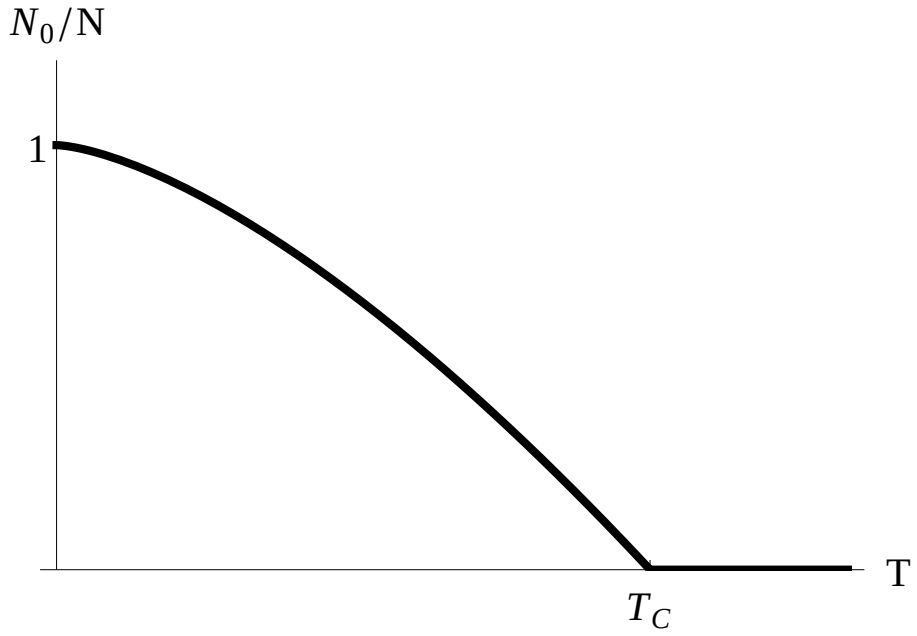


Figure 1.1: A graph showing the condensate fraction as a function of temperature. Above the critical temperature the condensate fraction is 0, while below the critical temperature the ground state becomes macroscopically occupied.

In this thesis, I consider bosonic atoms which are trapped in a harmonic confining potential

$$V(x,y,z) = \frac{1}{2}m\omega_x^2 x^2 + \frac{1}{2}m\omega_y^2 y^2 + \frac{1}{2}m\omega_z^2 z^2. \tag{1.1.5}$$

In this case, the three-dimensional density of states is $g(\epsilon) = \frac{\epsilon^2}{2\hbar^3\omega_x\omega_y\omega_z}$. According to the above considerations, the critical temperature is then given by $T_\mathrm{c} \approx 0.94\hbar(N\omega_x\omega_y\omega_z)^{1/3}$ and the condensate fraction below the critical temperature is $N_0/N = 1 - (T/T_\mathrm{c})^3$.

In practice, getting down to a low enough temperature is not the only requirement to observe a BEC. This is because at temperatures low enough to observe a BEC the thermodynamic equilibrium corresponds to the crystalline phase. This

means that the BEC is not an equilibrium but rather a metastable state of matter. The main low temperature decay mechanism out of this metastable state is 3-body recombination - formation of molecules which bring the system into the thermodynamically stable solid state.

In order to usefully realize a BEC, the 3-body recombination rate should be small enough that the metastable state persists over long enough times to experiment upon. Recombination effects can be quenched in a number of ways. One possibility is to use a dilute gas so that collisions leading to 3-body recombination (and other inelastic processes) are rare. A typical BEC experiment has a density of the order of $10^{13} - 10^{15}\mathrm{atoms/cm}^3$. At these low densities the temperature required to observe quantum effects is typically of the order of $\mu K$. Another possibility for reducing the 3-body recombination rate is to trap the gas far from any material walls where interactions with many atoms in the wall would favour recombination. This is one reason why magnetic and optical traps are favoured above physical traps.

Note also that although inelastic collisions are suppressed, 2-body collisions may still redistribute the energy so that kinetic equilibrium (or thermalization) with respect to these collisions is possible. These 2-body collisions are also the source of interaction effects, which may be characterized by the s-wave scattering length as shall be discussed in section 1.3.

### 1.1.2 Off-Diagonal Long-Range Order and the Order Parameter

One definition of a BEC is simply the presence of macroscopic occupation of the ground state such that $n_0/N \sim \mathcal{O}(1)$. This is not the case when dealing with interacting particles as then the condensate occupation number is no longer given

solely by a single quantum state of the system.

A more general definition of a BEC was given by Penrose and Onsager and relates to the presence of off-diagonal long-range order. Consider the N particle (symmetric) bosonic wavefunction $\Psi(r_1, r_2, ..., r_N)$. The single-particle reduced density matrix is then

$$\begin{aligned} n^{(1)}(r, r') &= \langle \hat{\Psi}^\dagger(r)\hat{\Psi}(r')\rangle \\ &= N\sum_j \int \mathrm{d}r_2 ... \mathrm{d}r_N \, p_j \Psi_j^*(r, r_2, ..., r_N)\Psi_j(r', r_2, ..., r_N), \end{aligned} \tag{1.1.6}$$

where $\hat{\Psi}_j^\dagger(r)$ and $\hat{\Psi}_j(r)$ are the field operators corresponding to creation and annihilation of a particle in state $j$ at position $r$ and $p_j$ is the probability of finding the system in the state $j$. This expression gives the probability amplitude that the system remains in the same state if you remove a particle from position $r'$ and replace it at position $r$. Writing Eq. (1.1.6) in this way highlights that the single particle density matrix is Hermitian and so may be diagonalized by an appropriate orthonormal basis comprising of the single particle eigenfunctions,

$$\hat{\Psi}(r) = \sum_\alpha \psi_\alpha(r) a_\alpha, \tag{1.1.7}$$

where $a_\alpha$ annihilates a particle from state $\alpha$. The single particle density matrix may then be written in this representation as

$$n^{(1)}(r, r') = \sum_\alpha N_\alpha \psi_\alpha^*(r)\psi_\alpha(r'). \tag{1.1.8}$$

Here, $N_i = \langle a_i^\dagger a_i\rangle$ is the average particle occupation of state $i$, which also corre-

sponds to an eigenvalue of the system. This can be seen from the equation

$$\int \mathrm{d}r' n^{(1)}(r,r')\psi_i(r') = N_i\psi_i(r), \tag{1.1.9}$$

where in order to perform the integral I have utilized the orthonormality of the basis set. In a translationally invariant system, in which momentum is a good quantum number, the single particle density matrix is a function of the relative co-ordinate only,

$$n^{(1)}(r,r') = n^{(1)}(r-r') = \frac{1}{V}\int \mathrm{d}k\, n(k) e^{-ik(r-r')/\hbar}, \tag{1.1.10}$$

and the solutions of Eq. (1.1.9) are plane waves $\psi_i = \frac{1}{\sqrt{V}} e^{ik_i r/\hbar}$.

The momentum distribution is then given by

$$\begin{aligned} n(k) &= \langle \hat{\Psi}^\dagger(r)\hat{\Psi}(r')\rangle \\ &= \int \mathrm{d}r\mathrm{d}r'\, n^{(1)}(r',r) e^{ik(r-r')/\hbar} \\ &= \sum_i N_i \delta(k-k_i), \end{aligned} \tag{1.1.11}$$

where the last equation comes from substituting Eq. (1.1.8). If one of the eigenvalues (call it $N_0$ for simplicity) is macroscopically large so that $N_0 \sim N$ then one can write

$$n(k) = N_0\delta(k-k_0) + \sum_{i\neq 0} N_i\delta(k-k_i) = N_0\delta(k-k_0) + \bar{n}(k). \tag{1.1.12}$$

Putting this back into the single particle density matrix Eq. (1.1.10), one can see that in the thermodynamic limit ($N, V \to \infty$ while $N_0/V = n_0$ remains finite) then

at large distances,

$$\lim_{|r-r'|\to\infty} n^{(1)}(r,r') = \begin{cases} 0 & \text{if } n(k) \text{ is a smooth function} \\ n_0 & \text{if } n(k) \text{ is singular.} \end{cases}$$

This is known as off-diagonal long-range order (ODLRO) as it appears in the off-diagonal part of the single particle density matrix ($r \neq r'$) and persists as $r - r' \to \infty$. A BEC is defined by the existence of such ODLRO, which in turn is down to at least one of the eigenvalues being of macroscopic size and implies macroscopic occupation of at least one state. If more than one of the eigenvalues are macroscopic in size this means that more than one state is macroscopically occupied. This is known as a fractured condensate and will not be considered in this thesis. This definition of BEC applies also to non-uniform and strongly interacting systems. It does not directly apply to finite systems as will be considered further in chapter 2.

ODLRO is an example of quantum coherence because a particle always has a finite probability of vanishing from one part of the condensate and appearing in another part. In fact, because the single particle density matrix is constant at large distance this implies that the averages carried out in Eq. (1.1.6) can be performed independently

$$\left\langle \hat{\Psi}^\dagger(r)\hat{\Psi}(r') \right\rangle = \left\langle \hat{\Psi}^\dagger(r) \right\rangle \left\langle \hat{\Psi}(r') \right\rangle. \tag{1.1.13}$$

It is clear then that in the presence of ODLRO, the averages $\left\langle \hat{\Psi}^\dagger(r) \right\rangle$ and $\left\langle \hat{\Psi}(r') \right\rangle$ are non-zero. The field can be split into the condensed and (small) non-condensed parts, $\hat{\Psi} = \Psi_0 + \delta\hat{\Psi}$. Macroscopic occupation implies that adding or removing one particle makes little difference to the ground state. One can then assume (follow-

ing Bogoliubov) that $a_0^\dagger = a_0 = \sqrt{N_0}$ so that from Eq. (1.1.7) it is clear $\Psi_0 = \sqrt{N_0}\psi_0$, while $\delta\hat{\Psi} = \sum_{i\neq 0} \psi_i a_i$. $\Psi_0$ is an order parameter which describes the (ordered) BEC phase and vanishes above the transition temperature. As $\Psi_0$ is a complex number, it is characterized by a modulus and a phase. One can make a gauge transformation by multiplying a phase factor without altering the physical properties of the system. This symmetry is broken by the BEC, which spontaneously picks a value of phase so that the order parameter $\Psi_0 = \left\langle \hat{\Psi}_0 \right\rangle$ has non-zero average. This order parameter forms the basis for theoretical considerations of the BEC as will be explored in section 1.3

## 1.2 Trapping and Cooling Atoms

In this section I will outline some of the key concepts and techniques routinely used to both trap and cool atoms in order to form and observe BECs.

### 1.2.1 The Zeeman Effect

In order to understand the methods of trapping and cooling atoms it is first important to understand the structure of these atoms. Here I will focus only on $Rb^{87}$ although the concepts can easily be generalized. The total angular momentum of an atom is given by the sum of the electronic and nuclear spins **F = I + J**. For $Rb^{87}$, $J = 1/2$ due to a single valance electron in the outer shell, while $I = 3/2$. According to the rules for adding spins this yields two possibilities, $F = 1, 2$. The (hyperfine) interaction between the nuclear and atomic spins is given by

$$H_{\mathrm{HF}} = A\mathbf{I}\cdot\mathbf{J} = \frac{A}{2}(F(F+1) - I(I+1) - J(J+1)) = \frac{A}{2}\Big(F(F+1) - \frac{9}{2}\Big), \quad (1.2.1)$$

where $A$ is a coupling constant. Without the presence of an external field, the difference in energy between the two hyperfine states $F = 1, 2$ is $\Delta E = 2A$. An external magnetic field couples to the electronic and nuclear spins. The coupling to the nuclear spin may be safely neglected in most experimental situations as it is approximately 3 orders of magnitude smaller than the coupling to the electronic spin. Considering an external field in in the z-direction, the Hamiltonian is

$$H = H_{\mathrm{HF}} + g\mu_{\mathrm{B}} J_z B, \tag{1.2.2}$$

where $g = 2$ is the Landé g-factor, $\mu_{\mathrm{B}} = 9.274 \times 10^{-24}$J T$^{-1}$ is the Bohr magneton and B is the magnetic field strength. The hyperfine interaction can be written in terms of the raising and lowering operators $H_{\mathrm{HF}} = AI_z J_z + \frac{A}{2}(I_+ J_- + I_- J_+)$ where $I_\pm = I_x \pm iI_y$ and likewise for $J$. In the basis of states $|m_I, M_J\rangle$ where $m_I = \pm 3/2, \pm 1/2$ and $m_J = \pm 1/2$, this Hamiltonian conserves the z component of angular momentum so that only states with the same value of $m_F = m_I + m_J$ are coupled. Utilizing the identity $I_\pm|m_{\mathrm{I}}\rangle = \sqrt{I(I+1) - m_{\mathrm{I}}(m_{\mathrm{I}} \pm 1)}|m_{\mathrm{I}} \pm 1\rangle$, and likewise for $J$, the Hamiltonian may then be diagonalized by the finding the eigenvalues as summarized in the following table:

| | |
|---|---|
| $m_F = 2$ | $E = \frac{3}{4}A + \mu_{\mathrm{B}} B$ |
| $m_F = 1$ | $E = -\frac{1}{4}A \pm \sqrt{\frac{3}{4}A^2 + \frac{1}{4}(A + 2\mu_{\mathrm{B}} B)^2}$ |
| $m_F = 0$ | $E = -\frac{1}{4}A \pm \sqrt{A^2 + \mu_{\mathrm{B}}^2 B^2}$ |
| $m_F = -1$ | $E = -\frac{1}{4}A \pm \sqrt{\frac{3}{4}A^2 + \frac{1}{4}(A - 2\mu_{\mathrm{B}} B)^2}$ |
| $m_F = -2$ | $E = \frac{3}{4}A - \mu_{\mathrm{B}} B$ |

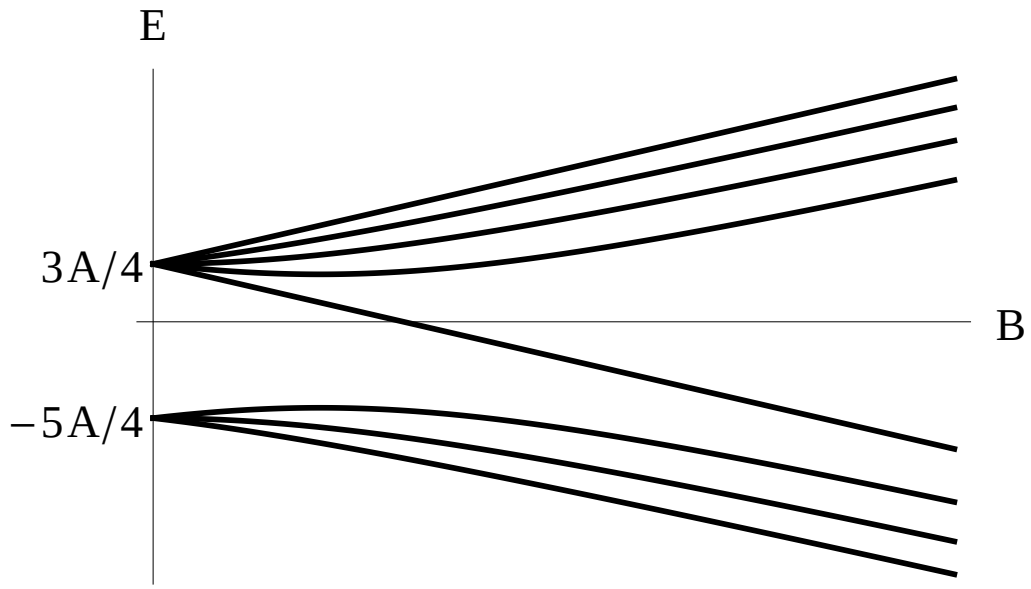


Figure 1.2: A graph showing the energy of the hyperfine states as a function of external magnetic field for $Rb^{87}$ atoms with $I = 3/2$.

These (hyperfine) energy levels are plotted in Fig. (1.2) where it is obvious that at low magnetic fields the energies approach the two hyperfine levels $F = 1, 2$, while at high fields the levels vary linearly with the field, $E \approx \pm\mu_{\mathrm{B}}B$. If the energy of an hyperfine state decreases as the field is increased then atoms in this state are driven to areas of high field, while if the energy of the hyperfine state increases as the field is increased then atoms in this state are driven to areas of low field. This is known as the Zeeman effect and provides the basis for methods of magnetic trapping as outlined in the following section.

### 1.2.2 Atomic Trapping

As has been shown in the previous section, the energy of an hyperfine state depends on the external magnetic field strength. This means that in an inhomogeneous magnetic field, atoms feel a spatially-dependent trapping potential. Atoms

in high-field-seeking hyperfine states are trapped at the maxima of the field, while those in low-field-seeking hyperfine states are trapped in minima of the field. In the absence of charge and current density, the Maxwell equations are $\nabla \cdot \mathbf{B} = 0$ and $\nabla \times \mathbf{B} = 0$, so that $\nabla^2 B_i = 0$. It is then possible to show that

$$\nabla^2 |\mathbf{B}|^2 = \nabla_k \nabla_k B_i B_i = 2\nabla_k B_i \nabla_k B_i = 2B_i \nabla^2 B_i + 2(\nabla_k B_i)^2 > 0. \tag{1.2.3}$$

This means that the magnetic field strength $|\mathbf{B}|^2$ cannot acquire a maxima in the vacuum, as this requires $\partial^2_{x,y,z}|\mathbf{B}|^2 < 0$ for all of $x, y$ and $z$. In conclusion, only atoms in low-field-seeking hyperfine states are able to be trapped.

The simplest magnetic trap is known as a *quadrupole trap* which is formed by a field varying linearly in all directions,

$$\mathbf{B} = B'(x, y, -2z). \tag{1.2.4}$$

Here $B'$ is the magnetic field gradient and $|\mathbf{B}| = B'\sqrt{x^2 + y^2 + 4z^2}$. Note that the gradient in the z-component is twice that in the x,y-components and of opposite sign in order to have zero divergence as per the Maxwell equation above. Such a trap suffers from so-called Majorana transitions, in which atoms in low-field-seeking states may transition into a high-field-seeking state and hence be ejected from the trap. These transitions become important when the frequency associated with the atomic motion in the field is greater than the frequency associated with the transition between hyperfine states. As can be seen from Fig. (1.2), the high- and low-field-seeking states become degenerate, having energy $E = 3A/4$ as $B \to 0$ so that near the minimum of the trap there is significant loss of particles.

In order to remove the problem of Majorana transitions it is preferable to have

a non-zero minimum of the magnetic field. One way of achieving this is to superimpose a rotating uniform magnetic field, known as a *time-averaged orbiting potential (TOP) trap*. The magnetic field is then given by

$$\mathbf{B}(t) = (B'x + B_0 \cos\omega t, B'y + B_0 \sin\omega t, -2B'z). \tag{1.2.5}$$

Here $\omega$ is chosen to be much lower than the frequency associated with transitions between hyperfine states ($\sim 10^6$Hz) to avoid Majorana transitions. It must also be much lower than the Larmor frequency, which is the frequency of precession of the magnetic moment of the atoms so that the magnetic moment adiabatically follows the potential. On the other hand, $\omega$ must be larger than the frequency associated with atomic motion ($\sim 10^2$Hz) so that the atoms only feel the time-averaged effective potential,

$$\langle B \rangle = \frac{\omega}{2\pi} \int_0^{2\pi/\omega} \mathrm{d}t \, |\mathbf{B}(t)| = B_0 + \frac{B'^2}{4B_0}(x^2 + y^2 + 8z^2). \tag{1.2.6}$$

It is clear that the trap minimum is no longer at $B = 0$ but rather a finite value $B = B_0$ so that the effect of Majorana transitions is suppressed. Note also that the time-averaged potential has a harmonic rather than a linear form.

The final possibility I will consider is a static potential which has non-zero minimum known as an *Ioffe-Pritchard trap*. Three sets of coils are typically used:

$$\mathbf{B} = B_0 \begin{pmatrix} 0 \\ 0 \\ 1 \end{pmatrix} + B' \begin{pmatrix} x \\ -y \\ 0 \end{pmatrix} + \frac{B''}{2} \begin{pmatrix} -xz \\ -yz \\ z^2 - \frac{1}{2}(x^2 + y^2) \end{pmatrix}. \tag{1.2.7}$$

The last term of Eq. (1.2.7) provides an axially symmetric trapping potential known

as a magnetic bottle. The second term of Eq. (1.2.7) is known as an Ioffe bar and gives rise to a field which breaks the rotational invariance about the central axis of the magnetic bottle. The first term of Eq. (1.2.7) gives rise to a uniform field which allows one to tune the value of $B_0$. For large $B_0$ so that only quadratic terms are retained, the field strength is given by

$$B = B_0 + \frac{1}{2}B''z^2 + \frac{1}{2}\left(\frac{(B')^2}{B_0} - \frac{B''}{2}\right)(x^2 + y^2). \tag{1.2.8}$$

Such a trap clearly has a non-zero minimum so that Majorana transitions are suppressed and also has harmonic form. This will be of particular relevance when considering an experimental realization of the results of this thesis using an atom chip as described in chapter 10.1.

Since the height of the atomic potential is given by the Bohr magneton $\mu_{\mathrm{B}} = e\hbar/2m_e = 0.67\mathrm{KT}^{-1}$, temperatures of the order of tens of mK must be reached before atoms can be magnetically trapped. Such pre-cooling can be carried out cryogenically for instance by a dilution refrigerator [47]. Once the particles are trapped, then they are further cooled to obtain a BEC.

### 1.2.3 Atomic Cooling

A laser gives rise to a time-dependent electric field. For weak electric fields, the interaction between the light and atoms is dominated by the dipole moment $d$ induced in the atoms, $H = -\mathbf{d} \cdot \varepsilon$, where $\varepsilon(r,t) = \varepsilon(r,\omega)e^{-i\omega t} + \varepsilon(r,-\omega)e^{i\omega t}$ is the electric field. Here $e^{\pm i\omega t}$ corresponds to the absorption or emission of a photon from the laser with energy $\omega$. A second order time-dependent perturbative

treatment of this field gives a shift in energy (known as a Stark shift) given by

$$\Delta E(r) = -\frac{1}{2}\alpha(\omega)|\varepsilon(r)|^2. \tag{1.2.9}$$

Here,

$$\alpha(\omega) = \sum_{\mathrm{e}} |\langle e|\mathbf{d}\cdot\hat{\varepsilon}|g\rangle|^2 \frac{2(E_{\mathrm{e}}-E_{\mathrm{g}})}{(E_{\mathrm{e}}-E_{\mathrm{g}})^2-(\omega+i\eta)^2}, \tag{1.2.10}$$

where $e, g$ are the excited and ground states of the system, $1/\eta$ is the lifetime of an excited state and $\alpha(\omega)$ is known as the dynamic polarizability. This spatially dependent field gives rise to a radiative force $\mathbf{F} = -\nabla(\Delta E(\mathbf{r}))$. This force acts to push atoms to areas of high field if the laser is blue-detuned ($\omega - (E_{\mathrm{e}} - E_{\mathrm{g}}) > 0$) and towards areas of low field if the laser is red-detuned ($\omega - (E_{\mathrm{e}} - E_{\mathrm{g}}) < 0$). In such a way an optical trapping of atoms may be achieved by focusing a red-detuned laser. A combination of magnetic and optical trapping gives rise to a *magneto-optical trap (MOT)*.

The radiative force of a laser can also be used to slow and hence cool atoms. Imagine two counter-propagating laser beams (red) detuned to a frequency just below that of an atomic transition. The rate at which a single atom absorbs such photons is proportional to the Lorentzian $\dot{N}_{\mathrm{ph}} \propto A(\omega) = \eta/[(\omega - (E_{\mathrm{e}} - E_{\mathrm{g}}))^2 + (\eta/2)^2]$. An atom at rest will, on average, absorb as many left moving photons from one laser as it will right moving photons from the other laser. If however the atom is moving with velocity $v$ parallel to the direction of the lasers, then the frequency of the photons is Doppler shifted in the rest frame of the atom so that $\dot{N}_{\mathrm{R}} \propto A(\omega[1 - v/c])$ and $\dot{N}_{\mathrm{L}} \propto A(\omega[1 + v/c])$, where c is the speed of the photons. This means that an atom moving to the right will absorb more left-moving photons than right-moving photons, while an atom moving to the left will absorb

more right-moving photons than left-moving photons. This mismatch in absorption of photons from one side gives rise to a force that tends to decelerate the atoms. As the average kinetic energy of the atoms decreases, so to does the temperature so that the sample is cooled. By placing such a co-propagating pair of lasers in all three spatial directions the atoms can be slowed in all directions. This cooling effect is countered by a heating effect due to absorption of photons travelling in the same direction as the atom. This means that such Doppler cooling techniques have a minimum temperature limit, which is of the order of $100\mu$K.

Further cooling of atoms is usually achieved using evaporative cooling techniques. At the simplest level, by removing the most energetic atoms from the trap the remaining atoms re-thermalize to a lower temperature as the average energy of the system is now lower. This technique relies on the thermalization time of the atoms (by 2-body collisions) being much shorter than the 3-body recombination time (which leads to trap losses). There are two main ways of achieving evaporative cooling. The first is to modify the form of the trapping potential so that the trap is made less deep and the most energetic particles are no longer contained. The second is to use radio-frequency radiation to induce Majorana transitions in atoms of high enough energy so that these atoms are transferred into high-field-seeking states and are no longer trapped.

If the energy threshold for removing atoms is too low, then there are significant losses from the trap. Increasing the energy threshold means that the temperature drop per atom lost is larger, however this also decreases the rate of evaporation as statistically fewer particles have high enough energy to leave the trap. In reality, a balance must be sought between cooling the sample fast enough that particle loss due to other processes (mainly 3-body recombination) is not an issue, but

slow enough that a high number of particles are retained in the trap. Such evaporative cooling techniques are able to lower the temperature beyond the critical temperature for observing condensation ($\sim 100$nK).

## 1.3 Theoretical Background

### 1.3.1 The Gross-Pitaevskii Equation

As has already been discussed, the BEC phase is dominated by 2-body interactions, while 3-body and higher processes may safely be neglected. At low energies, the 2-body interactions are dominated by s-wave scattering and characterized by a single constant - the s-wave scattering length $a_{\rm s}$. In the Born approximation, the scattering length is given by

$$a_{\rm s} = \frac{m}{4\pi\hbar^2} U(0), \tag{1.3.1}$$

where $U(k-k')$ is the Fourier transform of the atom-atom interaction potential. Rearranging this equation gives an effective interaction potential for the atoms, $g = U(0) = \frac{4\pi\hbar^2 a_{\rm s}}{m}$.

At zero temperature, when the ground state of the BEC is fully occupied, one may replace the ground state wavefunction with a classical field i.e. the complex order parameter of section 1.1. The action describing the condensate trapped in the external potential $V(r,t)$ is

$$S = \int \mathrm{d}t\mathrm{d}r \left[ i\hbar\Psi_0^\dagger(r,t)\partial_t\Psi_0(r,t) - \frac{\hbar^2}{2m}|\nabla\Psi_0(r,t)|^2 - V(r,t)|\Psi_0(r,t)|^2 - \frac{g}{2}|\Psi_0(r,t)|^4 \right]. \tag{1.3.2}$$

By computing the equation of motion of the order parameter, $\frac{\delta S}{\delta \Psi^*(r,t)} = 0$, one obtains the Gross-Pitaevskii equation,

$$i\hbar\partial_t \Psi_0(r,t) = \left(-\frac{\hbar^2}{2m}\nabla^2 + V(r,t) + g|\Psi_0(r,t)|^2\right)\Psi_0(r,t). \tag{1.3.3}$$

This equation is the main tool for theoretical investigations of BECs. It is a mean field equation in which the order parameter must be found in a self-consistent way.

As the order parameter is a complex field, it can be parametrized in terms of its modulus and phase as $\Psi_0(r,t) = \sqrt{n(r,t)}e^{i\phi(r,t)}$, where $n(r,t)$ is the density of the condensate and $\phi(r,t)$ is the phase. Substituting this form of the order parameter into the Gross-Pitaevskii equation (1.3.3) gives

$$-n\hbar\dot{\phi} + \frac{i\hbar}{2}\dot{n} = Vn + gn^2 - i\frac{\hbar^2 n}{2m}\nabla^2\phi + \frac{\hbar^2 n}{2m}(\nabla\phi)^2 - i\frac{\hbar^2}{4m}\nabla n\nabla\phi - \frac{\hbar^2}{4m}\nabla^2 n + \frac{\hbar^2}{8mn}(\nabla n)^2. \tag{1.3.4}$$

The imaginary terms give rise to the continuity equation

$$\dot{n} = -\frac{\hbar}{m}(n\nabla^2\phi + \nabla n\nabla\phi) = -\frac{\hbar}{m}\nabla(n\nabla\phi). \tag{1.3.5}$$

Here, $v = \frac{\hbar}{m}\nabla\phi$ is the superfluid velocity and $j = nv$ is the current density. The equation arising from the real terms is

$$\begin{aligned} -\hbar\dot{\phi} &= ng + V + \frac{\hbar^2}{2m}(\nabla\phi)^2 - \frac{\hbar^2}{2m\sqrt{n}}\nabla^2\sqrt{n} \\ &= ng + V + \frac{1}{2}mv^2 - \frac{\hbar^2}{2m\sqrt{n}}\nabla^2\sqrt{n}. \end{aligned} \tag{1.3.6}$$

Eqs. (1.3.5)-(1.3.6) are together equivalent to the Gross-Pitaevskii equation. This

is sometimes known as the hydrodynamic description of a Bose-condensate as it is written in terms of the density and superfluid-velocity and Eq. ((1.3.6)) has the form of a generalized Bernoulli equation. The final term of Eq. (1.3.6) is known as the quantum pressure and may be neglected in the limit that the length-scale characterizing the density variations is much smaller than the healing length $\xi = 1/(mc)$. This is known as the Thomas-Fermi approximation and in this limit, Eq. (1.3.6) reduces to the classical Euler equation for an inviscid, irrotational ($\nabla \times v = 0$) flow with pressure $P = gn^2/2$.

### 1.3.2 Bogoliubov Theory

Consider the Hamiltonian describing an atomic gas in a three-dimensional box interacting via an effective contact potential,

$$H = \int \mathrm{d}r \left[ -\hat{\Psi}^\dagger(r) \frac{\hbar^2}{2m} \nabla^2 \hat{\Psi}(r) + \frac{g}{2} \hat{\Psi}^\dagger(r) \hat{\Psi}^\dagger(r) \hat{\Psi}(r) \hat{\Psi}(r) \right], \tag{1.3.7}$$

where $\hat{\Psi}^\dagger(r)(\hat{\Psi}(r))$ are the fields which create (annihilate) a particle at position $r$ and $g$ is the effective interaction potential (defined above). One may then Fourier transform the fields $\hat{\Psi}(r) = \frac{1}{\sqrt{V}} \sum_k \hat{a}_k e^{i\mathbf{k}\cdot\mathbf{r}/\hbar}$ so that

$$H = \sum_k \frac{k^2}{2m} \hat{a}_k^\dagger \hat{a}_k + \frac{g}{2V} \sum_{k,k',q} \hat{a}_{k+q}^\dagger \hat{a}_{k'-q}^\dagger \hat{a}_k \hat{a}_{k'}. \tag{1.3.8}$$

As a BEC has a macroscopic number of the particles condensed into a single state, $\Psi_0$, it is natural to develop a perturbative expression $\hat{\Psi}(r) = \Psi_0(r) + \delta\hat{\Psi}(r)$, where $\delta\hat{\Psi}(r)$ describe small fluctuations from the condensed state and $\Psi_0(r)$ is the complex order parameter. This is equivalent to considering $\hat{a}_k = a_0 + \hat{a}_{k\neq 0} =$

$\sqrt{N_0} + \hat{a}_{k\neq 0}$ or $N = N_0 + \sum_{k\neq 0} \hat{a}_k^\dagger \hat{a}_k$, where $\hat{a}_{k\neq 0}$ are small compared to $\sqrt{N_0}$. Substituting this into the expression above, one should note that terms linear in $\hat{a}_{k\neq 0}$ do not appear due to momentum conservation so that the leading order fluctuational contribution is given by

$$H = \frac{g}{2V} N_0^2 + \sum_{k\neq 0} \left[ \frac{k^2}{2m} \hat{a}_k^\dagger \hat{a}_k + \frac{gN}{2V} \left( 2\hat{a}_k^\dagger \hat{a}_k + \hat{a}_k^\dagger \hat{a}_{-k}^\dagger + \hat{a}_k \hat{a}_{-k} \right) \right]. \tag{1.3.9}$$

One can diagonalize this Hamiltonian via a Bogoliubov transformation,

$$\hat{a}_k = u_k \hat{b}_k + v_{-k}^* \hat{b}_{-k}^\dagger. \tag{1.3.10}$$

Here, $\hat{b}^\dagger$ and $\hat{b}$ are creation and annihilation operators for the elementary excitations of the system. By choosing appropriate $u$ and $v$ so that non-diagonal terms vanish from the resultant Hamiltonian, one obtains

$$H = \frac{g}{2V} N_0^2 - \frac{1}{2} \sum_{k\neq 0} \left( \frac{k^2}{2m} + ng - \epsilon_k \right) + \sum_{k\neq 0} \epsilon_k \hat{b}_k^\dagger \hat{b}_k. \tag{1.3.11}$$

Here,

$$\epsilon_k = \sqrt{\frac{gn}{m} k^2 + \frac{k^4}{4m^2}}, \tag{1.3.12}$$

is the Bogoliubov dispersion relation for the excitations of the system. The interacting system has thus been re-written in terms of independent non-interacting quasi-particles which are elementary excitations with energy $\epsilon_k$. Such an approach can straightforwardly be adapted to include the presence of a trapping potential.

At high energy, the dispersion relation reduces to that of a free particle $\epsilon_k \sim \frac{k^2}{2m}$, while the low energy excitations have a linear spectrum $\epsilon_{k\to 0} \sim ck$ where

$c^2 = gn/m$ is the velocity of the excitation. By comparing the two terms under the square root in the dispersion relation, one may obtain a characteristic length scale $\xi = 1/mc$ which separates the phononic and free-particle regimes of the dispersion relation. This is known as the condensate healing length and may be thought of as a characteristic interaction length. It is also the length scale over which a BEC, if perturbed, will restore to its bulk values. These low energy phononic excitations form the basis of Luttinger liquid theory, in which a one-dimensional interacting system is written in the basis of its low energy phononic excitations as shown in chapter 2.

## 1.4 The Josephson Effect

In this section I will briefly describe the Josephson effect, which is a key concept of this thesis. The Josephson effect is a direct manifestation of the quantum coherence of a BEC. As already described above, this allows the BEC to be described by a complex order parameter with a definite phase. If two such systems are connected via a weak link (e.g. a tunnel junction), then Josephson predicted a particle current between them of the form

$$I_{\mathrm{J}} = I_{\mathrm{c}} \sin \Phi, \tag{1.4.1}$$

where $I_{\mathrm{c}}$ is a critical current and $\Phi = \phi_1 - \phi_2$ is the phase difference between the two systems [49]. This is known as the d.c. Josephson effect. In the presence of a non-zero chemical potential difference between the two systems, the phase

difference evolves according to

$$\dot{\Phi} = -\Delta\mu. \tag{1.4.2}$$

This is known as the a.c. Josephson effect. Such a current has been observed in many quantum systems including superconductors and Helium as well as cold atomic systems [3, 50–52]. In this thesis I am concerned primarily with the d.c. Josephson effect.

As a simple derivation of the Josephson equations, consider two condensates in a double well potential such that the wavefunction in each well is given by $\Psi_{1,2} = \sqrt{N_{1,2}}e^{i\phi_{1,2}}$. The tunnelling Hamiltonian is given by the overlap of the wavefunctions $H_T = -J(\Psi_1^\dagger\Psi_2 + \Psi_2^\dagger\Psi_1)$. Substituting in the form of the wavefunction gives the full Hamiltonian

$$\begin{aligned} H &= E_1N_1 + E_2N_2 - J\sqrt{N_1N_2}\left(e^{i(\phi_1-\phi_2)} + e^{-i(\phi_1-\phi_2)}\right) \\ &= E_0 + \frac{E_1 - E_2}{2}\Delta N - J\sqrt{N_{\mathrm{T}}^2 - \Delta N^2}\cos\Phi, \end{aligned} \tag{1.4.3}$$

where $E_0 = \frac{E_1+E_2}{2}N_{\mathrm{T}}$ is a constant, $2N_{1,2} = N_{\mathrm{T}} \pm \Delta N$ and $\Phi = \phi_1 - \phi_2$. In the limit that the difference in particle number is much smaller than the total number of particles then

$$H(\Delta N, \Phi) = E_0 + \frac{E_1 - E_2}{2}\Delta N - JN_{\mathrm{T}}\cos\Phi. \tag{1.4.4}$$

The Josephson equations (1.4.1) and (1.4.2) are then given by Hamilton's equations of motion where $\mu = \frac{E_1-E_2}{2}$ and $I_{\mathrm{c}} = JN_{\mathrm{T}}$. Including an interacting term in each well of the form $H_{\mathrm{int}} = g|\Psi|^4$ whilst setting the energy difference to zero

gives the pendulum Hamiltonian

$$H = \frac{E_{\mathrm{C}}}{2}\Delta N^2 - E_{\mathrm{J}}\cos\Phi, \tag{1.4.5}$$

where $E_{\mathrm{C}} = g$, $E_{\mathrm{J}} = J\sqrt{N_{\mathrm{T}}^2 - \Delta N^2}$ and I have neglected constant terms. In the limit of small oscillations and again neglecting constant terms, this may be approximated as a harmonic oscillator

$$H = \Big(\frac{E_{\mathrm{C}}}{2} - \frac{J}{2N_{\mathrm{T}}}\Big)\Delta N^2 + \frac{1}{2}JN_{\mathrm{T}}\Phi^2. \tag{1.4.6}$$

From Hamilton's equations of this system it is easy to see that the characteristic frequency of these oscillations is

$$\omega_{\mathrm{J}} = \sqrt{JN_{\mathrm{T}}\Big(E_{\mathrm{C}} - \frac{J}{N_{\mathrm{T}}}\Big)}. \tag{1.4.7}$$

If $E_{\mathrm{C}} \ll J/N_{\mathrm{T}}$ then one has Rabi-oscillations of the particle number about $0$ with frequency $\omega_{\mathrm{J}} = J$. On the other hand, if $E_{\mathrm{C}} \gg J/N_{\mathrm{T}}$ then one has Josephson oscillations at the plasma frequency $\omega_{\mathrm{J}} = \sqrt{JN_{\mathrm{T}}E_{\mathrm{C}}}$. In this Josephson limit, if the initial number imbalance is sufficiently large the average $\Delta N$ over many oscillations takes a finite value not equal to zero. Physically, this corresponds to a long-lived imbalance in particle number between the two wells caused by the quantum coherence. This effect is often known as 'self trapping' of a condensate and is analogous to the rotation modes of a classical pendulum which are oscillations with non-zero average momentum.

# Chapter 2

# ONE DIMENSIONAL PHYSICS

As outlined in the introduction, this thesis primarily concerns the one-dimensional behaviour of ultracold bosons. It is possible to construct a one dimensional geometry using a highly asymmetric harmonic trap such that the trapping potential is given by

$$V(x,y,z) = \frac{1}{2}m\omega^2 x^2 + \frac{1}{2}m\omega_\perp^2(y^2+z^2). \tag{2.0.1}$$

Here, $\omega_\perp$ is the transverse trapping frequency and is chosen to be higher than all other energy scales in the problem, $\omega_\perp \gg \omega$. This means that the energy required to excite an atom out of the transverse ground state ($\hbar\omega_\perp$) is not readily available so that motion of atoms is limited to zero point oscillations in the transverse directions. As a result, the transverse degrees of freedom are effectively frozen out of the problem leaving atoms free to travel only in one spatial direction. The length-scale of the confinement is given by the oscillator length $a_\perp = \sqrt{\hbar/(m\omega_\perp)}$.

In the limit that the distance between particles is much smaller than the healing length, then the (classical) mean field theory of the Gross-Pitaevskii equation remains relevant. The one dimensional density is related to the three dimensional density via $n_{1D} = N/L = n_{3D}\pi a_\perp^2$. This means that the mean field theory is ap-

plicable for $\xi/d = \sqrt{\frac{a_\perp^2}{8a_s} n_{1D}} \gg 1$ i.e. for dense quantum gases. To describe dilute quantum gases it is necessary to go beyond mean field theory. In this section I shall first outline some of the peculiarities of a 1D system as compared to the standard 3D picture, before giving an outline of the Luttinger liquid theory as a universal low energy description of one-dimensional systems.

## 2.1 Peculiarities of 1D

One-dimensional systems stand apart from systems of higher dimension because all fluctuations (quantum and thermal) can only travel longitudinally. This means that the effect of fluctuations is dramatically enhanced and therefore fluctuations play a much more important role in one-dimension. In fact, these enhanced fluctuations are responsible for preventing the phase coherence and long range order necessary for Bose-Einstein condensation. This shows itself in the presence of infra-red divergences that appear in the one-dimensional calculations. The Mermin-Wagner theorem states that no continuous symmetry may be broken in one dimension at any temperature for sufficiently short range interactions. This means that bosonic atoms interacting via a contact potential may not form a BEC as this requires the presence of long range order which is a broken symmetry phase (see chapter 1).

It should be noted that the Mermin-Wagner theorem is only strictly applicable to a homogeneous gas of atoms in the thermodynamic limit. A trapped gas is not homogeneous and the density of states is modified by the shape of the trapping potential. Unfortunately, for a harmonic trap in one dimension this still cannot save us and the strict critical temperature for the phase transition goes to zero.

However, although the symmetry cannot strictly be broken this does not preclude the formation of a 'quasi-condensate'. A quasi-condensate does not have strict long range order, but instead the phase fluctuations are suppressed over a sufficient distance that phase coherence exists on a scale much larger than the particle spacing but much smaller than the system size. Such a quasi-condensate may still be described by an order parameter and exhibits superfluidity even though it is not a true long-range ordered phase. The quasi-long range order is a consequence of the characteristic power-law correlations of one-dimensional systems.

Another peculiarity of one-dimensional systems is that the effect of particle interaction is enhanced. This is because as the particles are constrained to travel in only one dimension they cannot avoid collisions and hence interactions, as is possible in higher dimensions. This has two major consequences. Firstly, the idea of particle statistics is not very well defined in one dimension. This is because particle exchange must necessarily involve collision and it is then impossible to distinguish statistical phase from any phase shift acquired in collisions. Instead it is the effect of interactions which dominates the particle motion. An illustration of this concept is the Tonks-Girardeau gas. This is a gas of 'hardcore' bosonic particles i.e. particles that have an infinitely strong contact interaction. It can be shown that such a bosonic gas in one dimension can *exactly* be mapped on to a one-dimensional gas of non-interacting fermions. This highlights that what is key in determining the behaviour of the one-dimensional system is not the particle statistics - as in this case the bosons and fermions have exactly the same behaviour - but rather the form of the interaction.

The second important consequence of particles necessarily colliding and interactions dominating is the absence of single-particle excitations in one dimension.

If one imagined such a single-particle excitation it is clear that as it has more energy than neighbouring particles it would move at a higher velocity. As it is moving at a higher velocity and is unable to avoid collision with slower moving particles, that energy will gradually be spread among all of the particles in the system and the single-particle excitation will have turned into a collective excitation. The fact that only collective excitations exist in one dimension means that a one-dimensional system can always be written in terms of a basis of these collective excitations. This leads directly to the idea of bosonization and the concept of a Luttinger liquid.

## 2.2 Luttinger Liquids

The historical development of Luttinger liquid theory can be traced back to 1950 when Tomonaga [53] first suggested that the excitations of a one-dimensional system could be described using a 'quantized field of sound waves' i.e. using bosonic excitations. This idea was developed into a model by Luttinger [54] in 1963, which had a linearised fermion dispersion, although he incorrectly solved this deriving that interacting and non-interacting systems would have the same excitations. The linear model (now known as the Luttinger model) was correctly solved by Mattis and Lieb [55] in 1965 using a Bogoliubov transform technique and expressing the excitation spectrum in terms of non-interacting bosonic collective modes. Then, in 1981, Haldane [56] showed that correction terms to add non-linearity to the linearised Luttinger model gave rise to non-linear couplings between these bosonic collective modes. He also showed that a bosonic perturbative expansion could be used to describe this and so the transformation technique

that solves the Luttinger model is a general method to solve for the low energy physics of the non-linear problem. Namely, the solution will have the same structure as the Luttinger model but with renormalized parameters. He coined the term 'Luttinger liquid' as a universality class for low energy one dimensional problems which have structure based on the solution to the Luttinger model but with renormalized parameters. This is analogous to the Fermi liquid universality class as an effective low energy theory for fermionic problems in higher dimensions, which have structure based on the solution of the Fermi gas but with parameters renormalized by the interactions.

Here I do not follow the historic construction of the Luttinger liquid outlined above but use the harmonic fluid approach to bosonization developed in parallel by Haldane [57]. I will outline this approach by following the excellent review of Cazalilla [58]. It was found that the low-energy structure of the results obtained previously for both bosons and fermions could be reproduced by considering the symmetrized/antisymmetrized states of a harmonic chain. Although the high energy structures of the Luttinger model and the harmonic chain model are quite different, they have equivalent low energy structure. This allows one to develop the theory independent of an exact model.

As the long wavelength (low energy) fluctuations are enhanced in one dimension, one needs to use variables that describe these low energy fluctuations. At low temperatures, the density $n(x)$ and phase $\phi(x)$ of the system are locally small and the bosonic field operator is described via

$$\Psi_B^\dagger(x) = \sqrt{n(x)}e^{-i\phi(x)}. \tag{2.2.1}$$

I define a cut-off momentum $k_c = 1/\xi$ and frequency $\omega_c \sim \mu$, where $\xi = \hbar/(mc)$

is the healing length and $\mu$ is the chemical potential. This provides an estimate of the momentum where the excitation spectrum deviates from the linear behaviour of the Bogoliubov spectrum Eq. (1.3.12). Modes with $\omega > \omega_c$ are defined as 'fast' modes $(n_>, \phi_>)$ and modes with $\omega < \omega_c$ are defined as 'slow' modes $(n_<, \phi_<)$ so that

$$\begin{aligned} \phi(x) &= \phi_<(x) + \phi_>(x), \\ n(x) &= n_<(x) + n_>(x). \end{aligned} \tag{2.2.2}$$

One can integrate out the fast modes from the problem to leave an effective description in terms of only the low energy modes. As such, I will now drop the (<,>) index and assume only the slow mode.

At low temperatures, $n(x)$ fluctuates around the average value so that

$$n(x) = n_0 + \Pi(x), \tag{2.2.3}$$

where $n_0 = N/L$ and $\Pi(x)$ describes density fluctuations. $\Pi(x)$ is canonically conjugate to $\phi(x)$ which describes the phase fluctuations,

$$\Big[\Pi(x), \phi(x')\Big] = i\delta(x - x'). \tag{2.2.4}$$

This commutation relation implies the existence of an uncertainty relation between the density and phase fluctuations i.e. if phase fluctuations are suppressed then density fluctuations are enhanced and vice versa. $\Pi(x)$ only describes *locally* small fluctuations, but this is not sufficient to describe all possible low-energy fluctuations of the density as it does not include short-wavelength fluctuations.

The linear Bogoliubov spectrum gives rise to phonons with energy $\epsilon_k = \pm ck$, where $c = \sqrt{gn/m}$ is the speed of sound. There are two types of density fluctuation with low energy. The first type are long wavelength fluctuations that oscillate around either one of the points $\pm ck$. The second type are short wavelength fluctuations that oscillate between these points leading to density fluctuations of the form $\cos(2kx)$. The longer wavelength density fluctuations lead to a small change in the local momentum $k(x) = k + \pi\Pi(x)$. This is also reflected in the shorter wavelength fluctuations that now oscillate as $\cos\Big(2\Theta(x)\Big)$ where

$$\frac{1}{\pi}\partial_x\Theta(x) = n_0 + \Pi(x). \tag{2.2.5}$$

Integrating this equation gives

$$\Theta(L) - \Theta(0) = \pi N, \tag{2.2.6}$$

where N is the total particle number. $\Theta(x)$ can be considered as a monotonically increasing function across the length of the wire. The location of particles is associated with points where $\Theta(x) = j\pi$ for integer $j$, as shown in Fig. (2.1). For this reason, $\Theta(x)$ is sometimes known as the particle labelling function. The density can then be expressed in terms of $\Theta(x)$ as

$$n(x) = \sum_{i=1}^{N}\delta(x_i - x) = \frac{1}{\pi}\partial_x\Theta(x)\sum_{n=-\infty}^{\infty}\delta(\Theta(x) - n\pi). \tag{2.2.7}$$

Using the Poisson summation formula

$$\sum_{n=-\infty}^{\infty} f(n) = \sum_{m=-\infty}^{\infty}\int_{-\infty}^{\infty}\mathrm{d}z\, f(z)e^{2m\pi iz},$$

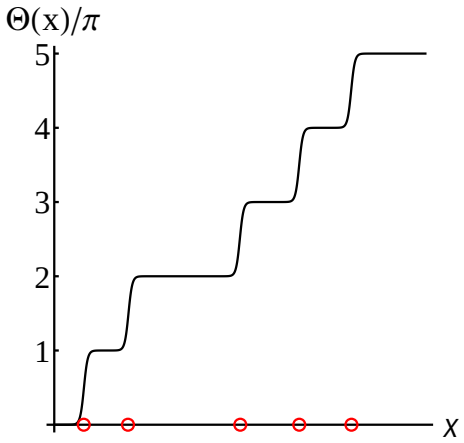


Figure 2.1: A sketch showing the particle labelling function $\Theta(x)$, based on [58]. Particle locations (red circles) are associated with kinks in $\Theta(x)$.

the density can be written as

$$n(x) = \frac{1}{\pi}\partial_x\Theta(x)\sum_{m=-\infty}^{\infty} e^{2mi\Theta(x)} = \Big(n_0 + \Pi(x)\Big)\sum_{m=-\infty}^{\infty} e^{2mi\Theta(x)}. \tag{2.2.8}$$

This means one can express the boson creation operator as

$$\Psi_B^\dagger \sim [n_0 + \Pi(x)]^{1/2}\sum_{m=-\infty}^{\infty} e^{2mi\Theta(x)}e^{-i\phi(x)}, \tag{2.2.9}$$

which is correct up to a pre-factor which depends on the high energy cut-off parameter.

Note that this construction applies equally to fermionic particles with one caveat - as the operators would need to anti-commute, one needs to add a phase factor $e^{i\pi}$ for each particle that is between the two fermions being exchanged. This is analogous to a Jordan-Wigner transformation and gives

$$\Psi_F^\dagger \sim [n_0 + \Pi(x)]^{1/2}\sum_{m=-\infty}^{\infty} e^{(2m+1)i\Theta(x)}e^{-i\theta(x)}. \tag{2.2.10}$$

I now apply this construction to a bosonic system interacting via a general two-body interaction described by the Hamiltonian

$$H = \frac{\hbar^2}{2m}\int \mathrm{d}x\, \partial_x\Psi^\dagger(x)\partial_x\Psi(x) + \frac{1}{2}\int \mathrm{d}x\mathrm{d}x'\, V(x-x')n(x)n(x'). \tag{2.2.11}$$

Substituting Eq. (2.2.9) into this Hamiltonian and keeping only the leading order (quadratic) terms ($m \to 0$) gives

$$H = \frac{\hbar^2}{2m}\int \mathrm{d}x\, n_0\Big(\partial_x\phi(x)\Big)^2 + \frac{1}{2}\int \mathrm{d}x\, \frac{V_0}{\pi^2}\Big(\partial_x\Theta(x) - \pi n_0\Big)^2, \tag{2.2.12}$$

where the interaction is point-like so that $V(x) = V_0\delta(x)$. The coefficients are then relabelled so that

$$cK = \frac{\pi\hbar n_0}{m}, \qquad \frac{c}{K} = \frac{V_0}{\hbar\pi}. \tag{2.2.13}$$

Defining $\Theta(x) = \pi n_0 x - \theta(x)$ so that $\Pi(x) = -\frac{1}{\pi}\partial_x\theta$, the Hamiltonian becomes

$$H = \frac{\hbar}{2\pi}\int \mathrm{d}x\, \Big[cK\Big(\partial_x\phi(x)\Big)^2 + \frac{c}{K}\Big(\partial_x\theta(x)\Big)^2\Big], \tag{2.2.14}$$

known as the Luttinger Hamiltonian. This gives rise to a corresponding action, which may be written in terms of either $\phi(x)$ or $\theta(x)$ by integrating out the relevant fields:

$$S = \frac{\hbar}{2\pi K}\int \mathrm{d}x\, \mathrm{d}\tau\, \Big[c\Big(\partial_x\theta\Big)^2 + \frac{1}{c}\Big(\partial_\tau\theta\Big)^2\Big], \tag{2.2.15}$$

$$S = \frac{\hbar K}{2\pi}\int \mathrm{d}x\, \mathrm{d}\tau\, \Big[c\Big(\partial_x\phi\Big)^2 + \frac{1}{c}\Big(\partial_\tau\phi\Big)^2\Big]. \tag{2.2.16}$$

These dual representations describe the system in terms of either the low energy density or phase fluctuations. To obtain Eq. (2.2.14) I have thrown away higher

order terms, but it can be shown [59] that these terms do not change the form of the Hamiltonian, rather the only effect they have is to renormalize the parameters $v$ and $K$. This is then a universal effective field theory which describes the system in terms of the low energy excitations of the system. As the low energy excitations are phonons, which can always be described in terms of bosonic creation and annihilation operators, the process of deriving this Hamiltonian is often known as *bosonization*.

The phenomenological parameter $K$ is known as the Luttinger parameter and is a dimensionless parameter which describes the interactions. It is clear from Eq. (2.2.14) that when $K$ is large, the density fluctuates rapidly, while the phase fluctuations are suppressed so that the phase field behaves classically. This allows the formation of a quasi-condensate in a weakly interacting Bose gas as described above. In the opposite limit of small $K$, the phase oscillates rapidly while the density fluctuations are suppressed. It should be noted that $K = 1$ corresponds both to non-interacting fermions and a Tonks-Girardeau gas of hard-core interacting bosons. $K \to \infty$ corresponds to non-interacting bosons. Repulsively interacting fermions are described by $0 < K < 1$, while attractively interacting fermions have $K > 1$. Part of the power of the Luttinger theory is that it describes both fermions and bosons on equal footing with all differences defined not by the particle statistics but the value of the Luttinger parameter. In general, $K$ depends on the microscopic properties of the particular system under consideration. It can be approximated numerically or in certain circumstances may be extracted from an exact solution obtained from e.g. the Bethe-ansatz.

The Luttinger action (2.2.16) forms the basis of my considerations of the bosonic current in a one-dimensional geometry as described in section III of this thesis.

# Part II

# TECHNIQUES

# Chapter 3

# FUNCTIONAL INTEGRATION

The field, or functional integral is a powerful method in statistical physics. Here, I sketch a brief overview of this method and as an example, utilize it to calculate a correlation function for the Luttinger liquid. For a more complete review, I refer the reader to [60].

Consider the (imaginary time) partition function, defined as

$$Z = \det(i\omega - \hat{H})^{-1}\,, \tag{3.0.1}$$

where $\omega$ is the energy and $\hat{H}$ is the Hamiltonian. For simplicity, I consider a one-particle Hamiltonian such that $\hat{H}|\alpha\rangle = \epsilon_\alpha|\alpha\rangle$, where $\epsilon_\alpha$ are the eigenvalues and $|\alpha\rangle$ are the eigenvectors - a complete, orthonormal set of states. By diagonalizing the Hamiltonian in this way, the partition function may be written as

$$Z = \prod_\alpha \frac{1}{i\omega - \epsilon_\alpha}. \tag{3.0.2}$$

Now, borrowing the result of a simple Gaussian integral,

$$\int_{-\infty}^{\infty} \mathrm{d}x\, e^{-bx^2} = \sqrt{\frac{\pi}{b}}, \tag{3.0.3}$$

one may express

$$\frac{1}{i\omega - \epsilon_\alpha} = \frac{1}{\pi}\int_{-\infty}^{\infty} \mathrm{d}x\mathrm{d}y\, e^{-(i\omega-\epsilon_\alpha)(x^2+y^2)}. \tag{3.0.4}$$

Then, by making the transformation $c = x+iy$ and $c^* = x-iy$, which has Jacobian $1/(2i)$, this can be written as

$$\frac{1}{i\omega - \epsilon_\alpha} = \frac{1}{2\pi i}\int \mathrm{d}c^*\mathrm{d}c\, e^{-c^*(i\omega-\epsilon_\alpha)c}. \tag{3.0.5}$$

The partition function can then be written in the form of a *functional integral*:

$$\begin{aligned} Z &= \prod_\alpha \int \frac{\mathrm{d}c_\alpha^*\mathrm{d}c_\alpha}{2\pi i}\, e^{-c_\alpha^*(i\omega-\epsilon_\alpha)c_\alpha} \\ &= \int \mathrm{D}c^*\mathrm{D}c\, e^{-c^*(i\omega-\epsilon_\alpha)c}. \end{aligned} \tag{3.0.6}$$

Here, the symbolic notation $\mathrm{D}c^*\mathrm{D}c$ indicates integrating over all possible complex numbers, or in real space, $\Psi(r) = \langle r \,|\, \Psi\rangle = \sum_\alpha \langle r|c_\alpha|\alpha\rangle = \sum_\alpha c_\alpha \psi_\alpha(r)$ takes all possible values of the given Hilbert space.

All results for functional integration can then be obtained from the formula for Gaussian integration of N complex variables

$$\prod_n \int \frac{\mathrm{d}\phi_n^*\mathrm{d}\phi_n}{2\pi i} e^{-\sum_{i,j}\phi_i^* M_{ij}\phi_j + \sum_i (h_i^*\phi_i + \phi_i^* h_i)} = \frac{e^{\sum_{ij} h_i^*(M^{-1})_{ij}h_j}}{\det M}, \tag{3.0.7}$$

where $M$ is a $N \times N$ matrix. By differentiating both sides of this equation with

respect to $h_i$ and $h_j$ and then setting $h_{i,j} \to 0$, one obtains the definition of the correlation function as a functional integral

$$\langle \phi_i^* \phi_j \rangle = \frac{\prod_n \int \frac{\mathrm{d}\phi_n^* \mathrm{d}\phi_n}{2\pi i} \phi_i^* \phi_j e^{-\sum_{i,j} \phi_i^* M_{ij} \phi_j}}{\prod_n \int \frac{\mathrm{d}\phi_n^* \mathrm{d}\phi_n}{2\pi i} e^{-\sum_{i,j} \phi_i^* M_{ij} \phi_j}} = M_{ij}^{-1}. \tag{3.0.8}$$

In this way, the left hand side of Eq. (3.0.7) is like a generating function for different correlation relations. Of particular importance is the case of a real field in which $\phi^*(q) = \phi(-q)$. In this case, one has

$$\langle \phi^*(q_1)\phi(q_2) \rangle = \frac{\int \mathrm{D}\phi^*[q]\mathrm{D}\phi[q]\, \phi^*(q_1)\phi(q_2) e^{-\frac{1}{2}\sum_q \phi^*(q)M(q)\phi(q)}}{\int \mathrm{D}\phi^*[q]\mathrm{D}\phi[q]\, e^{-\frac{1}{2}\sum_q \phi^*(q)M(q)\phi(q)}} = \frac{1}{M(q_1)}\delta_{q_1,q_2}. \tag{3.0.9}$$

Finally one may note that in real time

$$Z = \det(\omega - \hat{H})^{-1} = \int \mathrm{D}c^* \mathrm{D}c\, e^{i\sum_\alpha c_\alpha^*(\omega - \epsilon_\alpha)c_\alpha}. \tag{3.0.10}$$

Writing the function in the exponent in terms of real space eigenvalues gives

$$\begin{aligned}
\sum_\alpha c_\alpha^*(\omega - \epsilon_\alpha)c_\alpha &= \sum_{\alpha\beta} c_\alpha^*(\omega - \epsilon_\alpha)c_\beta \delta_{\alpha\beta} \\
&= \sum_{\alpha\beta} c_\alpha^*(\omega - \epsilon_\alpha)c_\beta \int \mathrm{d}r\, \psi_\alpha^*(r)\psi_\beta(r) \\
&= \int \mathrm{d}r \sum_\alpha c_\alpha^* \psi_\alpha^*(r)(\omega - \epsilon_\alpha) \sum_\beta c_\beta \psi_\beta(r) \\
&= \int \mathrm{d}r\, \Psi^*(r)(\omega - \epsilon_\alpha)\Psi(r).
\end{aligned} \tag{3.0.11}$$

Fourier transforming this to the time representation gives

$$\int \mathrm{d}r\, \Psi^*(r)(\omega - \epsilon_\alpha)\Psi(r) \rightarrow \int \mathrm{d}r\, \Psi^*(r)(i\partial_t - \epsilon_\alpha)\Psi(r) = S[\Psi^*(r), \Psi(r)], \quad (3.0.12)$$

i.e. the classical action so that on restoring $\hbar$ one has

$$Z = \int \mathrm{D}\Psi^* \mathrm{D}\Psi\, e^{\frac{i}{\hbar} S[\Psi^*, \Psi]}. \quad (3.0.13)$$

The classical solution minimizes the action and gives the largest contribution to the integral. This functional framework allows, for instance, to consider fluctuations about such a classical solution. The Gaussian nature of the integrals involved mean that any quadratic theory may simply be solved. Also the presence of the exponential, which may be readily expanded for small parameters, gives rise naturally to perturbative solutions. This method is very powerful and can be used across many different areas of physics.

## 3.1 Evaluation of Luttinger Liquid Correlation Functions

As an example of the use of functional integration, I compute the Luttinger liquid correlation function for exponentials of the phase, as will be utilized later in this thesis. The arguments here are parallel to those of Giamarachi [59] who presents a much more general review of Luttinger liquid correlation functions. In the infinite channel limit, the Fourier transform of the Luttinger liquid action Eq. ( 2.2.16) is

given by

$$S_{LL} = \frac{K}{2\pi c}\frac{1}{\beta\Omega}\sum_q \phi^*(q)\Big[\omega^2 + c^2k^2\Big]\phi(q), \tag{3.1.1}$$

where $q = (k, \omega)$. One may consider the general correlation function

$$\left\langle e^{\,i\sum\limits_j A_j\phi(r_j)} \right\rangle_{S_{\rm LL}}. \tag{3.1.2}$$

Taking the Fourier transform of the sum in the exponent gives

$$i\sum_j A_j\phi(r_j) = \frac{i}{2\beta\Omega}\sum_q A^*(q)\phi(q) + \phi^*(q)A(q). \tag{3.1.3}$$

The average may now be computed by completing the square in the functional integral:

$$\begin{aligned}
\left\langle e^{i\sum_j A_j\phi(r_j)} \right\rangle &= \left\langle e^{\frac{i}{2\beta\Omega}\sum\limits_q A^*(q)\phi(q)+\phi^*(q)A(q)} \right\rangle \\
&= \int \mathrm{D}\phi^*\mathrm{D}\phi\, e^{\frac{-1}{2\beta\Omega}\sum\limits_q\left[\frac{K}{\pi c}(\omega^2+c^2k^2)\phi^*(q)\phi(q) - iA^*(q)\phi(q) - i\phi^*(q)A(q)\right]} \\
&= \int \mathrm{D}\phi^*\mathrm{D}\phi\, e^{\frac{-1}{2\beta\Omega}\sum\limits_q\left[(\phi^*-iA^*M)M^{-1}(\phi-iMA)+A^*MA\right]} \\
&= e^{\frac{-1}{2\beta\Omega}\sum\limits_q A^*MA},
\end{aligned} \tag{3.1.4}$$

where $M^{-1} = \frac{K}{\pi c}(\omega^2 + c^2k^2)$ so that $M = \frac{\pi c}{K}\frac{1}{\omega^2+c^2k^2}$. Note that

$$\begin{aligned}
\sum_q A^*(q)MA(q) &= \sum_q \frac{\pi c}{K}\frac{1}{\omega^2+c^2k^2}\sum_{m,n} A_mA_n e^{iq(r_m-r_n)} \\
&= \sum_q \frac{\pi c}{K}\frac{1}{\omega^2+c^2k^2}\left[\left(\sum_n A_n\right)^2 - \sum_{m,n} A_mA_n\Big(1 - e^{iq(r_m-r_n)}\Big)\right],
\end{aligned} \tag{3.1.5}$$

so that at low energy ($q \ll 1$) the expression outside the bracket is divergent. Putting this result back into Eq. (3.1.4), one can see that for any $\sum_n A_n \neq 0$, the divergent term dominates and the correlation function is zero. The only non-zero correlations are for $\sum_n A_n = 0$.

Considering the simplest case, $A_1 = -A_2 = 1$, so that $\sum_{m,n} A_m A_n e^{iq(r_m - r_n)} = 2 - 2\cos(kx - \omega\tau)$, one has

$$\begin{aligned} F(r_1 - r_2) &= \frac{1}{\beta\Omega} \sum_q \frac{2\pi c}{K} \frac{1 - \cos(kx - \omega\tau)}{\omega^2 + c^2 k^2} \\ &= \frac{1}{\beta} \sum_{\omega_n} \int \frac{\mathrm{d}k}{2\pi} \frac{2\pi c}{K} \frac{1 - \cos(kx - \omega\tau)}{\omega^2 + c^2 k^2}, \end{aligned} \tag{3.1.6}$$

where $x$ and $\tau$ are the space and imaginary time differences between the two points and the sum in the final line is over bosonic Matsubara frequencies $\omega_n = \frac{2\pi n}{\beta}$. As an aside, note that one can use Eq. (3.0.9) to demonstrate that this result is equivalent to saying that $\langle e^{i(\phi_1 - \phi_2)} \rangle = e^{-\frac{1}{2}\langle(\phi_1 - \phi_2)^2\rangle}$, which holds in general for Luttinger liquids and will be used throughout this thesis. To evaluate the sum in Eq. (3.1.6), it is useful to split it into three parts;

$$\begin{aligned} f(r_1 - r_2) &= \frac{1}{\beta} \sum_n \frac{1 - \cos(kx - \omega_n\tau)}{\omega_n^2 + c^2 k^2} \\ &= \frac{1}{\beta} \sum_n \frac{1 - \frac{1}{2}e^{ikx}\, e^{-i\omega_n\tau} - \frac{1}{2}e^{-ikx}\, e^{i\omega_n\tau}}{\omega_n^2 + c^2 k^2} \\ &= S_1 - \frac{1}{2}e^{ikx} S_2 - \frac{1}{2}e^{-ikx} S_3. \end{aligned} \tag{3.1.7}$$

To evaluate the sum $\frac{1}{\beta}\sum_{\omega_n} g(i\omega_n)$, one can use the fact that the Bose distribution function $n_{\mathrm{B}}(\pm z)$ has poles at $z = i\omega_n$ with residue $\pm\frac{1}{\beta}$. Utilizing the contour, $\gamma_I$, depicted in figure 3.1, one can close the contour around the imaginary axis to

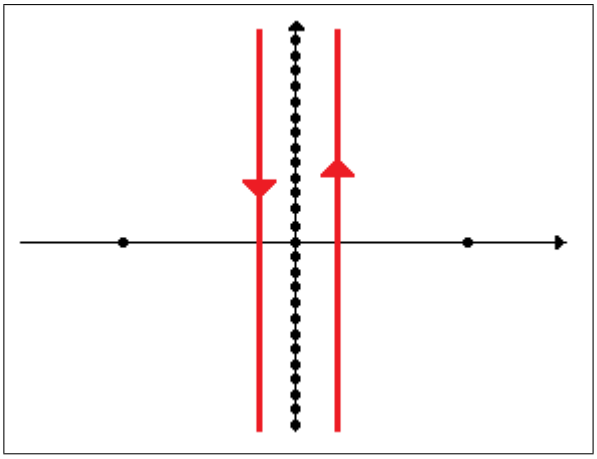

Figure 3.1: A sketch showing the contour $\gamma_I$, used to evaluate the Matsubara sum.

write the sum as

$$\frac{1}{\beta}\sum_{\omega_n} g(i\omega_n) = \oint_{\gamma_I} \frac{\mathrm{d}z}{2\pi i} n_{\mathrm{B}}(z) g(z). \tag{3.1.8}$$

An equivalent expression can be found by closing the contour in two semi-circles around the poles of $g(z)$. Applying this technique to each of the sums in Eq. (3.1.7) gives the following results:

$$\begin{aligned} S_1 &= \frac{1}{\beta}\sum_n \frac{1}{\omega_n^2 + c^2k^2} \\ &= \oint_{\gamma_I} \frac{\mathrm{d}z}{2\pi i} \frac{-n_{\mathrm{B}}(z)}{(z+|ck|)(z-|ck|)} \\ &= \frac{n_{\mathrm{B}}(|ck|) - n_{\mathrm{B}}(-|ck|)}{2|ck|} \\ &= \frac{n_{\mathrm{B}}(|ck|)}{|ck|} + \frac{1}{2|ck|}. \end{aligned} \tag{3.1.9}$$

To calculate $S_2$, consider first the case $\tau > 0$:

$$f(z) = \frac{-e^{-z\tau} n_{\mathrm{B}}(-z)}{(z+|ck|)(z-|ck|)}.$$

Now, $\lim_{z\to\infty} f(z) = e^{-z\tau} \to 0$ and $\lim_{z\to-\infty} f(z) = e^{z(\tau-\beta)} \to 0$ because $\tau < \beta$. This means I can extend my contour out to infinity and

$$\begin{aligned} S_2 &= \frac{1}{\beta}\sum_n \frac{e^{-i\omega_n\tau}}{\omega_n^2 + c^2k^2} \\ &= \oint_{\gamma_I} \frac{\mathrm{d}z}{2\pi i} \frac{-e^{-z\tau}\, n_{\mathrm{B}}(-z)}{(z+|ck|)(z-|ck|)} \\ &= \frac{n_{\mathrm{B}}(|ck|)e^{|ck|\tau} - n_{\mathrm{B}}(-|ck|)e^{-|ck|\tau}}{2|ck|} \\ &= \frac{n_{\mathrm{B}}(|ck|)\cosh(ck\tau)}{|ck|} + \frac{e^{-|ck|\tau}}{2|ck|}. \end{aligned} \tag{3.1.10}$$

Doing likewise for $\tau < 0$ gives the final expression

$$S_2 = \frac{1}{\beta}\sum_n \frac{e^{-i\omega_n\tau}}{\omega_n^2 + c^2k^2} = \frac{n_{\mathrm{B}}(|ck|)\cosh(ck\tau)}{|ck|} + \frac{e^{-|ck||\tau|}}{2|ck|}, \tag{3.1.11}$$

for any $\tau$. $S_3$ may then be computed in exactly the same way to give

$$S_3 = \frac{1}{\beta}\sum_n \frac{e^{i\omega_n\tau}}{\omega_n^2 + c^2k^2} = \frac{n_{\mathrm{B}}(|ck|)\cosh(ck\tau)}{|ck|} + \frac{e^{-|ck||\tau|}}{2|ck|}. \tag{3.1.12}$$

Combining Eqs. (3.1.9),(3.1.11) and (3.1.12) gives the result of the sum as

$$\begin{aligned} f(x,\tau) &= S_1 - \frac{1}{2}e^{ikx}S_2 - \frac{1}{2}e^{-ikx}S_3 \\ &= \frac{n_{\mathrm{B}}(|ck|)}{|ck|} + \frac{1}{2|ck|} - \cos(kx)\left[\frac{n_{\mathrm{B}}(|ck|)\cosh(ck\tau)}{|ck|} + \frac{e^{-|ck||\tau|}}{2|ck|}\right] \\ &= \frac{n_{\mathrm{B}}(|ck|)}{|ck|}(1 - \cos(kx)\cosh(kc\tau)) + \frac{1}{2|ck|}\Big(1 - \cos(kx)e^{-|ck||\tau|}\Big). \end{aligned} \tag{3.1.13}$$

To integrate this with respect to k, I must cut off the (divergent) large k behaviour. In this case, the cut-off is the healing length, $\xi$, which is the smallest length-scale in the system and defines the extent of the (linear) Luttinger approximation (see

chapter 2).

$$\begin{aligned}F(x,\tau) =&\frac{c}{K}\int_{-\infty}^{\infty}\mathrm{d}k\, e^{-\xi|k|}\frac{n_{\mathrm{B}}(|ck|)}{|ck|}(1-\cos(kx)\cosh(kc\tau)) + \frac{1}{2|ck|}\Big(1-\cos(kx)e^{-|ck||\tau|}\Big)\\ =&\frac{1}{K}\int_{0}^{\infty}\frac{\mathrm{d}k}{k}\, e^{-\xi k}\Big[(1+n_{\mathrm{B}}(ck))\Big(1-\cos(kx)e^{-kc|\tau|}\Big) + n_{\mathrm{B}}(ck)\Big(1-\cos(kx)e^{kc|\tau|}\Big)\Big]\\ =&\frac{1}{K}\int_{-\infty}^{\infty}\frac{\mathrm{d}k}{k}\, e^{-\xi|k|}n_{\mathrm{B}}(ck)\Big(1-\cos(kx)e^{kc|\tau|}\Big). \end{aligned} \tag{3.1.14}$$

To evaluate this integral, first note that $n_{\mathrm{B}}(ck)$ has poles up the imaginary axis at $kc\beta = 2\pi i n$ with residue $\frac{1}{c\beta}$. Note there is no pole at $k = 0$ as in this case the numerator of the integral always gives zero. The integral may then be tackled in three parts:

$$\begin{aligned}\int_{-\infty}^{\infty}\frac{\mathrm{d}k}{k}e^{-\xi|k|}n_{\mathrm{B}}(ck) &= \sum_{n}\frac{1}{n}e^{\frac{-\xi 2\pi n}{\beta c}}\\ &= -\log\Big(1-e^{\frac{-\xi 2\pi}{\beta c}}\Big)\\ &= -\log\Big(1-1+\frac{\xi 2\pi}{\beta c}\Big)\\ &= \frac{1}{2}\log\Big(\frac{\beta^2c^2}{4\xi^2\pi^2}\Big). \end{aligned} \tag{3.1.15}$$

$$\begin{aligned}\int_{-\infty}^{\infty}\frac{\mathrm{d}k}{k}e^{-\xi|k|}n_{\mathrm{B}}(ck)e^{k(i|x|+c|\tau|)} &= \sum_{n>0}\frac{1}{n}e^{-\frac{2\pi n|x|}{\beta c}+\frac{2\pi n i|\tau|}{\beta}}\\ &= -\log\Big(1-e^{-\frac{2\pi|x|}{\beta c}+\frac{2\pi i|\tau|}{\beta}}\Big)\\ &= -\log\Big(2\sinh\Big(\frac{\pi|x|}{\beta c}-\frac{\pi i|\tau|}{\beta}\Big)\Big)+\Big(\frac{\pi|x|}{\beta c}-\frac{\pi i|\tau|}{\beta}\Big). \end{aligned} \tag{3.1.16}$$

$$\begin{aligned}\int_{-\infty}^{\infty}\frac{\mathrm{d}k}{k}e^{-\xi|k|}n_{\mathrm{B}}(ck)e^{k(-i|x|+c|\tau|)} &= \sum_{n>0}\frac{1}{n}e^{-\frac{2\pi n|x|}{\beta c}-\frac{2\pi ni|\tau|}{\beta}}\\ &= -\log\left(1-e^{-\frac{2\pi|x|}{\beta c}-\frac{2\pi i|\tau|}{\beta}}\right)\\ &= -\log\left(2\sinh\left(\frac{\pi|x|}{\beta c}+\frac{\pi i|\tau|}{\beta}\right)\right)+\left(\frac{\pi|x|}{\beta c}+\frac{\pi i|\tau|}{\beta}\right).\end{aligned} \tag{3.1.17}$$

Combining these terms gives,

$$F(x,\tau)=\frac{1}{2K}\log\left[\left(\frac{\beta c}{\xi\pi}\right)^2\left(\sinh^2\left(\frac{\pi x}{\beta c}\right)+\sin^2\left(\frac{\pi\tau}{\beta}\right)\right)\right]-\frac{\pi|x|}{K\beta c}. \tag{3.1.18}$$

Note that the last term arises from the divergence in the limit $\beta\to 0$, $\tau=0$, where the integral becomes

$$\begin{aligned}\int\frac{\mathrm{d}k}{k}(1-\cos(kx))n_{\mathrm{B}}(kc) &= \frac{2}{\beta c}\int\frac{\mathrm{d}k}{k^2}\sin^2\left(\frac{kx}{2}\right)\\ &= \frac{\pi|x|}{\beta c}.\end{aligned} \tag{3.1.19}$$

As I am considering low temperatures, I can safely neglect this (high temperature) divergent behaviour leaving

$$F(x,\tau)=\langle[\phi(x,\tau)-\phi(0,0)]^2\rangle=\frac{1}{2K}\log\left[\frac{\beta^2c^2}{\xi^2\pi^2}\left(\sin^2\left(\frac{\pi\tau}{\beta}\right)+\sinh^2\left(\frac{\pi x}{c\beta}\right)\right)\right]. \tag{3.1.20}$$

This means that

$$\langle e^{i(\phi(x,\tau)-\phi(0,0))}\rangle=e^{-\frac{1}{2}F(x,\tau)}=\left[\frac{\beta^2c^2}{\xi^2\pi^2}\left(\sin^2\left(\frac{\pi\tau}{\beta}\right)+\sinh^2\left(\frac{\pi x}{c\beta}\right)\right)\right]^{-\frac{1}{4K}}, \tag{3.1.21}$$

an example of the power-law correlations of one-dimensional physics.

# Chapter 4

# RENORMALIZATION GROUP ANALYSIS

This chapter provides a summary of the Renormalization Group (RG) method, focusing primarily on Wilson's momentum-shell approach. I will then provide a worked example of this method by summarizing the work of Kane and Fisher [8,9] on a single impurity in a Luttinger liquid. This forms the basis of the analysis in chapter 9 as the geometry under consideration can be thought of as a generalization of the Kane-Fisher impurity. An historical background and further examples of the use of RG may be found in refs [59–62].

RG is a theoretical technique which may be used to determine how relevant a perturbation is at low energies. Consider a system described at low energies (below an energy cut-off $\Lambda$) by an action $S[\phi]$, where $\phi$ is the relevant field. This system may then be perturbed by an action $S_{\rm pert}[\phi] \propto g$, where $g$ is a coupling coefficient characterizing the perturbation. The RG analysis proceeds in three stages:

The first stage is 'coarse-graining' the action. This may be done in a number of different ways depending on the problem under consideration (e.g. Kadanoff's block spin analysis of the Ising model [60, 63]). Following Wilson, one can *artificially* define a scale separating the system into higher and lower energy fields.

As such, one can introduce a parameter $b \geq 1$ such that the low-energy ('slow') fields $\phi_<(\omega)$ have energy $|\omega| < \Lambda/b$, while the high energy ('fast') fields $\phi_>(\omega)$ have energy $\Lambda/b < |\omega| < \Lambda$.

The second stage of the RG procedure is sometimes known as decimation. The partition function is given as the trace over all states, equivalent to a functional integral over all field configurations $\phi$. One can explicitly integrate out the fast field configurations $\phi_>$ (i.e. perform the partial trace over these states). In order to compute this integration one must often proceed perturbatively (assuming the coupling constant is small). The partition function is then *exactly* expressed as the functional integral over the lower energy field configurations $\phi_<$ weighted by an effective action, $S^{eff}[\phi_<]$ given by the result of the integration. This effective action may (in general) have a form wildly different to that of the bare (unrenormalized) action, in which case this process is not useful. However, if the effective action has the same structure as the bare action one may proceed with the final stage.

To complete the RG procedure, one must rescale the fields and energy so that the non-perturbed part of the resulting effective action is the same as the bare action (i.e. the non-perturbed part of the action is invariant, or a fixed point, of the RG mapping). For instance, the UV cut-off of the effective action is $\Lambda/b$, so to scale this back to the bare value of the cut-off ($\Lambda$) one must rescale energy in the effective action as $\omega' = b\omega$. Then, as the rescaled field $\phi'_<$ is equivalent to the original field $\phi$, one may simply re-label so that the rescaled effective action is now written in terms of the original field $S^{eff}[\phi'_<] \to S^{eff}[\phi]$. The only difference to the original action is that the coupling constant has been *renormalized* to some different value, $g \to g \times \alpha$, where $\alpha$ is a multiplicative factor which is due to the

effect of the fast modes which have now been integrated out.

As the structure of the renormalized action is the same as that of the bare action, this process may be iterated many times. The result of each iteration is to further renormalize the coupling constant, $g \rightarrow \alpha^n g$. This iteration procedure is responsible for the name 'Renormalization Group'. Formally, the renormalization process outlined above is a mapping between two actions with different coupling constants. The mapping is closed (because all actions have the same structure) and associative (due to the multiplicative effect of the iteration procedure). There also exists a unitary transform (b=1 corresponding to not integrating out any fields) so that the mapping has the structure of a semigroup. Note it does not have the structure of a full group as no inverse mapping can be defined within the closed set. However, this is a formal definition included for completeness and has little use in the practical application of this theory.

By considering the flow equations generated in the continuum limit of this iterative procedure one may determine the low energy behaviour. If the coupling constant flows to larger values as the RG procedure is iterated, the perturbation is considered 'relevant' and dominates the low energy behaviour. If the coupling constant flows to smaller values as the RG procedure is iterated, the perturbation is considered 'irrelevant' and may be ignored in the low energy limit. If the coupling constant is unchanged by RG it is known as a 'marginal' perturbation. A fixed point is invariant under RG and is classified as stable (unstable) if all flows in its vicinity flow toward (away from) it. This leads to the idea of universality as many different actions may exhibit the same low energy behaviour if they exist within the basin of attraction of the same RG fixed point.

Having introduced some of the key concepts, it is perhaps most instructive to

illustrate the RG procedure with a concrete example.

## 4.1 Single Impurity in a Luttinger Liquid

The problem of a Luttinger liquid with a single impurity was considered by Kane and Fisher who used an RG approach to determine the low energy behaviour of the system [8, 9, 59, 60]. The geometry of interest for this thesis as outlined in the introduction and detailed in chapter 6 is a generalization of the single impurity problem. This section will outline the solution of Kane and Fisher to the single impurity problem both as a worked example of the RG ideas introduced above and a basis for the generalization of this problem in section III.

Consider first the case of a *weak impurity* in which the impurity potential acts as a small perturbation to the free flow. The impurity couples to the Luttinger liquid via the action $S_{\text{imp}} = \int \mathrm{d}\tau \mathrm{d}x V(x) n(x)$, where $V(x)$ is the impurity potential and $n(x)$ is the density. The density must be considered to leading order in back scattering components (see Eq. (2.2.7)). Assuming a point-like impurity $V(x) = V_0 \delta(x)$, one has

$$S_{\text{imp}} = V_0 \int \mathrm{d}\tau \Big[ n_0 - \frac{1}{\pi} \partial_x \theta(0) + 2 n_0 \cos(2\theta(0)) \Big]. \tag{4.1.1}$$

The first two terms represent the forward-scattering and may be removed by a simple gauge transformation. The final term is the back-scattering and contains all the interesting physics. As this is written in terms of the density fluctuations, one must use the Luttinger representation Eq. (2.2.15) so that

$$S = \frac{1}{2\pi K c} \int \mathrm{d}x \mathrm{d}\tau \Big[ c^2 (\partial_x \theta)^2 + (\partial_\tau \theta)^2 \Big] + \tilde{V}_0 \int \mathrm{d}\tau \cos 2\theta(0) \ . \tag{4.1.2}$$

This action is Gaussian at all points except for $x = 0$ so that the field $\theta(x)$ may be integrated out except for $\theta(0) = \theta_0$. Using the Lagrange multiplier $\lambda$ one may write

$$\begin{aligned} e^{-S^{eff}} &= \int \mathrm{D}\theta\mathrm{D}\lambda e^{-S_{\mathrm{LL}}+i\int \mathrm{d}\tau\lambda(\tau)[\theta_0-\theta(x=0,\tau)]} \\ &= \int \mathrm{D}\theta\mathrm{D}\lambda e^{-\frac{1}{2\pi Kc}\int \frac{\mathrm{d}\omega\mathrm{d}q}{4\pi^2}(c^2q^2+\omega^2)|\theta(q,\omega)|^2+i\int \frac{\mathrm{d}\omega}{2\pi}\lambda(-\omega)\left[\theta_0(\omega)-\int \frac{\mathrm{d}q}{2\pi}\theta(q,\omega)\right]} \\ &= \int \mathrm{D}\lambda e^{-\frac{1}{2}\int \frac{\mathrm{d}\omega}{2\pi}\frac{\mathrm{d}q}{2\pi}\frac{K\pi c}{c^2q^2+\omega^2}|\lambda(\omega)|^2+i\int \frac{\mathrm{d}\omega}{2\pi}\lambda(-\omega)\theta_0(\omega)} \\ &= \int \mathrm{D}\lambda e^{-\frac{1}{2}\int \frac{\mathrm{d}\omega}{2\pi}\frac{K\pi}{2|\omega|}|\lambda(\omega)|^2+i\int \frac{\mathrm{d}\omega}{2\pi}\lambda(-\omega)\theta_0(\omega)} \\ &= e^{-\frac{1}{2}\int \frac{\mathrm{d}\omega}{2\pi}\frac{2|\omega|}{K\pi}|\theta_0(\omega)|^2}. \end{aligned} \tag{4.1.3}$$

Finally, by rescaling the field so $2\theta_0 \to \theta$, the weak impurity in a Luttinger liquid is described by the action

$$S = \frac{1}{8\pi^2}\int_{|\omega|<\Lambda} \mathrm{d}\omega \frac{|\omega|}{K}|\theta(\omega)|^2 + \tilde{V}_0 \int \mathrm{d}\tau \cos\theta(\tau) \ , \tag{4.1.4}$$

where $\Lambda$ is the UV cut-off which defines the extent to which the Luttinger action is valid. To proceed with the RG, one defines the fast modes $\theta_>$ with $\Lambda/b < |\omega| < \Lambda$ and the slow modes $\theta_<$ with $|\omega| < \Lambda/b$. One should note that $\theta(\tau) = \theta_<(\tau)+\theta_>(\tau)$, where e.g. $\theta_<(\tau) = \int_{|\omega|<\Lambda} \frac{\mathrm{d}\omega}{2\pi}\theta(\omega)e^{-i\omega\tau}$. One must now integrate out the fast modes,

$$\begin{aligned} \int \mathrm{D}\theta_> e^{-S} &= e^{-S_s[\theta_<]}\int \mathrm{D}\theta_> e^{-S_f[\theta_>]-\tilde{V}_0\int \mathrm{d}\tau\cos(\theta_<(\tau)+\theta_>(\tau))} \\ &= e^{-S_s[\theta_<]}\int \mathrm{D}\theta_> e^{-S_f[\theta_>]}\left(1-\tilde{V}_0\int \mathrm{d}\tau\cos(\theta_<(\tau)+\theta_>(\tau))+...\right) \\ &= e^{-S_s[\theta_<]}\left\langle 1-\tilde{V}_0\int \mathrm{d}\tau\cos(\theta_<(\tau)+\theta_>(\tau))+...\right\rangle_f \\ &= e^{-S_s[\theta_<]-\tilde{V}_0\int \mathrm{d}\tau\langle\cos(\theta_<(\tau)+\theta_>(\tau))\rangle_f}, \end{aligned} \tag{4.1.5}$$

where $S_{s,f}$ is the slow(fast) part of the $\omega$ integral in Eq. (4.1.4) and I have assumed that $\tilde{V}_0$ is small. To compute this average, I use the identity $\langle e^{iA}\rangle = e^{-\frac{1}{2}\langle A^2\rangle}$ as demonstrated in chapter 3. This means that $\langle \cos A\rangle = e^{-\frac{1}{2}\langle A^2\rangle}$, while $\langle \sin A\rangle = 0$. Substituting these identities gives

$$\begin{aligned}\left\langle \cos(\theta_<(\tau)+\theta_>(\tau))\right\rangle_f &= \cos\theta_<\left\langle\cos\theta_>\right\rangle_f - \sin\theta_<\left\langle\sin\theta_>\right\rangle_f \\ &= \cos\theta_< e^{-\frac{1}{2}\left\langle\theta_>^2(\tau)\right\rangle_f}.\end{aligned} \tag{4.1.6}$$

Finally, one may use the functional identity Eq. (3.0.9) applied to the action $S_f[\theta_>]$ to show that

$$\langle\theta_>(\omega_1)\theta_>(\omega_2)\rangle = 4\pi^2 K\delta_{-\omega_1,\omega_2}\frac{1}{|\omega|}. \tag{4.1.7}$$

This means that

$$\begin{aligned}\left\langle\theta_>(\tau)\theta_>(\tau)\right\rangle_f &= \int_f \frac{\mathrm{d}\omega_1\mathrm{d}\omega_2}{4\pi^2}\left\langle\theta_>(\omega_1)\theta_>(\omega_2)\right\rangle_f \\ &= \int_f \frac{\mathrm{d}\omega_1\mathrm{d}\omega_2}{4\pi^2}4\pi^2 K\delta_{-\omega_1,\omega_2}\frac{1}{|\omega|} \\ &= \int_f \mathrm{d}\omega\frac{K}{|\omega|} \\ &= 2\int_{\Lambda/b}^{\Lambda}\mathrm{d}\omega\frac{K}{\omega} \\ &= 2K\log b.\end{aligned} \tag{4.1.8}$$

Combining all of these results, one sees that the remaining action is given by

$$S_b = \frac{1}{8\pi^2}\int_{|\omega|<\Lambda/b}\mathrm{d}\omega\frac{|\omega|}{K}|\theta_<(\omega)|^2 + \tilde{V}_0 e^{-K\log b}\int\mathrm{d}\tau\cos\theta_<(\tau). \tag{4.1.9}$$

It is clear on comparison with Eq. (4.1.4) that only two things have changed in

the action - the limits of the $\omega$ integral and a multiplicative factor altering the impurity coupling. In order to bring the UV cut-off energy back to $\Lambda$, I rescale the energy $\omega' = b\omega$ so that $\tau' = \tau/b$. I also want to leave the cosine term invariant [$\theta(\tau') = \theta(\tau)$] so from the definition of the Fourier transform $\theta(\tau) = \int \frac{\mathrm{d}\omega}{2\pi}\theta(\omega)e^{-i\omega\tau}$ it is clear that $\theta'(\omega') = \theta(\omega)/b$. Applying these rescalings and then re-labelling the fields gives

$$S_b = \frac{1}{8\pi^2}\int_{|\omega|<\Lambda} \mathrm{d}\omega \frac{|\omega|}{K}|\theta_<(\omega)|^2 + \tilde{V}_0 b^{1-K}\int \mathrm{d}\tau \cos\theta(\tau). \tag{4.1.10}$$

All terms are equivalent to the original (bare) action, with the coupling renormalized by the factor $\tilde{V}_0(b) = b^{1-K}\tilde{V}_0$. Assuming that $b$ is very close to $1$, one can express this renormalization flow as a differential equation

$$\frac{\mathrm{d}\log\tilde{V}_0}{\mathrm{d}\log b} = 1 - K. \tag{4.1.11}$$

One can now iterate this process, integrating out all modes down to an IR cut-off, $\omega_0$, so that at this energy scale the coupling is given by $\tilde{V}_0(\Lambda/\omega_0)^{1-K}$. By definition, $\Lambda > \omega_0$, so that for $K > 1$ the coupling constant is an irrelevant perturbation at low energies as the impurity potential is decreasing relative to the fluctuations, while for $K < 1$ the coupling constant is a relevant perturbation at low energies because the coupling constant is increasing relative to fluctuations.

This problem can also be considered from the *strong impurity* limit. Here, rather than using the impurity potential (which is now a large parameter), the strong impurity is the same as a weak link and so it is simpler to consider two semi-infinite Luttinger leads weakly connected by a tunnelling barrier. The left

semi-infinite lead may be expressed in phase variables as

$$S_{\rm L} = \frac{K}{2\pi c}\int_{-\infty}^{0} {\rm d}x \int {\rm d}\tau \Big[c^2(\partial_x \phi_{\rm L})^2 + (\partial_\tau \phi_{\rm L})^2\Big] \quad = \frac{K}{4\pi c}\int \frac{{\rm d}\omega {\rm d}q}{4\pi^2}(c^2q^2+\omega^2)|\phi_{\rm L}|^2,$$

and similar for the right lead. Using the notation $\Psi(x) = \sqrt{n(x)}e^{i\phi(x)}$, the coupling between the two leads may be written

$$S_{\rm t} = t\int {\rm d}\tau \Big[\Psi_{\rm L}^\dagger(0)\Psi_{\rm R}(0) + h.c.\Big] \sim t\int {\rm d}\tau \cos(\phi_{\rm L}(0) - \phi_{\rm R}(0)). \tag{4.1.12}$$

As was the case for the weak impurity, the action is Gaussian at all points except for $x = 0$ and so the fields away from this point may be integrated out. This leaves

$$S_{\rm L(R)} = \frac{K}{4\pi^2}\int_{|\omega|<\Lambda} {\rm d}\omega|\omega||\phi_{\rm L(R)}(\omega)|^2. \tag{4.1.13}$$

Then, defining $\phi_\pm = \phi_{\rm L} \pm \phi_{\rm R}$ the action of the leads can be expressed as

$$\begin{aligned} S_{\rm L} + S_{\rm R} &= \frac{K}{4\pi^2}\int_{|\omega|<\Lambda} {\rm d}\omega|\omega| \left[\left|\frac{\phi_+ + \phi_-}{2}\right|^2 + \left|\frac{\phi_+ + \phi_-}{2}\right|^2\right] \\ &= \frac{K}{8\pi^2}\int_{|\omega|<\Lambda} {\rm d}\omega|\omega|\Big[|\phi_+|^2 + |\phi_-|^2\Big]. \end{aligned} \tag{4.1.14}$$

The $\phi_+$ part of the action is Gaussian and may simply be integrated out. The remaining action may be relabelled $\phi_- \to \phi$ so that

$$S = \frac{K}{8\pi^2}\int_{|\omega|<\Lambda} {\rm d}\omega|\omega||\phi(\omega)|^2 + t\int {\rm d}\tau \cos\phi(\tau). \tag{4.1.15}$$

This action for the strong impurity in the Luttinger liquid is dual to Eq. (4.1.4) for

the weak link. The RG equation is obtained in exactly the same way giving

$$\frac{\mathrm{d}\log t}{\mathrm{d}\log b} = 1 - \frac{1}{K}. \tag{4.1.16}$$

This means that for $K > 1$, the tunnelling energy (t) increases relative to the fluctuations at lower energy scales meaning it is more energetically favourable to tunnel particles through the barrier. On the contrary, for $K < 1$ the tunnelling energy decreases relative to the fluctuations at lower energy scales meaning that tunnelling between the two leads becomes less likely.

From these two limits, one can construct a picture of the RG flows. In both cases the $K < 1$ flow is away from the (unstable) 'no impurity' fixed point and towards the (stable) 'infinite impurity' fixed point. Also, in both cases the $K > 1$ flow is away from the (unstable) 'infinite impurity' fixed point and towards the (stable) 'no impurity' fixed point. In other words, the low energy (long time) effects of adding an impurity to a Luttinger liquid are drastically different depending on the value of $K$. For $K < 1$, the effect of adding an impurity - however small - will eventually be the same as cutting the Luttinger liquid in to two separate parts. For $K > 1$, the effect of adding an impurity - however large - will eventually be negligible.

# Chapter 5

# KELDYSH TECHNIQUE

In this chapter I give an overview of the Keldysh technique, based to a large extent on the introductory chapters of the excellent textbook by Kamanev [64]. The Keldysh method is a powerful technique in modern field theory and is most useful in studying disordered or non-equilibrium systems. For a more complete review I refer the reader to the textbooks of Kamanev [64], Stefanucci and van Leeuwen [65] or Altland and Simons [60].

In quantum mechanics, the time evolution of a system is defined by the Schrödinger equation,

$$i\partial_t|\Psi(t)\rangle = \hat{H}|\Psi(t)\rangle. \tag{5.0.1}$$

For a time-independent Hamiltonian $\hat{H}(t) = \hat{H}(t_0)$ the solution is given as

$$|\Psi(t)\rangle = e^{-i\hat{H}(t_0)(t-t_0)}|\Psi(t_0)\rangle \tag{5.0.2}$$

and is uniquely defined for any initial condition $|\Psi(t_0)\rangle$.

One may define a Unitary evolution operator which maps a state at one time

on to the state at a different time,

$$|\Psi(t)\rangle = \hat{U}(t,t')|\Psi(t')\rangle. \tag{5.0.3}$$

To obtain this operator one may split the time interval into infinitely many slices so that over each slice the Hamiltonian is approximately time-independent. Then using Eq. (5.0.2) one may write

$$\hat{U}(t,t') = \lim_{N\to\infty} e^{-i\hat{H}(t-\Delta_t)\Delta_t} e^{-i\hat{H}(t-2\Delta_t)\Delta_t} \dots e^{-i\hat{H}(t-N\Delta_t)\Delta_t} e^{-i\hat{H}(t')\Delta_t}. \tag{5.0.4}$$

Note that in this expression it is important that as $t' < t$, the operators must be ordered so that those acting at earlier times are to the right and so act on the state $|\Psi(t')\rangle$ first. This is known as time ordering and is often represented by the operator $\mathbb{T}$. As $\hat{H}(t_i)$ commutes with $\hat{H}(t_j)$ for all $i, j$, time ordering the expression does not modify the result because in this case, $e^{\hat{H}(t_i)}e^{\hat{H}(t_j)} = e^{\hat{H}(t_i)+\hat{H}(t_j)}$. The evolution operator may then be written as

$$\hat{U}(t,t') = \mathbb{T}e^{-i\int_{t'}^{t} \mathrm{d}t\, \hat{H}(t)}. \tag{5.0.5}$$

It should also be noted that if $t' > t$, for this expression to make sense the operators should be anti time ordered so that operators acting at later times are to the right. This is carried out by the action of the anti time ordering operator $\bar{\mathbb{T}}$. Two important properties of $\hat{U}(t,t')$ which are clear from Eq. (5.0.5) are:

$$\hat{U}(t,t) = 1, \tag{5.0.6}$$

$$\hat{U}(t_3,t_2)\hat{U}(t_2,t_1) = \hat{U}(t_3,t_1). \tag{5.0.7}$$

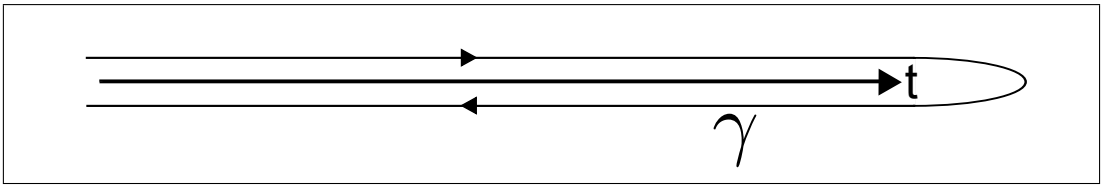


Figure 5.1: A graph showing the Keldysh time contour $\gamma$.

One may now use this definition of the evolution operator to compute the expectation value of some operator. Suppose one has a non-equilibrium, many-body, interacting system in which the final state is unknown. The equilibrium theory relies on knowledge of the final state [66] so must be adapted. Instead, Schwinger [67] suggested a theory in which only knowledge of the initial (known) state is necessary,

$$\langle\hat{\mathcal{O}}(t)\rangle = \langle\Psi(t)|\hat{\mathcal{O}}(t)|\Psi(t)\rangle = \langle\Psi_0|\hat{U}(t_0,t)\hat{\mathcal{O}(t)}\hat{U}(t,t_0)|\Psi_0\rangle. \tag{5.0.8}$$

In order to calculate an observable both the forward and backward time-evolution of the operator are required. This can be written in a more compact way with the help of a time contour, first introduced by Keldysh [68], which travels from $t=-\infty$ to $t=\infty$ before looping round and travelling from $t=\infty$ back to $t=-\infty$ as is illustrated in Fig. (5.1). In this way, one has eliminated the issue of not knowing the final state of the system at the expense of doubling the degrees of freedom of the problem. By time ordering the operators along this contour, one obtains

$$\begin{aligned}\langle\hat{\mathcal{O}}(t)\rangle &= \langle\Psi_0|\bar{\mathbb{T}}\left[e^{-i\int_t^{t_0}\mathrm{d}t\,\hat{H}(t)}\right]\hat{\mathcal{O}}(t)\mathbb{T}\left[e^{-i\int_{t_0}^{t}\mathrm{d}t\,\hat{H}(t)}\right]|\Psi_0\rangle \\ &= \langle\Psi_0|\mathcal{T}\left[e^{-i\int_\gamma \mathrm{d}z\,\hat{H}(z)}\hat{\mathcal{O}}(t_\pm)\right]|\Psi_0\rangle,\end{aligned} \tag{5.0.9}$$

where $\mathcal{T}$ is the contour-ordering operator and $z$ is the contour time; $t_+$ on the

upper (forward) branch of the Keldysh contour and $t_-$ on the lower (backward) branch.

In a similar approach to chapter 3, the partition function can be expressed as a functional integral

$$Z = \int \mathrm{D}\Psi^* \mathrm{D}\Psi e^{i\int_\gamma \mathrm{d}z \Psi^*(z) G^{-1} \Psi(z)}, \tag{5.0.10}$$

where $G^{-1} = i\partial_t - \epsilon$, although it is often easier to deal with the forward and backward branches of the Keldysh contour separately so that

$$S = \int_{-\infty}^{\infty} \mathrm{d}t \Big[ \Psi^*(t_+) G^{-1} \Psi(t_+) - \Psi^*(t_-) G^{-1} \Psi(t_-) \Big]. \tag{5.0.11}$$

Any classical field is the same on both the forward and backward branches of the contour so that $Z = 1$.

When considering the Green's functions of Eq. (5.0.10), there are four possibilities depending on whether the time arguments of the operators appear on the upper or lower branch of the Keldysh contour:

$$iG^{\pm\pm} = \langle \Psi^*(t_\pm) \Psi(t_\pm) \rangle = \int \mathrm{D}\Psi^* \mathrm{D}\Psi \, \Psi^*(t_\pm) \Psi(t_\pm) e^{iS[\Psi^*, \Psi]}. \tag{5.0.12}$$

$G^{++}$ and $G^{--}$ are the time and anti-time ordered Green's functions respectively, while $G^{+-}$ and $G^{-+}$ are sometimes known as the lesser and greater Green's functions $G^<, G^>$. These Green's functions are not independent as it may be shown that $G^{++} + G^{--} = G^< + G^>$. A more compact notation may be obtained by making a Keldysh rotation: $\Psi^{\mathrm{cl}} = \Psi(t_+) + \Psi(t_-)$, $\Psi^{\mathrm{q}} = \Psi(t_+) - \Psi(t_-)$. These are called the *classical* and *quantum* components because for a purely classical field

(so that $\Psi^{\mathrm{q}} = 0$) the action is zero as the field takes the same value on the forward and backward branches of the contour. These Green's functions are sometimes expressed via a $2 \times 2$ matrix

$$\left\langle \Psi^{\alpha}(t)\Psi^{*\,\beta}(t')\right\rangle = iG^{\alpha\beta}(t,t') = \begin{pmatrix} iG^{\mathrm{K}}(t,t') & iG^{\mathrm{R}}(t,t') \\ iG^{\mathrm{A}}(t,t') & 0 \end{pmatrix}. \tag{5.0.13}$$

Here, $G^{\mathrm{R}}(t,t') = G^{\mathrm{cl,q}}(t,t') = \theta(t-t')(G^{>} - G^{<})$ is the retarded Green function, $G^{\mathrm{A}}(t,t') = G^{\mathrm{q,cl}}(t,t') = \theta(t'-t)(G^{<} - G^{>})$ is the advanced Green function and $G^{\mathrm{K}}(t,t') = G^{\mathrm{cl,cl}}(t,t') = G^{>} + G^{<}$ is the Keldysh Green function. These Green's functions may be generated from the action

$$S[\Psi^*,\Psi] = \int_{-\infty}^{\infty} \mathrm{d}t\mathrm{d}t' \begin{pmatrix} \Psi^{*\,\mathrm{cl}}(t), & \Psi^{*\,\mathrm{q}}(t) \end{pmatrix} \begin{pmatrix} 0 & [G^{-1}(t,t')]^{\mathrm{A}} \\ [G^{-1}(t,t')]^{\mathrm{R}} & [G^{-1}(t,t')]^{\mathrm{K}} \end{pmatrix} \begin{pmatrix} \Psi^{\mathrm{cl}}(t') \\ \Psi^{\mathrm{q}}(t') \end{pmatrix} \tag{5.0.14}$$

which is obtained by performing the Keldysh rotation to the action 5.0.11. It should be remembered that the continuum notation of the functional integral is the infinite limit of a discrete number of slices along the time contour. The causality structure of the retarded(advanced) Green's function is maintained in this continuum notation by the regularization $i\partial_t \to \omega \pm i\delta$, where $\delta \to 0$. The energy poles are then located in the lower(upper) half of the complex plane giving rise to the correct theta functions on Fourier transformation. Also, the inverse of the Keldysh Green function is not directly accessible from the Keldysh rotation of the continuum action but may be obtained via the fluctuation dissipation theorem,

$$G^{\mathrm{K}}(\omega) = \coth\frac{\omega-\mu}{2T}[G^{\mathrm{R}}(\omega) - G^{\mathrm{A}}(\omega)]. \tag{5.0.15}$$

# Part III

# STATICS

# Chapter 6

# THE MODEL

In the following chapter I will introduce the model that I have used to study the one-dimensional bosonic flow as in Simpson, et al [30]. I consider a flow of ultracold bosonic atoms through a one-dimensional channel, where each end of the channel is connected via a weak tunnelling link to a macroscopic three-dimensional reservoir of Bose-condensed atoms. I consider the reservoirs to have equal chemical potential so that it is purely the phase difference between the reservoirs that drives the particle current through the channel. Such a geometry can be implemented through the use of potential shaping on an atom chip, as is described in chapter 10. A schematic diagram of the system in question is shown in Fig. (6.1), while Fig. (6.2) is a sketch showing the phase notations used in the model.

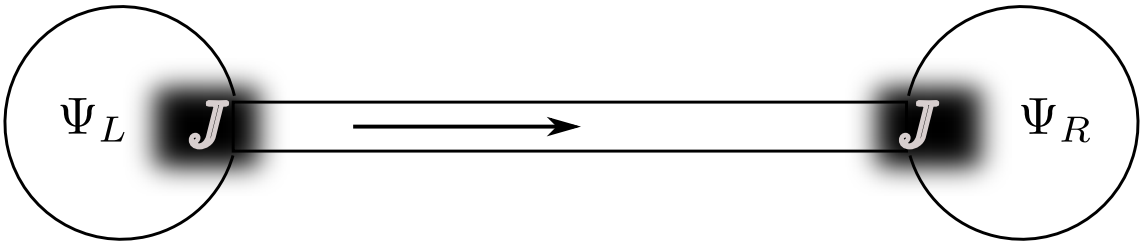


Figure 6.1: 1d channel connected to 3d reservoirs.

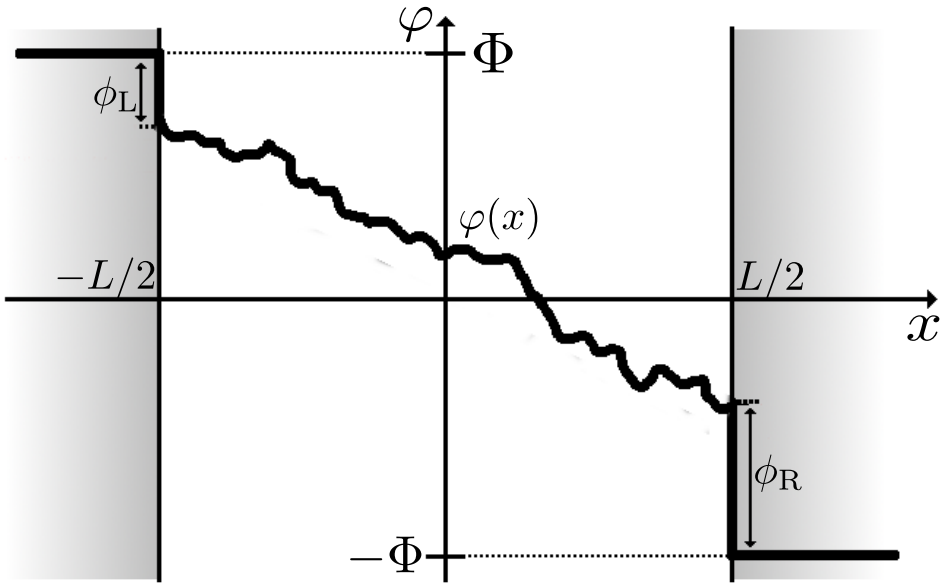


Figure 6.2: A sketch showing the phase notations used in the model: $\pm\Phi$ are the phases of the reservoirs, $\phi_{\mathrm{L,R}}$ are phase jumps located at the tunnel barriers and $\varphi(x)$ is the phase field in the Luttinger channel.

The left and right reservoirs are macroscopic and three-dimensional so that at low temperatures the atoms contained within them may condense to form a Bose-Einstein Condensate. This may be described in the standard way by an order parameter $\Psi_{\mathrm{L,R}} = \sqrt{N_{\mathrm{L,R}}}\mathrm{e}^{i\Phi_{\mathrm{L,R}}}$. I have assumed that the reservoirs have been equilibrated to the same chemical potential so that they must have equal particle densities, $n_{\mathrm{L}} = n_{\mathrm{R}}$. Phase is only well defined in a relative way, for instance against an external reference, allowing me to choose $\Phi_{\mathrm{L}} = -\Phi_{\mathrm{R}} \equiv \Phi$ without loss of generality. The particle current through the channel is thus driven only by the phase difference $2\Phi$. Substituting this form of the order parameter gives the reservoir action in the standard Gross-Pitaevskii form [43, 44]

$$S_{\eta=\mathrm{L,R}} = \int_0^\beta \mathrm{d}\tau \Big[\frac{1}{2}\dot{N}_\eta - \dot{\Phi}_\eta N_\eta + V_{\mathrm{ext}} N_\eta + \frac{g}{2}N_\eta^2\Big], \tag{6.0.1}$$

where $V_{\rm ext}$ is the external reservoir trapping potential generated by the atom chip and $g = 4\pi\hbar^2 a_{\rm s}/m$ is the interaction energy for particles with scattering length $a_{\rm s}$ and mass $m$.

I consider the 1D channel to be of length $L$ and containing $N$ bosons. These bosons do not form a full condensate due to the absence of long range order in 1D systems, however, as discussed in chapter 2 there exists a characteristic radius of phase fluctuations which can be larger than the healing length (known as quasi-long range order) so that locally the system behaves in the same way as a full condensate. This gives rise to a one-dimensional quasi-condensate which may also be described by an order parameter $\psi(x,t) = \sqrt{n_0 - \frac{1}{\pi}\partial_x\theta(x,t)}\mathrm{e}^{i\varphi(x,t)}$, where $\varphi$ is a phase field and $\partial_x\theta$ denotes density fluctuations around the mean density $n_0 = N/L$. The model can be written in terms of either of the canonically conjugate variables $\partial_x\theta$ or $\varphi$. As the phase-difference is driving the particle current, I choose to write the model in terms of $\varphi$ alone. Note that the dual representation is considered in Appendix A. Assuming that the length of the 1D channel is much longer than the healing length of the bosons, the quasi-condensate takes the standard Luttinger-liquid form [58, 59]

$$S_{\rm LL} = \frac{K}{2\pi c}\int_0^\beta \mathrm{d}\tau \int_{-L/2}^{L/2} \mathrm{d}x \Big[(\partial_\tau\varphi)^2 + c^2(\partial_x\varphi)^2\Big]. \tag{6.0.2}$$

Here $\xi \equiv 1/mc$ is the healing length, $c$ is the sound velocity, $m$ is the bosonic mass and $K \equiv \pi n\xi$ is the Luttinger parameter. In particular, I consider the case of weakly interacting bosons in which the healing length is much larger than the distance between bosons so that $K \gg 1$.

The weak link between the reservoirs and 1D channel may be described by the standard tunnelling Hamiltonian. I will assume that the tunnelling is sym-

metric so that the tunnelling energy of each barrier is equal, $J_{\mathrm{L}} = J_{\mathrm{R}} = J$. This assumption will be justified a posteriori as I will demonstrate that a difference in tunnelling energy is a marginal parameter in the RG and so will not alter the characteristic behaviour of the flow (see Appendix B). The tunnelling action is thus given as

$$S_{\mathrm{T}} = 2J \int_0^\beta \mathrm{d}\tau \Big[ \cos\phi_{\mathrm{R}} + \cos\phi_{\mathrm{L}} \Big], \tag{6.0.3}$$

where $\phi_{\mathrm{L,R}}$ are the phase differences between the reservoirs and the ends of the channel ($x = \pm L/2$). This tunnelling action is appropriate only when the overlap of the wavefunctions across the classically forbidden region is small, which imposes the constraint $J \ll cK/\xi \equiv \pi nc$.

It is interesting at this point to notice the similarity of this model to a condensed matter model previously studied: supercurrent along a 1D channel connected via tunnelling barriers to two bulk superconductors differing only by the phase of the superconducting order parameter [69–72]. The only significant difference between the superconducting case and the bosonic model of interest is the value of the Luttinger parameter, where $K \geq 1$ for bosons and $K \leq 1$ for fermions (with $K = 1$ describing the Tonks-Giradeau gas of hard-core bosons, which can be equivalently mapped on to a non-interacting gas of fermions). This thesis will demonstrate that despite apparent similarities between these models, the behaviour of the bosonic system is completely different to the parallel superconducting system.

# Chapter 7

# PERTURBATION THEORY

In this chapter I will perform perturbation theory on the action of Eqs. (6.0.1) - (6.0.3), following the standard analysis used to compute the supercurrent in the parallel superconducting problem [69,70]. I will demonstrate that in the bosonic case, the perturbative approach completely fails due to divergences in the leading order of the expansion. I begin by expanding the partition function in terms of the tunnelling, which is assumed to be weak;

$$\begin{aligned} Z &= \int \mathrm{D}\Phi_{\mathrm{L}}\,\mathrm{D}\Phi_{\mathrm{R}}\,\mathrm{D}\varphi\, e^{-S_{\mathrm{L}}-S_{\mathrm{R}}-S_{\mathrm{LL}}-S_{\mathrm{T}}} \\ &= \int \mathrm{D}\Phi_{\mathrm{L}}\,\mathrm{D}\Phi_{\mathrm{R}}\, e^{-S_{\mathrm{L}}-S_{\mathrm{R}}} \int \mathrm{D}\varphi\, e^{-S_{\mathrm{LL}}}\left(1 - S_{\mathrm{T}} + \frac{1}{2}S_{\mathrm{T}}^2 + ...\right) \\ &= \int \mathrm{D}\Phi_{\mathrm{L}}\,\mathrm{D}\Phi_{\mathrm{R}}\, e^{-S_{\mathrm{L}}-S_{\mathrm{R}}} \left\langle 1 - S_{\mathrm{T}} + \frac{1}{2}S_{\mathrm{T}}^2 + ... \right\rangle_{S_{\mathrm{LL}}}. \end{aligned} \tag{7.0.1}$$

The Josephson current is given by $I \propto \frac{\partial \log Z}{\partial \Delta\Phi}$, where $\Delta\Phi = \Phi_{\mathrm{L}} - \Phi_{\mathrm{R}}$ is the phase difference so that the only terms which will contribute to the Josephson current are those containing the phase difference. The lowest order term of this form is second order in $S_{\mathrm{T}}$ and corresponds to particles that start and end their motion in opposite reservoirs. This means that, to leading order, one may replace $S_{\mathrm{T}}$ with

the effective action $S_{\rm T}^{eff}$ containing only the relevant terms from $S_{\rm T}^2$ so that

$$S_{\rm T}^{eff} = -J^2 \int \mathrm{d}\tau\, \mathrm{d}\tau' \Big[ e^{i(\Phi_{\rm L}+\Phi_{\rm R}-\varphi(-L/2,\tau)-\varphi(L/2,\tau'))} + e^{-i(\Phi_{\rm L}+\Phi_{\rm R}-\varphi(-L/2,\tau)-\varphi(L/2,\tau'))} + e^{i(\Phi_{\rm L}-\Phi_{\rm R}-\varphi(-L/2,\tau)+\varphi(L/2,\tau'))} + e^{-i(\Phi_{\rm L}-\Phi_{\rm R}-\varphi(-L/2,\tau)+\varphi(L/2,\tau'))} \Big]. \tag{7.0.2}$$

The problem then reduces to computing the averages of the type

$$\left\langle e^{i(\pm\varphi(-L/2,\tau)\pm\varphi(L/2,\tau'))} \right\rangle_{S_{\rm LL}} = \left\langle e^{i\sum\limits_j A_j\varphi_j} \right\rangle_{S_{\rm LL}}, \tag{7.0.3}$$

where $\varphi_j = \varphi(r_j)$, as considered in chapter 3. Using Eq. (3.1.20), the average may be written as

$$\langle S_{\rm T}^{eff} \rangle = -2J^2 \iint \mathrm{d}\tau_1 \mathrm{d}\tau_2\, \cos(\Phi_L(\tau_1) - \Phi_R(\tau_2)) e^{-\frac{1}{4K}\log\left[\frac{\beta^2c^2}{\xi^2\pi^2}\left(\sin^2\left(\frac{\pi(\tau_2-\tau_1)}{\beta}\right)+\sinh^2\left(\frac{\pi L}{c\beta}\right)\right)\right]}. \tag{7.0.4}$$

Making the transformation $\tau_{1,2} = \tau \mp \frac{\Delta\tau}{2}$ gives

$$\langle S_{\rm T}^{eff} \rangle = -2J^2 \int \mathrm{d}\tau\, \cos(\Phi_L - \Phi_R) \int \mathrm{d}\Delta\tau\, e^{-\frac{1}{4K}\log\left[\frac{\beta^2c^2}{\xi^2\pi^2}\left(\sin^2\left(\frac{\pi\Delta\tau}{\beta}\right)+\sinh^2\left(\frac{\pi L}{c\beta}\right)\right)\right]}. \tag{7.0.5}$$

The leading order term of the Free Energy is thus given by

$$\mathcal{F} = -\frac{1}{\beta}\log Z = 2J^2 \cos(\Phi_L - \Phi_R) \int \mathrm{d}\Delta\tau\, e^{-\frac{1}{4K}\log\left[\frac{\beta^2c^2}{\xi^2\pi^2}\left(\sin^2\left(\frac{\pi\Delta\tau}{\beta}\right)+\sinh^2\left(\frac{\pi L}{c\beta}\right)\right)\right]}. \tag{7.0.6}$$

At zero temperature ($\beta \to \infty$), this may be written as

$$\mathcal{F} = 2J^2 \cos(\Phi_L - \Phi_R) \int_{-\infty}^{\infty} \mathrm{d}\Delta\tau\, e^{-\frac{1}{4K}\log\left[\frac{L^2}{\xi^2}\left(\frac{c^2\Delta\tau^2}{L^2}+1\right)\right]}$$

$$= 2J^2 \frac{L}{c}\left(\frac{L}{\xi}\right)^{-\frac{1}{2K}} \cos(\Phi_L - \Phi_R) \int_{-\infty}^{\infty} \mathrm{d}n \left(n^2+1\right)^{-\frac{1}{4K}}$$
$$= 2\frac{J^2}{\mu}\left(\frac{L}{\xi}\right)^{1-\frac{1}{2K}} I_0 \cos(\Phi_L - \Phi_R). \tag{7.0.7}$$

It should also be noted that the solution to the integral $I_0$ is a beta function,

$$I_0 = \int_{-\infty}^{\infty} \mathrm{d}n (1+n^2)^{-1/4K} = B\Big(\frac{1}{2}, \frac{1}{4K} - \frac{1}{2}\Big),$$

valid only for $K < 1/2$ and diverging otherwise. It is apparent that the perturbation theory diverges for all $K > 1/2$ and so a different approach is required in this regime. As we are interested in weakly interacting Bosons, for which $K \gg 1$, then certainly we require an alternative approach. In the next section I will develop a (non-perturbative) mean field approach to the problem.

# Chapter 8

# MEAN FIELD THEORY

I continue my analysis by searching for a non-trivial mean-field (MF) phase configuration for the model (6.0.1)–(6.0.3). The tunnelling part of the model introduces boundary conditions to the phase in the channel $\varphi(x)$ defined in terms of the phase drops at the barriers:

$$\begin{aligned} \varphi(-L/2) &= \Phi_{\rm L} - \phi_{\rm L} & \qquad \varphi(L/2) &= \Phi_{\rm R} + \phi_{\rm R} \\ &= \Phi - \phi_{\rm L}, & &= \phi_{\rm R} - \Phi. \end{aligned} \tag{8.0.1}$$

I write down an ansatz for the phase field as a stationary solution satisfying the above boundary conditions:

$$\varphi_0(x) = -\phi_- - 2(\Phi - \phi_+)\frac{x}{L}\,, \qquad \phi_\pm \equiv \frac{1}{2}(\phi_{\rm L} \pm \phi_{\rm R}). \tag{8.0.2}$$

This linear phase solution describes constant superflow between the reservoirs, $\mathcal{I} = nv$, where the velocity is given as $v = (1/m)\partial_x\varphi_0(x) = -2(\Phi - \phi_+)/mL$. An example of this phase profile is illustrated schematically in Fig (8.1) to give clarification to the notations used above.

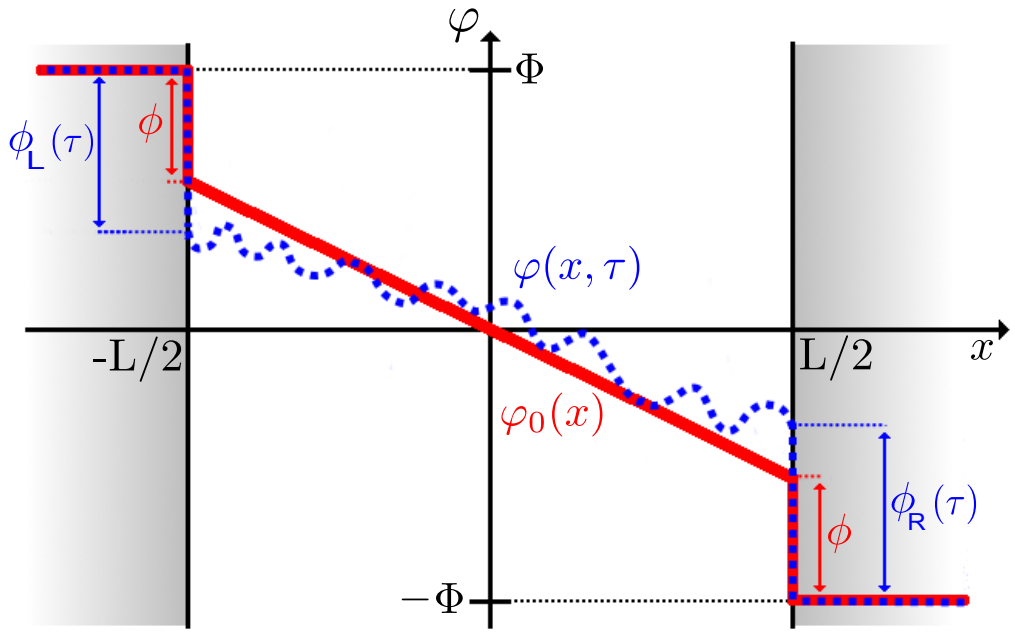


Figure 8.1: Phase profile along the channel: the solid (red) line, $\varphi_0(x)$ shows a symmetric phase configuration ($\phi_L = \phi_R = \phi$) made up of a linear superfluid contribution and phase jumps, $\phi$ at each tunnel barrier. The dashed (blue) line represents a possible fluctuation around the MF phase profile. Figure and caption from Simpson, et al [30].

The energy $E$ of a phase configuration is obtained by substituting the mean field ansatz of Eq. (8.0.2) into the model (6.0.2)–(6.0.3). This gives a contribution from the kinetic energy of the superflow, $\frac{1}{2}mNv^2$, and a contribution from the Josephson energy, $-2J(\cos\phi_R + \cos\phi_L)$ . The total dimensionless energy, $\varepsilon \equiv E/J_c$, can then be written via the phase drops $\phi_\pm$ as

$$\varepsilon = \quad 2(\Phi - \phi_+)^2 - 4\alpha\cos\phi_+\cos\phi_- \qquad\qquad \alpha \equiv J/J_c. \tag{8.0.3}$$

I have defined the energy scale $J_c \equiv n/mL \ll \pi nc$ so that $\alpha$ can take values from $0$ to $\gg 1$ without violating the conditions under which the tunnelling Hamiltonian, Eq. (6.0.3) remains valid. The energy profile (8.0.3) is depicted in Fig. (8.2) for a

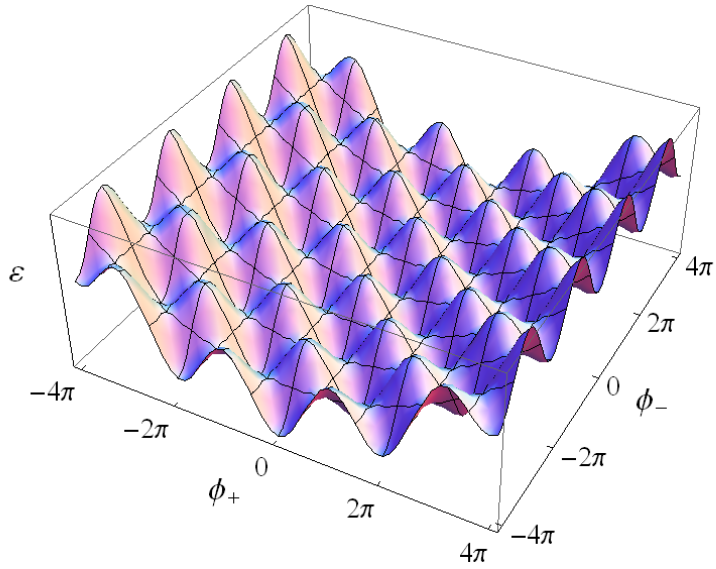


Figure 8.2: A graph of the MF energy profile for $\Phi = 0$.

fixed $\Phi$ and a cut from this at $\phi_- = 0$ in Fig. (8.3) shows the form of the washboard potential for $\phi_+$.

Minimizing this energy with respect to both $\phi_+$ and $\phi_-$ for a fixed external phase difference $2\Phi$ gives all possible MF solutions as described by the equations

$$\Phi - \phi_+ = \alpha \sin\phi_+ \cos\phi_- \,, \tag{8.0.4a}$$

$$\cos\phi_+ \sin\phi_- = 0 \,. \tag{8.0.4b}$$

The stability of these solutions may be obtained from the determinant of the (Hessian) matrix of second derivatives,

$$H[\phi_+, \phi_-] = \begin{pmatrix} 4 + 4\alpha\cos\phi_+\cos\phi_- & -4\alpha\sin\phi_+\sin\phi_- \\ -4\alpha\sin\phi_+\sin\phi_- & 4\alpha\cos\phi_+\cos\phi_- \end{pmatrix},$$

$$D[\phi_+, \phi_-] = 16[\alpha^2\cos^2\phi_+\cos^2\phi_- + \alpha\cos\phi_+\cos\phi_- - \alpha^2\sin^2\phi_+\sin^2\phi_-]. \tag{8.0.5}$$

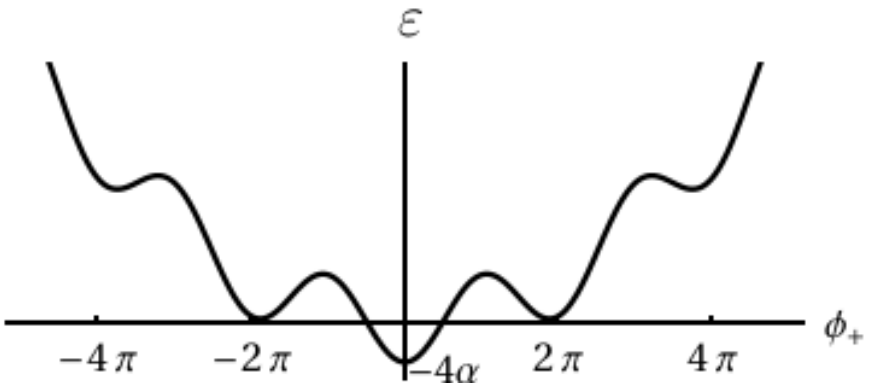


Figure 8.3: A cross-section of the energy profile for $\phi_- = 0$ and $\Phi = 0$, illustrating the form of the 'washboard' potential for $\phi_+$.

Looking first at Eq. (8.0.4b), the two possible solutions are $\cos\phi_+ = 0$ or $\sin\phi_- = 0$. From (8.0.5) it is evident that for $\cos\phi_+ = 0$ one has $D[\phi_+, \phi_-] \leq 0$ so that this is always an unstable (saddle point) solution. Since the dimensionless energy (8.0.3) is a $2\pi$-periodic function of $\phi_-$, I only consider solutions to Eq. (8.0.4b) in the interval $\phi_- \in [0, 2\pi)$. This means that $\phi_- = 0, \pi$, with $\phi_- = 0$ corresponding to symmetric phase drops at the tunnel barriers so that $\phi_{\rm R} = \phi_{\rm L} = \phi_+$, and $\phi_- = \pi$ corresponding to asymmetric phase drops at the tunnel boundaries so that $\phi_{\rm L} = \phi_{\rm R} + 2\pi$. For these symmetric and asymmetric branches the remaining minimization condition Eq. (8.0.4a) becomes

$$\Phi - \phi_+ = \pm\alpha \sin\phi_+. \tag{8.0.6}$$

Note that for $\alpha < 1$, Eq. (8.0.6) has a unique solution, however for $\alpha > 1$ new solutions emerge around $\phi_+ = j\pi$ (where j is an odd integer for the symmetric branch and an even integer for the asymmetric branch). With $\alpha$ continuing to increase, the region in which the two solutions co-exist increases in size until for $\alpha \gg 1$ there are multiple solutions of $\phi_+$ for any given $\Phi$. This is illustrated for

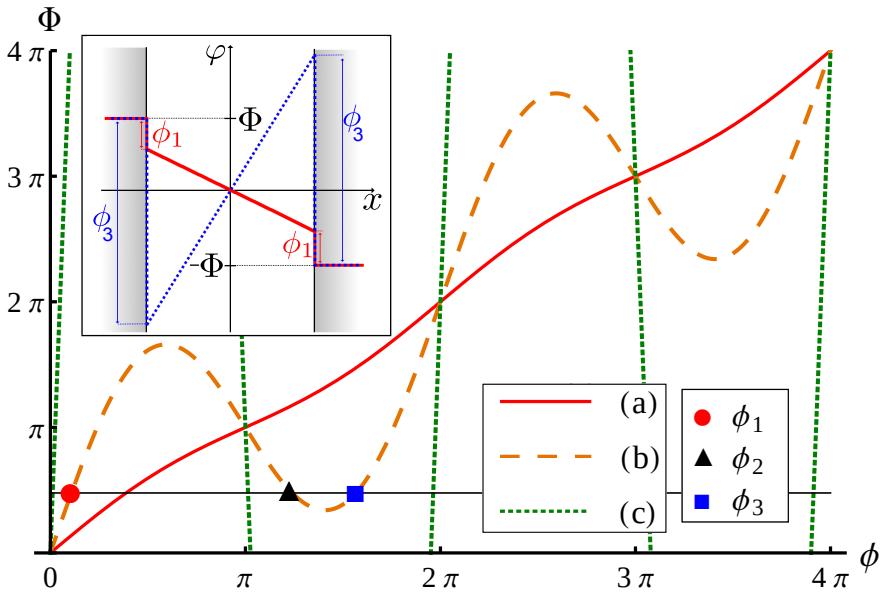


Figure 8.4: The graphical solution to Eq. (8.0.6) for $\cos\phi_- = 1$. (a) $\alpha \ll 1$ a unique solution. (b) $\alpha \approx \pi/2$ an additional pair of solutions emerge. (c) $\alpha \gg 1$ many possible solutions exist. The inset shows the two (symmetric) solutions $\phi_1$ and $\phi_3$, while $\phi_2$ corresponds to a maximum of the energy.

the symmetric case in Fig (8.4). I will now demonstrate that each of the equations (8.0.6) for the symmetric and asymmetric branches has at least one stable solution in some interval of $\Phi$ and that remarkably there always exists some region in which these intervals overlap.

Substituting $\phi_- = 0, \pi$ into the Hessian matrix (8.0.5) gives eigenvalues $\lambda_1 = \pm 4\alpha\cos\phi_+$ and $\lambda_2 = 4 \pm 4\alpha\cos\phi_+$. Solutions are stable when both eigenvalues of the Hessian matrix are positive so that stable solutions must satisfy $\pm\cos\phi_+ > 0$. This indicates that $\phi_- = 0$ gives stable solutions around $\phi_+ = 2j\pi$ (where j is an integer), while $\phi_- = \pi$ gives stable solutions around $\phi_+ = (2j+1)\pi$. The lowest energy solution of Eq. (8.0.6) around $\Phi = 0$ is thus on the symmetric branch and is given by $\phi_+ \approx \Phi/(1+\alpha)$. For small $\alpha$ it remains stable until $\phi_+ = \pi/2$, which

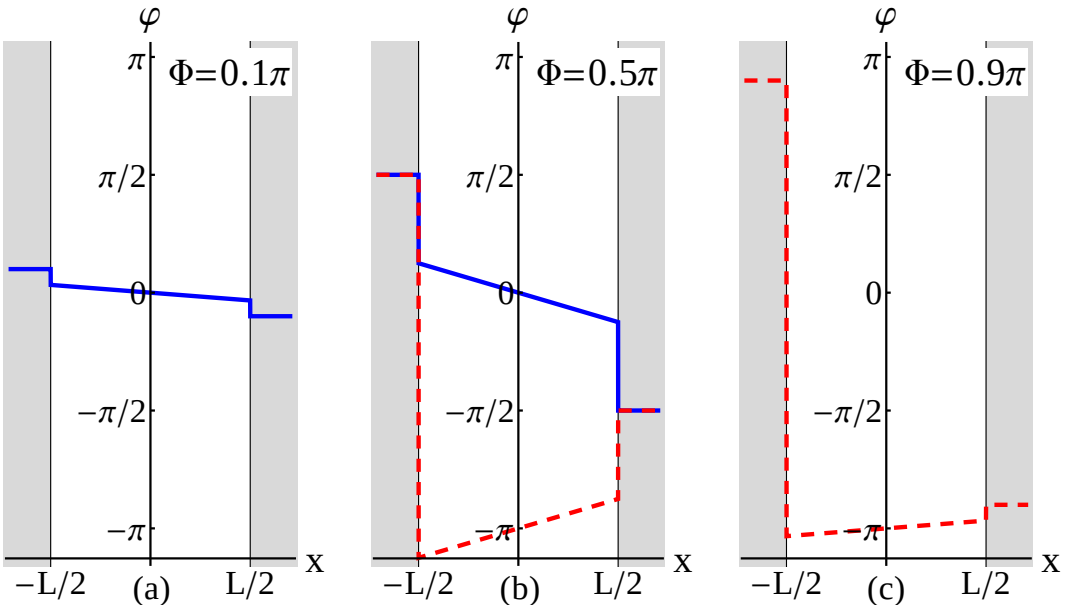


Figure 8.5: The MF phase profile in the channel for $\alpha < 1$ ($J < J_c$): (a) and (c) are unique symmetric/asymmetric solutions near $\Phi = 0$ or $\pi$, respectively; (b) these two solutions become degenerate at $\Phi = \pi/2$, with one of them becoming metastable slightly above or below $\pi/2$. Figure from Simpson, et al [30].

corresponds to increasing $\Phi$ up to $\Phi = \pi/2 + \alpha$. Likewise, the lowest energy solution around $\Phi = \pi$ is on the asymmetric branch and remains stable in the region $\phi_+ \in [\pi/2, 3\pi/2]$ corresponding to $\Phi \in [\pi/2 - \alpha, 3\pi/2 + \alpha]$. In the interval of width $2\alpha$ centred at $\Phi = \pi/2$ both the symmetric and asymmetric solutions coexist. The symmetric solution is stable and the asymmetric solution metastable for $\Phi < \pi/2$, while the asymmetric solution is stable and the symmetric solution metastable for $\Phi > \pi/2$. This is illustrated in Fig. 8.5. It is clear that this pattern is repeated as $\Phi$ is increased further, with the symmetric solution around $\Phi = 2\pi$ stable in the region $\Phi \in [3\pi/2 - \alpha, 5\pi/2 + \alpha]$, the asymmetric solution around $\Phi = 3\pi$ stable in the region $\Phi \in [5\pi/2 - \alpha, 7\pi/2 + \alpha]$ and so on. Each value of $\Phi = (2j + 1)\pi/2$ sits at the centre of a region of coexistence of width $2\alpha$ between consecutive symmetric and asymmetric solutions.

As $\alpha$ is increased, two new solutions of Eq. (8.0.6) emerge when $\alpha > 1$ around the points $\Phi = (2j+1)\pi$ for the symmetric branch [see Fig. (8.4)] and around the points $\Phi = 2j\pi$ for the asymmetric branch. These new solutions remain unstable until $\alpha$ increases to $\pi/2$, corresponding to the point at which the two solutions coexist in the full interval $[0, \pi]$. As $\alpha$ is further increased, these new solutions become (meta)stable, while new pairs of metastable solutions emerge for integer values of $\pi/2$ as illustrated in Fig. 8.6. All metastable solutions exist above the ground state energy in the continuum of phononic fluctuations.

Using Eqs. (8.0.2) and (8.0.6), the superflow along the channel is $\mathcal{I} = \frac{n}{m}\partial_x\varphi(x) = \mp 2J\sin\phi_+$, where the sign is determined by $\cos\phi_- = \pm 1$. This means that $\mathcal{I} = -2J\sin\phi_+\cos\phi_- = -J(\sin(\phi_+ + \phi_-) + \sin(\phi_+ - \phi_-)) = -J(\sin\phi_{\rm L} + \sin\phi_{\rm R})$, which gives the sum of the Josephson currents at the left and right barrier, as expected. The non-triviality arises from the dependence of the superflow on the external phase difference, $2\Phi$, given by Eqs. (8.0.4).

The energy of the MF configurations (8.0.6) is $\varepsilon = 2\alpha^2\sin^2\phi_+ \mp 4\alpha\cos\phi_+$, where the first term is the energy of the (linear) superflow and the second term is the Josephson energy. For $\alpha < 1$ (i.e. for $J \ll J_{\rm c}$), then it is clearly energetically favourable for the phase difference to accumulate at the Josephson barriers. For the symmetric branch, this means that $\phi_{\rm L} = \phi_{\rm R} \approx \Phi$, while for the asymmetric branch $\phi_{\rm L} = \Phi + \pi$ and $\phi_{\rm R} = \Phi - \pi$. As a result, near the energy minimum $\Phi = \pi$, almost the entire phase drop, $2\pi$, occurs at one of the barriers, as illustrated in Fig. (8.5). Each branch carries a current, $\mathcal{I} = \mp 2J\sin\Phi$, which has $4\pi$-periodicity with respect to the overall phase difference, $2\Phi$. However, the symmetric branch is stable for $2\Phi < \pi + 2\alpha$ while the asymmetric branch is stable for $2\Phi > \pi - 2\alpha$. This means that the correct $2\pi$-periodicity is restored by jumps between the two

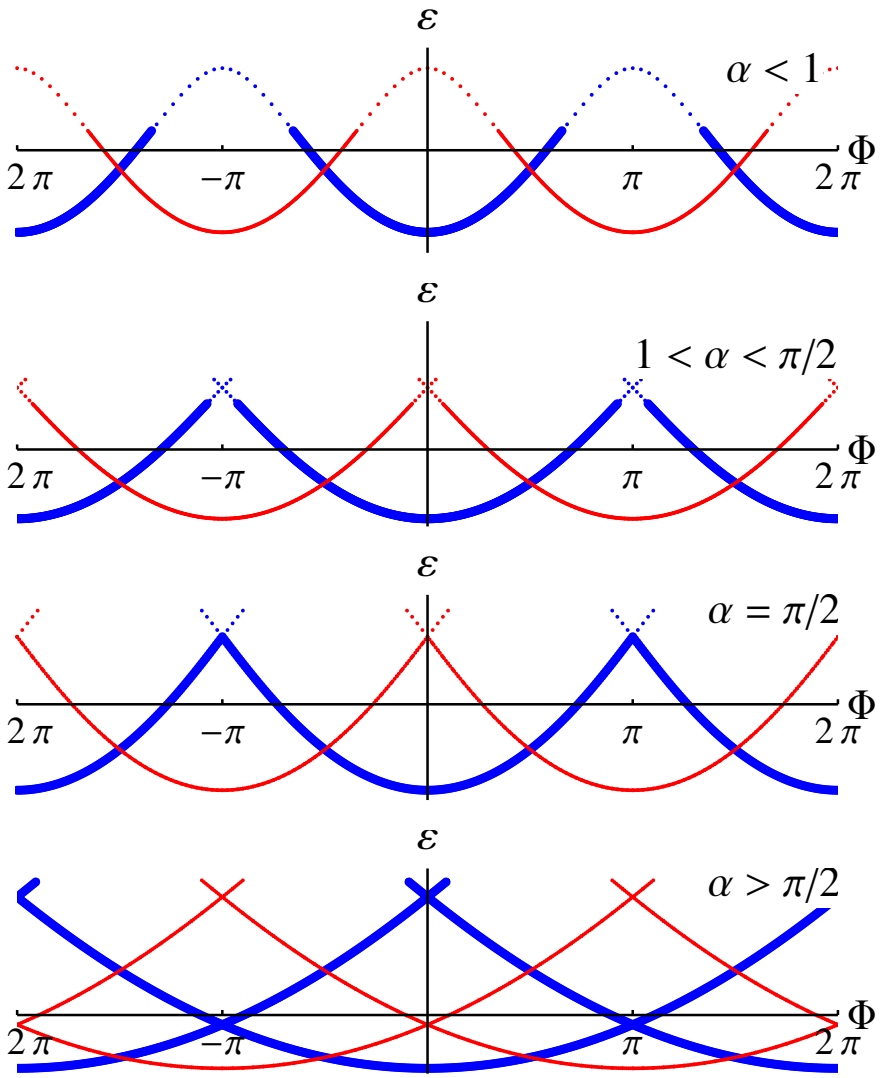


Figure 8.6: The Mean Field energies $\varepsilon = 2\alpha^2 \sin^2 \phi_+ \mp 4\alpha \cos \phi_+$ on the symmetric (thick blue) and asymmetric (thin red) branches shown as a function of external phase difference, $2\Phi$. Four different values of $\alpha$ are shown to illustrate the different cases described in the text: $\alpha < 1$ - a unique solution, $1 < \alpha < \pi/2$ - new solutions emerge but are unstable, $\alpha = \pi/2$ - the energy is bistable for all values of $\Phi$, $\alpha > \pi/2$ - new metastable solutions emerge around integer values of $\pi/2$. All stable energies lie in the interval $-4\alpha \leqslant \varepsilon \leqslant 2\alpha^2$. Dashed lines represent unstable solutions and are shown as a guide for the eye.

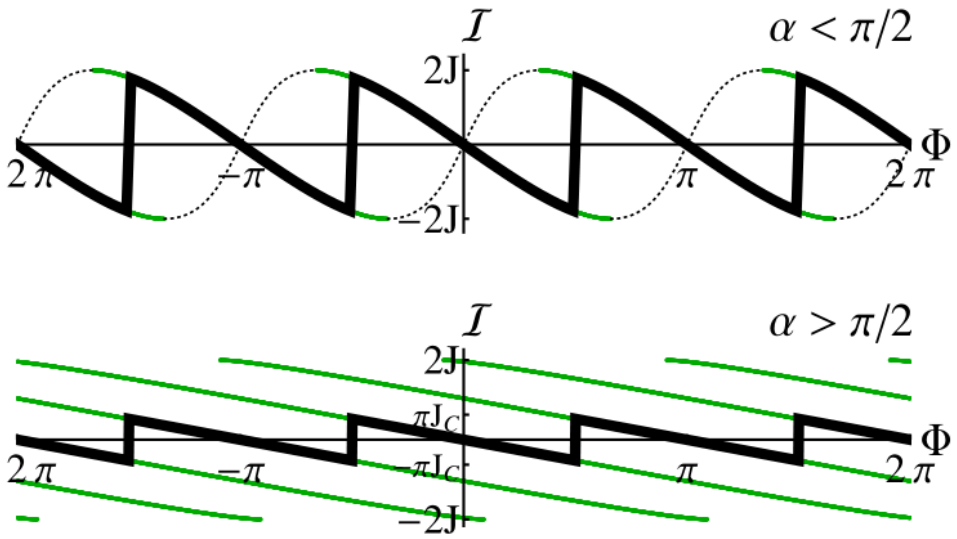


Figure 8.7: The superflow, $\mathcal{I} = \mp 2J \sin \phi_+$, as a function of the external phase difference $2\Phi$. For $\alpha < \pi/2$ the superflow has the form of a piecewise sinusoid, while for $\alpha > \pi/2$ the superflow has saw-tooth form. Thick black (thin green) lines represent the stable (metastable) superflow, while dashed lines represent unstable solutions which have been drawn as a guide for the eyes. Figure from Simpson, et al [30].

branches. These jumps can occur anywhere within the interval of coexistence of the two branches, i.e. in the window of width $2\alpha$ centred at the crossing point.

It should be noted that although Eq. (8.0.6) appears similar to one deriving from the standard analysis of a Superconducting Quantum Interference Device (SQUID) [50], in the bosonic case the correct $2\pi$-periodicity with respect to the external phase difference can only be recovered by discontinuous jumps between symmetric and asymmetric branches for all values of the tunnelling energy $\alpha$. This is not true for a SQUID where each branch retains independent $2\pi$-periodicity and discontinuities only arise for $\alpha > 1$ corresponding to the emergence of new solutions.

As expected, the metastable energy solutions are also reflected in the form

of the superflow, $\mathcal{I} = -J_c \, \mathrm{d}\varepsilon / \, \mathrm{d}(2\Phi)$, as shown in Fig. 8.7. For $\alpha < \pi/2$, the superflow behaves as a piecewise sinusoid, while for $\alpha > \pi/2$ it behaves as a sawtooth function with $\mathcal{I} = -2J_c\Phi$ for $\Phi \in [-\pi/2, \pi/2]$ and periodically repeated for all $\Phi$. In the limit $\alpha \gg 1$, the maximal possible superflow saturates at $\mathcal{I} = \pi J_c$, justifying the labelling of $J_c$ as a critical current.

The discontinuities in the current occur as the solution switches from the symmetric to the asymmetric branch. As shown in Fig. (8.7), the sign of the current changes across the discontinuity indicating a change in the direction of the flow. The jumps may occur anywhere within the region of co-existence of the two branches so that the metastable solutions should be experimentally observable through hysteresis loops in the superflow. A possible future experimental realisation of these results will be discussed in chapter 10.

These features in the bosonic flow have no counterpart in the parallel superconducting situation where the current is always given perturbatively as a sinusoidal function of the phase difference. I will now demonstrate that the MF solution I have obtained is robust against phase fluctuations and so is relevant at low energies.

# Chapter 9

# FLUCTUATIONS

In the following chapter I will analyse the full fluctuating action and use it to show that phase fluctuations about the mean field solution of the previous chapter are irrelevant (in the RG sense). This means that at low energies the effect of fluctuations can be ignored and the mean field solution is sufficient. This implies that the fluctuations cannot provide a mechanism to switch between the symmetric and asymmetric branches of the mean field solution so that the level crossings in the energy, Fig. (8.6), are not avoided.

## 9.1 Fluctuating Action

The mean field solution found in the previous chapter has the form

$$\varphi_0(x) = -\phi_- - \frac{2x}{L}(\Phi - \phi_+). \tag{9.1.1}$$

The full solution can be expressed in terms of fluctuations around this mean field solution. An example of such a fluctuation is illustrated in Fig. (8.1). The fluctuations are thus defined as the difference between the full solution and the MF

solution:

$$\begin{aligned}\widetilde{\phi}_{\mathrm{L}}(\tau) &= \phi_{\mathrm{L}}(\tau) - \phi_{\mathrm{L}},\\ \widetilde{\phi}_{\mathrm{R}}(\tau) &= \phi_{\mathrm{R}}(\tau) - \phi_{\mathrm{R}},\\ \widetilde{\varphi}(x,\tau) &= \varphi(x,\tau) - \varphi_0(x).\end{aligned} \tag{9.1.2}$$

The full ($\tau$-dependent) solution must satisfy the same boundary conditions as the MF solution, Eq. (8.0.1), so that the (fluctuating) phase jumps at the boundaries are always equal to the (fluctuating) difference in phase between the reservoirs and the ends of the channel. This means that the boundary conditions on the fluctuating fields are given by

$$\begin{aligned}\varphi(-L/2,\tau) = \Phi - \phi_{\mathrm{L}}(\tau) &\Rightarrow \widetilde{\varphi}(-L/2,\tau) = -\widetilde{\phi}_{\mathrm{L}}(\tau),\\ \varphi(L/2,\tau) = -\Phi + \phi_{\mathrm{R}}(\tau) &\Rightarrow \widetilde{\varphi}(L/2,\tau) = \widetilde{\phi}_{\mathrm{R}}(\tau).\end{aligned} \tag{9.1.3}$$

As was the case for the MF solution, it is convenient to define the symmetric and asymmetric combinations

$$2\widetilde{\phi}_{\pm}(\tau) = \widetilde{\phi}_{\mathrm{L}}(\tau) \pm \widetilde{\phi}_{\mathrm{R}}(\tau). \tag{9.1.4}$$

Using these definitions, I wish to express the action in terms of the symmetric and asymmetric fluctuations. I will then integrate out all of the (Gaussian) fluctuations along the channel to obtain an effective action only in terms of the symmetric and asymmetric fluctuating fields parallel to [73].

I begin by expressing the impurity action in terms of these fields:

$$\begin{aligned} S_{\rm Tun} &= 2J\int \mathrm{d}\tau\,[\cos\phi_{\rm L}(\tau)+\cos\phi_{\rm R}(\tau)] \\ &= 4J\int \mathrm{d}\tau\,\cos(\phi_+ + \widetilde{\phi}_+(\tau))\cos(\phi_- + \widetilde{\phi}_-(\tau)). \end{aligned} \tag{9.1.5}$$

Next, I consider the Luttinger action describing the quasi-condensate in the channel

$$S_{\rm LL} = \frac{Kc}{2\pi}\int \mathrm{d}x\mathrm{d}\tau\left[\frac{1}{c^2}(\partial_\tau\varphi)^2+(\partial_x\varphi)^2\right]. \tag{9.1.6}$$

I wish to Fourier transform the field $\widetilde{\varphi}(x,\tau)$ subject to the boundary conditions (9.1.3). These are inhomogeneous boundary conditions, so I write the field as the sum of a linear term which correctly describes the boundary conditions and a fluctuating term that must have homogeneous (Dirichlet) boundary conditions $\bar{\varphi}(\pm L/2,\tau)=0$:

$$\begin{aligned} \widetilde{\varphi}(x,\tau) &= -\widetilde{\phi}_{\rm L}(\tau)+\left(\frac{\widetilde{\phi}_{\rm L}(\tau)+\widetilde{\phi}_{\rm R}(\tau)}{L}\right)\left(x+\frac{L}{2}\right)+\bar{\varphi}(x,\tau) \\ &= -\widetilde{\phi}_-(\tau)+\frac{2x}{L}\widetilde{\phi}_+(\tau)+\bar{\varphi}(x,\tau). \end{aligned} \tag{9.1.7}$$

The field $\bar{\varphi}(x,\tau)$ may be written in terms of a Fourier sum, giving

$$\widetilde{\varphi}(x,\tau) = -\widetilde{\phi}_-(\tau)+\frac{2x}{L}\widetilde{\phi}_+(\tau)+\sum_{n=1}^{\infty}\left[\varphi_n^{\rm e}(\tau)\cos\frac{(2n-1)\pi x}{L}+\varphi_n^{\rm o}(\tau)\sin\frac{2\pi n x}{L}\right], \tag{9.1.8}$$

where $\varphi_n^{\rm e,o}(\tau)$ are the Fourier coefficients. One can then substitute the full solution, $\varphi(x,\tau)=\varphi_0(x)+\widetilde{\varphi}(x,\tau)$, into the action (9.1.6) and evaluate the spatial integrals as follows:

$$\partial_x\varphi(x,\tau) = -\frac{2}{L}(\Phi-\phi_+(\tau))+\sum_{n=1}^{\infty}\left(\frac{2\pi n}{L}\varphi_n^{\rm o}(\tau)\cos\frac{2\pi n x}{L} - \frac{(2n-1)\pi}{L}\varphi_n^{\rm e}(\tau)\sin\frac{(2n-1)\pi x}{L}\right),$$

$$\int_{-\frac{L}{2}}^{\frac{L}{2}}\mathrm{d}x\,[\partial_x\varphi(x,\tau)]^2 = \frac{4}{L}(\Phi-\phi_+-\widetilde{\phi}_+(\tau))^2+\sum_{n=1}^{\infty}\frac{2\pi^2n^2}{L}(\varphi_n^{\rm o}(\tau))^2+\sum_{n=1}^{\infty}\frac{\pi^2(2n-1)^2}{2L}(\varphi_n^{\rm e}(\tau))^2. \tag{9.1.9}$$

$$\partial_\tau\varphi(x,\tau) = -\partial_\tau\widetilde{\phi}_-(\tau)+\frac{2x}{L}\partial_\tau\widetilde{\phi}_+(\tau)+\sum_{n=1}^{\infty}\left(\partial_\tau\varphi_n^{o}(\tau)\sin\frac{2\pi n x}{L}+\partial_\tau\varphi_n^{e}(\tau)\cos\frac{(2n-1)\pi x}{L}\right),$$

$$\begin{aligned}\int_{-\frac{L}{2}}^{\frac{L}{2}}\mathrm{d}x\,[\partial_\tau\varphi(x,\tau)]^2 =& L(\partial_\tau\widetilde{\phi}_-(\tau))^2+\frac{L}{3}(\partial_\tau\widetilde{\phi}_+(\tau))^2+\sum_{n=1}^{\infty}\left[\frac{L}{2}\Big((\partial_\tau\varphi_n^{\rm o}(\tau))^2+(\partial_\tau\varphi_n^{\rm e}(\tau))^2\Big)\right.\\ &\left.-\frac{4L(-1)^n}{\pi}\Big(\frac{1}{2n}\partial_\tau\widetilde{\phi}_+(\tau)\partial_\tau\varphi_n^{\rm o}(\tau)-\frac{1}{2n-1}\partial_\tau\widetilde{\phi}_-(\tau)\partial_\tau\varphi_n^{\rm e}(\tau)\Big)\right].\end{aligned} \tag{9.1.10}$$

I now take the Fourier transform in $\tau$ of Eqs. (9.1.9)-(9.1.10) and combine this with Eq. (9.1.5) to get the full action. This may conveniently be written in four parts as $S = S_\varepsilon + S_{\rm b} + S_{\rm o} + S_{\rm e}$, where

$$S_\varepsilon = \int\mathrm{d}\tau\Big[2J_{\rm c}(\Phi-\phi_+)^2-4J_{\rm c}(\Phi-\phi_+)\widetilde{\phi}_+(\tau)+4J\cos(\phi_++\widetilde{\phi}_+(\tau))\cos(\phi_-+\widetilde{\phi}_-(\tau))\Big], \tag{9.1.11}$$

and

$$
\begin{aligned}
S_{\rm b} &= \frac{Kc}{2\pi}\int\frac{{\rm d}\omega}{2\pi}\left[\frac{4}{L}|\widetilde{\phi}_+(\omega)|^2+\frac{L\omega^2}{c^2}|\widetilde{\phi}_-(\omega)|^2+\frac{L\omega^2}{3c^2}|\widetilde{\phi}_+(\omega)|^2\right],\\
S_{\rm o} &= \frac{Kc}{2\pi}\int\frac{{\rm d}\omega}{2\pi}\sum_{n=1}^{\infty}\left[\frac{1}{2}\left(\frac{4\pi^2n^2}{L}+\frac{L\omega^2}{c^2}\right)|\varphi_n^{\rm o}(\omega)|^2-\frac{2L(-1)^n\omega^2}{n\pi c^2}\widetilde{\phi}_+(\omega)\varphi_n^{\rm o}(-\omega)\right],\\
S_{\rm e} &= \frac{Kc}{2\pi}\int\frac{{\rm d}\omega}{2\pi}\sum_{n=1}^{\infty}\left[\frac{1}{2}\left(\frac{(2n-1)^2\pi^2}{L}+\frac{L\omega^2}{c^2}\right)|\varphi_n^{\rm e}(\omega)|^2+\frac{4L(-1)^n\omega^2}{\pi(2n-1)c^2}\widetilde{\phi}_-(\omega)\varphi_n^{\rm e}(-\omega)\right].
\end{aligned}
\tag{9.1.12}
$$

The only non-Gaussian part of this action is $S_\varepsilon$ and since this does not depend on the fields in the channel, $\varphi^{\rm e}$ and $\varphi^{\rm o}$, they may be integrated out. It is clear that the action does not mix the even and odd parts of the fluctuational field and so they may be integrated out independently. I first integrate out the odd modes, $\varphi_n^{\rm o}$, where the full details of evaluating the sum in the third line is included in Appendix C for completion.

$$
\begin{aligned}
\int{\rm D}\varphi_n^{\rm o}\,e^{-S[\varphi_n^{\rm o}]} &= \int{\rm D}\varphi_n^{o}e^{-\frac{Kc}{2\pi}\int\frac{{\rm d}\omega}{2\pi}\sum_{n=1}^{\infty}\left(\frac{1}{2}\left(\frac{4\pi^2n^2}{L}+\frac{L\omega^2}{c^2}\right)|\varphi_n^{\rm o}(\omega)|^2-\frac{2L(-1)^n\omega^2}{n\pi c^2}\widetilde{\phi}_+(\omega)\varphi_n^{\rm o}(-\omega)\right)}\\
&= \exp\left[\frac{Kc}{2\pi}\int\frac{{\rm d}\omega}{2\pi}\sum_{n=1}^{\infty}\frac{2L^3\omega^4|\widetilde{\phi}_+(\omega)|^2}{n^2\pi^2c^2(4\pi^2n^2c^2+L^2\omega^2)}\right]\\
&= \exp\left[\frac{Kc}{2\pi}\int\frac{{\rm d}\omega}{2\pi}|\widetilde{\phi}_+(\omega)|^2\frac{L^3\omega^4}{2\pi^4c^4}\sum_{n=1}^{\infty}\frac{1}{n^2\left(n^2+\frac{\omega^2L^2}{4\pi^2c^2}\right)}\right]\\
&= \exp\left[\frac{Kc}{2\pi}\int\frac{{\rm d}\omega}{2\pi}|\widetilde{\phi}_+(\omega)|^2\frac{L^3\omega^4}{2\pi^4c^4}\left(\frac{16\pi^4c^4}{2\omega^4L^4}+\frac{\pi^24\pi^2c^2}{6\omega^2L^2}-\frac{\pi8\pi^3c^3}{2\omega^3L^3}\coth\left(\frac{\omega L}{2c}\right)\right)\right]\\
&= \exp\left[\frac{Kc}{2\pi}\int\frac{{\rm d}\omega}{2\pi}|\widetilde{\phi}_+(\omega)|^2\left(\frac{4}{L}+\frac{\omega^2L}{3c^2}-\frac{2\omega}{c}\coth\left(\frac{\omega L}{2c}\right)\right)\right],\\
S_{\rm o}^{eff} &= \frac{Kc}{2\pi}\int\frac{{\rm d}\omega}{2\pi}|\widetilde{\phi}_+(\omega)|^2\left(\frac{2\omega}{c}\coth\left(\frac{\omega L}{2c}\right)-\frac{4}{L}-\frac{\omega^2L}{3c^2}\right).
\end{aligned}
\tag{9.1.13}
$$

Similarly, integrating out the even modes, $\varphi_n^{\rm e}$, gives

$$\begin{aligned}
\int \mathrm{D}\varphi_n^{\rm o}\, e^{-S[\varphi_n^{\rm o}]} &= \int \mathrm{D}\varphi_n^{o} e^{-\frac{Kc}{2\pi}\int\frac{\mathrm{d}\omega}{2\pi}\sum_{n=1}^{\infty}\left(\frac{1}{2}\left(\frac{(2n-1)^2\pi^2}{L}+\frac{L\omega^2}{c^2}\right)\right)|\varphi_n^{\rm e}(\omega)|^2+\frac{4L(-1)^n\omega^2}{\pi(2n-1)c^2}\widetilde{\phi}_-(\omega)\varphi_n^{\rm e}(-\omega)} \\
&= \exp\left[\frac{Kc}{2\pi}\int\frac{\mathrm{d}\omega}{2\pi}\sum_{n=1}^{\infty}\frac{16L^2\omega^4|\widetilde{\phi}_-(\omega)|^2}{2(2n-1)^2\pi^2c^4\left(\frac{(2n-1)^2\pi^2}{L}+\frac{L\omega^2}{c^2}\right)}\right] \\
&= \exp\left[\frac{Kc}{2\pi}\int\frac{\mathrm{d}\omega}{2\pi}|\widetilde{\phi}_-(\omega)|^2\frac{8L^3\omega^4}{\pi^4c^4}\sum_{n=1}^{\infty}\frac{1}{(2n-1)^2\left((2n-1)^2+\frac{\omega^2L^2}{\pi^2c^2}\right)}\right] \\
&= \exp\left[\frac{Kc}{2\pi}\int\frac{\mathrm{d}\omega}{2\pi}|\widetilde{\phi}_-(\omega)|^2\frac{8L^3\omega^4}{\pi^4c^4}\frac{\pi^4c^3}{8L^3\omega^3}\left(\frac{L\omega}{c}-2\tanh\left(\frac{L\omega}{2c}\right)\right)\right], \\
S_{\rm e}^{eff} &= \frac{Kc}{2\pi}\int\frac{\mathrm{d}\omega}{2\pi}|\widetilde{\phi}_-(\omega)|^2\left(\frac{2\omega}{c}\tanh\left(\frac{\omega L}{2c}\right)-\frac{L\omega^2}{c^2}\right). \qquad (9.1.14)
\end{aligned}$$

Combining Eqs. (9.1.13)-(9.1.14) with Eq. (9.1.12) gives the full effective action $S^{eff} = S_{\rm fl} + S_\varepsilon$, where

$$S_{\rm fl} = \int\frac{\mathrm{d}\omega}{2\pi}\frac{K\omega}{\pi}\left[\coth\left(\frac{\omega L}{2c}\right)|\widetilde{\phi}_+(\omega)|^2+\tanh\left(\frac{\omega L}{2c}\right)|\widetilde{\phi}_-(\omega)|^2\right]. \qquad (9.1.15)$$

It should be noted that taking the limit $\omega \to 0$ of the full effective action gives the zero mode of Eq. (9.1.15) along with $S_\varepsilon$ (9.1.11). This returns the 'washboard' potential of the mean field solution, Eq. (8.0.3), for the full $\tau-$dependent fields, as expected.

The action (9.1.15) may be further simplified as all relevant energies are greater than the lowest possible phononic energy allowed by the system, $\omega \gg c/L$, so that

$$S_{\rm fl} = \int\frac{\mathrm{d}\omega}{2\pi}\frac{K}{\pi}|\omega|\left[|\widetilde{\phi}_+(\omega)|^2+|\widetilde{\phi}_-(\omega)|^2\right]. \qquad (9.1.16)$$

## 9.2 RG Analysis

The fluctuational action of Eqs. (9.1.11) and (9.1.16) can be studied by performing the standard renormalization group (RG) analysis as outlined for a single impurity in chapter 4. To this end, I split the fields into the fast and slow modes, $\phi_\pm(\tau) = \phi^>_\pm(\tau) + \phi^<_\pm(\tau)$, where the fast modes have Fourier components with energy $\Lambda/b < |\omega| < \Lambda$, while the slow modes have Fourier components with energy $|\omega| < \Lambda/b$. I wish to integrate out the fast modes, $\phi^>_\pm(\tau)$ in the standard way. As action (9.1.16) does not mix the symmetric and asymmetric fluctuations these calculations may be performed independently. What's more, because the coefficient in the action (9.1.16) is the same for both the symmetric and asymmetric terms, the results of the symmetric and asymmetric calculations are identical. Integrating out fast modes is equivalent to performing the average $\langle \ldots \rangle_> \equiv \int \mathcal{D}\phi^> (\ldots) e^{-S^>_{\rm fl}} / \int \mathcal{D}\phi^> e^{-S^>_{\rm fl}}$, where $S^>_{\rm fl}$ is the fast part of action (9.1.16).

Using the identity

$$\Big\langle \exp\Big[\pm i\widetilde{\phi}^>_\pm\Big]\Big\rangle_> \equiv \exp\Big[-\frac{1}{2}\Big\langle\Big(\widetilde{\phi}_\pm\Big)^2\Big\rangle_>\Big], \tag{9.2.1}$$

as demonstrated in chapter 3, the symmetric (asymmetric) non-Gaussian part of the action (9.1.11) is then renormalized according to

$$\Big\langle \cos\Big[\phi_\pm + \widetilde{\phi}^<_\pm(\tau) + \widetilde{\phi}^>_\pm(\tau)\Big]\Big\rangle_{>,\pm} = \exp\left[-\frac{1}{2}\Big\langle\Big(\widetilde{\phi}^>_\pm(\tau)\Big)^2\Big\rangle_{>,\pm}\right] \cos\Big[\phi_\pm + \widetilde{\phi}^<_\pm(\tau)\Big]. \tag{9.2.2}$$

To compute this average, I first perform a Fourier transform

$$\langle(\widetilde{\phi}^>_\pm(\tau))^2\rangle_{>,\pm} = \int\limits_> \frac{\mathrm{d}\omega_1}{2\pi}\frac{\mathrm{d}\omega_2}{2\pi}\, e^{i\tau(\omega_1+\omega_2)} \langle\widetilde{\phi}_\pm(\omega_1)\widetilde{\phi}_\pm(\omega_2)\rangle_{>,\pm}. \tag{9.2.3}$$

The average is then given by the standard functional integral identity Eq. (3.0.9). Applying this identity to the symmetric (asymmetric) fast part of the action Eq. (9.1.16) gives the average

$$\langle\widetilde{\phi}(\omega_1)\widetilde{\phi}(\omega_2)\rangle_{>,\pm} = \frac{\pi^2}{K|\omega_1|}\delta_{-\omega_1,\omega_2}, \tag{9.2.4}$$

so that

$$\langle(\widetilde{\phi}^{>}_{\pm}(\tau))^2\rangle_{>,\pm} = \frac{1}{4K}\int_{>}\frac{\mathrm{d}\omega}{|\omega|} = \frac{1}{2K}\int_{\Lambda/b}^{\Lambda}\frac{\mathrm{d}\omega}{|\omega|} = \frac{1}{2K}\log b. \tag{9.2.5}$$

The combined effect of integrating out the fast symmetric and asymmetric fluctuations is thus to rescale the cosines

$$\begin{aligned}
&\Big\langle\cos\Big[\phi_+ + \widetilde{\phi}^{<}_{+}(\tau) + \widetilde{\phi}^{>}_{+}(\tau)\Big]\cos\Big[\phi_- + \widetilde{\phi}^{<}_{-}(\tau) + \widetilde{\phi}^{>}_{-}(\tau)\Big]\Big\rangle_{>}\\
&= \exp\Big[-\frac{1}{2}\Big\langle(\widetilde{\phi}^{>}_{+}(\tau))^2\Big\rangle_{>,+} - \frac{1}{2}\Big\langle(\widetilde{\phi}^{>}_{-}(\tau))^2\Big\rangle_{>,-}\Big]\cos\Big[\phi_+ + \widetilde{\phi}^{<}_{+}(\tau)\Big]\cos\Big[\phi_- + \widetilde{\phi}^{<}_{-}(\tau)\Big]\\
&= \exp\Big[-\frac{1}{2K}\log b\Big]\cos\Big[\phi_+ + \widetilde{\phi}^{<}_{+}(\tau)\Big]\cos\Big[\phi_- + \widetilde{\phi}^{<}_{-}(\tau)\Big].
\end{aligned} \tag{9.2.6}$$

As a final step in the RG procedure, I rescale the resulting action similar to chapter 4. This scales the $\omega$ integrals so that they have the same form as before integrating out the fast modes so that the process can be iterated. The result is that in each iteration of the RG procedure the tunnelling term is renormalized by a factor of $b^{1-1/(2K)}$. Performing this procedure in infinitesimally small increments gives rise to the Gell-Mann Low equation describing how $\alpha$ changes as the energy is rescaled (the renormalization flow equation),

$$\frac{\mathrm{d}\log\alpha}{\mathrm{d}\log b} = 1 - \frac{1}{2K}. \tag{9.2.7}$$

The renormalized dimensionless tunnelling energy is given by integrating Eq. (9.2.7) between the upper and lower energy cut-offs. The UV cut-off is given by the

chemical potential $\Lambda \sim c/\xi$, while the infra-red cut-off is given by $\omega_{min} \sim \max\{T, c/L\}$. This means that the tunnelling energy at the scale of $\omega_{min}$ is given as $\alpha(\omega_{min}) = \alpha_0(\Lambda/\omega_{min})^{1-\frac{1}{2K}}$, where $\alpha_0 = J/J_c$ is the bare value of the dimensionless tunnelling energy.

It is clear from Eq. (9.2.7) that there is a critical value of the Luttinger parameter, $K = 1/2$: for $K < 1/2$, the tunnelling energy flows to smaller values while for $K > 1/2$ the tunnelling energy flows to larger values.

For $K < 1/2$ this means that $\alpha$ is an irrelevant parameter (in the RG sense), which corresponds to the situation in which the height of the 'washboard' potential is decreasing relative to the energy of the fluctuations. This means that in the low temperature limit the fluctuations will dominate and so would wash out all features of the mean field solution.

Likewise, for $K > 1/2$ (including the case $K \gg 1$ pertinent to the cold bosonic atoms under consideration) $\alpha$ is a relevant parameter (in the RG sense), which means that the height of the 'washboard' potential is increasing relative to the fluctuations. This means that in the low temperature limit the fluctuations are too small to destroy the features of the MF solution found above. Consequently, the characteristic features of the MF solution found in chapter 8, namely cusps in the energy and corresponding jumps in the superflow, remain an essential feature of the full solution.

In particular, for $K > 1/2$, the fluctuations are not large enough to overcome the potential barrier separating the symmetric and asymmetric branches of the MF solution. This means that fluctuations cannot connect the different branches of the MF solution such that the level crossings of Fig. (8.6) cannot be avoided.

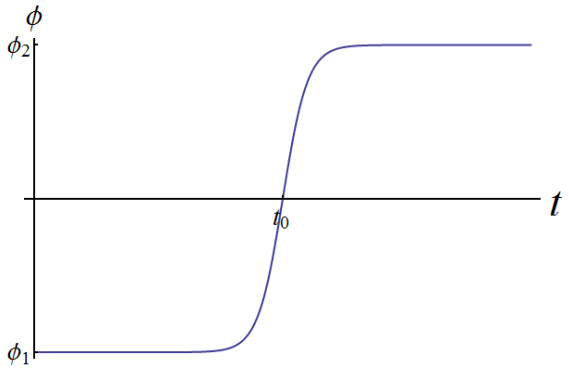


Figure 9.1: A graph sketching an instanton configuration between two minima, $\phi_1$ and $\phi_2$.

## 9.3 Instantonic Representation

In the previous section I used an RG analysis to demonstrate that for systems with $K > 1/2$, the washboard potential (which is a direct result of the geometry of the system) is a relevant perturbation and would not be washed out by fluctuations. In fact, because the height of the cosine is increasing relative to the fluctuational term there is no fluctuational mechanism which allows one to move between different minima of the potential, i.e. between different metastable branches of the MF solution.

An alternative way to see this result is to use an instantonic approach. This method allows to compute the probability amplitude of a particle tunnelling between two different minima of a potential. An instanton is a classical (saddle-point) solution of the Euclidean (imaginary time) action. The name 'instanton' stems from the idea that they are similar to solitons although in (imaginary) time rather than space. In fact, I can approximate an instanton as a theta function based on the idea that the time a particle spends tunnelling between minima is much shorter than the time it spends at the minima. This is illustrated in Fig. (9.1).

The fluctuational action Eq. (9.1.16) may be expanded in terms of a Coulomb gas using

$$\int \mathrm{d}\omega|\omega||\phi(\omega)|^2 = \int \mathrm{d}\tau_1\mathrm{d}\tau_2\, \dot{\phi}(\tau_1)U(\tau_1-\tau_2)\dot{\phi}(\tau_2), \tag{9.3.1}$$

where it is clear that

$$\begin{aligned} U(\tau) &= \int \mathrm{d}\omega \frac{1}{|\omega|} e^{i\omega\tau} \\ &= -\log\left|\frac{\tau}{\tau_\mathrm{c}}\right|^2, \end{aligned} \tag{9.3.2}$$

for an appropriate cut-off parameter $\tau_\mathrm{c}$. Substituting this, the action becomes

$$\begin{aligned} S = &-\frac{K}{\pi^2}\int \mathrm{d}\tau_1\mathrm{d}\tau_2\, \dot{\phi}_+(\tau_1)\log\left|\frac{(\tau_1-\tau_2)}{\tau_\mathrm{c}}\right|\dot{\phi}_+(\tau_2) - \frac{K}{\pi^2}\int \mathrm{d}\tau_1\mathrm{d}\tau_2\, \dot{\phi}_-(\tau_1)\log\left|\frac{(\tau_1-\tau_2)}{\tau_\mathrm{c}}\right|\dot{\phi}_-(\tau_2) \\ &+ \int \mathrm{d}\tau\Big[2J_\mathrm{c}(\Phi-\phi_+(\tau))^2 + 4J\cos\phi_+(\tau)\cos\phi_-(\tau)\Big]. \end{aligned} \tag{9.3.3}$$

The energy profile is illustrated in Fig. (9.2). At the lowest order, an instanton configuration connecting two metastable branches (minima of the energy profile) involves a shift in both $\phi_+$ and $\phi_-$ and is given by

$$\begin{aligned} \dot{\phi}_+ &= \pi[\delta(\tau) - \delta(\tau-\bar{\tau})], \\ \dot{\phi}_- &= \pi[\delta(\tau) - \delta(\tau-\bar{\tau})]. \end{aligned} \tag{9.3.4}$$

Here, $\bar{\tau}$ is the time spent in the metastable state. Substituting these configurations into the action Eq. (9.3.3) and ignoring constant terms gives the instantonic action

$$S_\mathrm{inst} = 4K\log\left|\frac{\bar{\tau}}{\tau_\mathrm{c}}\right| - \varepsilon\bar{\tau}, \tag{9.3.5}$$

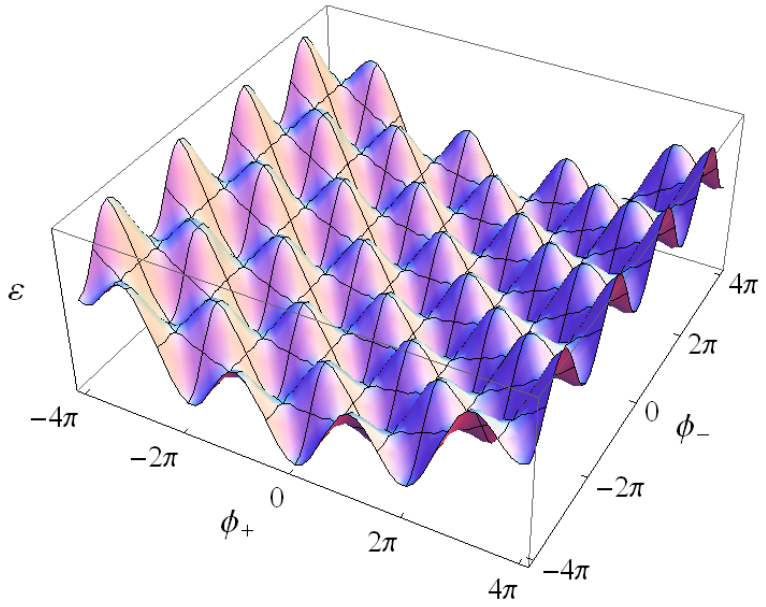


Figure 9.2: A graph showing the energy profile $\varepsilon[\phi_+, \phi_-]$. The instanton moves from one minimum of this profile to a neighbouring minimum.

where $\varepsilon = 2\pi J_c\left[\pi - 2(\Phi - \phi_+^0)\right]$ is the energy difference between the symmetric and asymmetric configurations with $\phi_+ = \phi_+^0$ and $\phi_+ = \phi_+^0 + \pi$, for a given $\Phi$. This 'single instanton' action is only valid in the limit $\varepsilon \ll 1$ i.e. close to the crossing point of the two solutions. Then, following [74, 75], the tunnelling rate between the two configurations is given as $\Gamma \sim \int \mathrm{d}t e^{-S[it]}$, where the Wick rotation has been applied to move to real times. This gives

$$\begin{aligned}\Gamma(\varepsilon) &\sim \int \mathrm{d}t e^{-4K\log(it)+\varepsilon(it)} \\ &= \int \mathrm{d}t (it)^{-4K} e^{i\varepsilon t} \\ &= \frac{2\pi}{\Gamma(4K)}\Theta(\varepsilon)\varepsilon^{4K-1},\end{aligned} \tag{9.3.6}$$

where the details of the integration are provided in Appendix C. Ignoring constant terms, the energy dependent tunnelling rate goes as $\Gamma(\varepsilon) \sim \varepsilon^{4K-1}$. As $\varepsilon < 1$,

the tunnelling is a relevant perturbation for $4K - 1 < 1$ and vanishes in the opposite limit. Rearranging this inequality, the tunnelling rate between different branches of the solutions is negligible in the limit $K > 1/2$, which corresponds exactly to the result from RG. As the tunnelling rate is suppressed, one can never have avoided crossings and the MF solution is stable against fluctuations.

In summary, the two complementary ways of viewing the problem demonstrate that for $K > 1/2$ the height of the tunnel barrier is increasing with respect to fluctuations at low energy scales and also the probability of tunnelling between metastable minima is vanishingly small. This instantonic picture therefore gives added weight to the idea that the MF solution developed in this thesis is robust against fluctuations and that a mechanism beyond the fluctuations is required to switch between different branches of this solution.

## 9.4 Discussion of Results

I have investigated the flow of particles along a one-dimensional channel linked via tunnel junctions to two reservoirs differing only by a constant phase and demonstrated that the bosonic superflow is dramatically different from the superconducting counterpart. I have shown how the perturbative solution pertinent to the superconducting problem [69,70,72,76] diverges for the bosonic flow implying the need for a non-perturbative mean field solution. This MF solution has striking features with no analogy in the superconducting current. In particular, the superflow is shown to always be (at least) bi-stable, with metastable configurations overlapping at the points $2\Phi = (2j + 1)\pi$ by an overlap proportional to the tunnelling energy $J$. This bi-stability ensures a $2\pi-$periodic solution

in the phase difference $2\Phi$ as the lowest energy solution alternates between two different branches: one in which the phase drop at the tunnelling barriers is distributed symmetrically on the left and right and one in which it is distributed asymmetrically between the two barriers. This is distinct from the superconducting case in which each branch of the solution retains $2\pi-$periodicity for small tunnelling $\alpha < 1$ [50]. As a consequence of this metastability, one would expect to see (sawtooth-like) jumps in the observed particle current as a function of $\Phi$ rather than the (smooth) sinusoidal function that follows from the perturbation theory.

It is of particular importance that these regions of metastability *do not* lead to 'avoided crossings' in which fluctuations smear out the cusps in the energy profile. Instead, I have demonstrated that fluctuations are irrelevant (in the RG sense) so that at low energy scales they are unable to drive transitions between metastable branches. In this way, the structure of the MF solution is robust against fluctuations. In section IV of this thesis I will investigate an alternative (non-fluctuational) method of transitioning between different branches of the MF solution, namely a quench.

It is interesting to note that both the RG and the perturbation theory give a cross over from perturbative to MF results at the point $K = 1/2$. At this special value of K (sometimes known as the Luther-Emery point), the system may be 're-fermionized' and expressed exactly in terms of a spinless fermionic model [59, 77]. It should also be noted that the system may be solved exactly at this point [78, 79] and interestingly shows a crossover from a sinusoidal current to a saw-tooth current as the tunnelling strength is increased.

Finally, a comment on the value $K = 1/2$. The critical $K$ for the supercon-

ducting case [69, 70, 72, 76] is $K = 1$ and not $K = 1/2$. The difference here lies with the fact that the superconducting system has an underlying SU(2) symmetry, while the spinless bosonic system under consideration does not. When there *is* the underlying SU(2) symmetry, this corresponds to $K_\sigma = 1$ in [69, 70, 72, 76] giving a current $I \propto \left(\frac{1}{k_f L}\right)^{\frac{1}{K_\rho}+\frac{1}{K_\sigma}-2} = \left(\frac{1}{k_f L}\right)^{\frac{1}{K_\rho}-1}$ with critical $K_\rho = 1$. However, when there is *no* underlying SU(2) symmetry, this corresponds to $K_\sigma$ being completely discarded as it is not well defined so that the current $I \propto \left(\frac{1}{k_f L}\right)^{\frac{1}{K_\rho}-2}$ with critical $K_\rho = 1/2$. This is equivalent to the transformation between the spinful and spinless cases $\frac{1}{K_\rho} + \frac{1}{K_\sigma} \to \frac{1}{K}$ as stated in [8, 9].

# Chapter 10

# EXPERIMENTAL IMPLEMENTATION

In this chapter I will discuss a possible experimental realization to observe the characteristic features of the bosonic flow described in this thesis. I will first outline how the model of chapter 6 may be realized by utilizing the power of potential shaping on an atom chip. I will then discuss the types of measurements which may be carried out in such an experiment, before performing a rough 'order of magnitude' type estimate for the magnitude of the observed current.

I am particularly indebted to Peter Krüger for helpful discussions as well as his work in designing a suitable atom chip to observe the features of the bosonic flow. All figures throughout this chapter have been generated from his code and have been used with his permission.

## 10.1 Experimental Setup

### 10.1.1 Introduction to Atom Chips

In order to experimentally observe the phenomena described in this thesis one may use ultracold bosonic atoms trapped above the surface of an atom chip.

Current carrying wires may be micro-fabricated into the chip, which combined with an external homogeneous bias field, trap the bosonic atoms above the surface [80], [81]. The Biot-Savart law states that

$$B = \frac{\mu_0}{4\pi} \int \frac{I \mathrm{d}\vec{\ell} \times \vec{r}}{|\vec{r}|^3}, \tag{10.1.1}$$

where $I$ is the current along the wire, $\mu_0 = 1.2566 \times 10^{-6} \mathrm{mkgs}^{-2}\mathrm{A}^{-2}$ is the permeability of free space and $\mathrm{d}\vec{\ell}$ is a unit vector pointing along the wire in the direction of the current. Consider an infinitely long wire along the x-axis whose magnetic field is compensated by a homogeneous bias field $B_0$ in the y-direction. Applying Eq. (10.1.1) with $\mathrm{d}\vec{\ell} = (\mathrm{d}x, 0, 0)$ gives

$$\begin{aligned} B_x &= 0, \\ B_y &= B_0 - \frac{\mu_0 I}{4\pi} \int_{-\infty}^{\infty} \mathrm{d}x \frac{z}{(x^2+y^2+z^2)^{3/2}} = B_0 - \frac{\mu_0 I}{2\pi} \frac{z}{y^2+z^2}, \\ B_z &= \frac{\mu_0 I}{4\pi} \int_{-\infty}^{\infty} \mathrm{d}x \frac{y}{(x^2+y^2+z^2)^{3/2}} = \frac{\mu_0 I}{2\pi} \frac{y}{y^2+z^2}. \end{aligned} \tag{10.1.2}$$

The minimum of the field ($B = 0$) is then at a height $z_0 = \frac{\mu_0 I}{2\pi B_0}$ above the wire and the field gradient at the minimum is given by $G = \frac{\mathrm{d}B}{\mathrm{d}z} = \frac{\mu_0 I}{2\pi z^2}$. Note that near the minimum of the trap it may be approximated as a quadrupole such that

$$B_x = 0, \qquad B_y = G(z - z_0), \qquad B_z = Gy. \tag{10.1.3}$$

It is clear that the trapping potential is orthogonal to the wire so that atoms have freedom of motion along the x-direction but are confined in the y,z- directions. A more realistic description of the wires on an atom chip may be obtained by con-

sidering the wire to have a finite width, $w$. Applying Eq. (10.1.1) to this situation gives

$$\begin{aligned} B_x &= 0, \\ B_y &= B_0 - \frac{\mu_0 I}{2\pi w}\left[\arctan\left(\frac{y+w/2}{z}\right) - \arctan\left(\frac{y-w/2}{z}\right)\right], \\ B_z &= \frac{\mu_0 I}{4\pi w}\log\left[\frac{(y+w/2)^2+z^2}{(y-w/2)^2+z^2}\right], \end{aligned} \tag{10.1.4}$$

which clearly reduce to Eqs. (10.1.2) in the limit $w \ll r$. Adding an homogeneous field along the x-direction shifts the minimum away from zero field and gives rise to an Ioffe-Pritchard trap (see Chapter 1). Such a geometry may be implemented on an atom chip by using a 'Z-shaped' wire (depicted schematically in Fig. (10.1) and for the real potential in Fig. (10.2)). Assuming semi-infinite wires, the contribution to the field from the end wires is

$$\begin{aligned} B_x &= \frac{\mu_0 I}{4\pi}\left[\frac{z}{(x+L/2)^2+z^2} + \frac{z}{(x-L/2)^2+z^2}\right] \approx \frac{2\mu_0 I}{\pi L^2} z, \\ B_y &= 0, \\ B_z &= \frac{\mu_0 I}{4\pi}\left[\frac{-x-L/2}{(x+L/2)^2+z^2} + \frac{-x+L/2}{(x-L/2)^2+z^2}\right] \approx -\frac{2\mu_0 I}{\pi L^2} x, \end{aligned} \tag{10.1.5}$$

where L is the length of the central part of the wire and the approximation is valid in the limit $L \gg r$. The total field for the Z-shaped trap is then given by the sum of Eqs. (10.1.2) and (10.1.5), often with the addition of an external homogeneous field parallel to x (sometimes known as an Ioffe field $B_I$),

$$B_Z = \left[(B_I + gz)^2 + G^2(z-z_0)^2 + (Gy - gx)^2\right]^{\frac{1}{2}}, \tag{10.1.6}$$

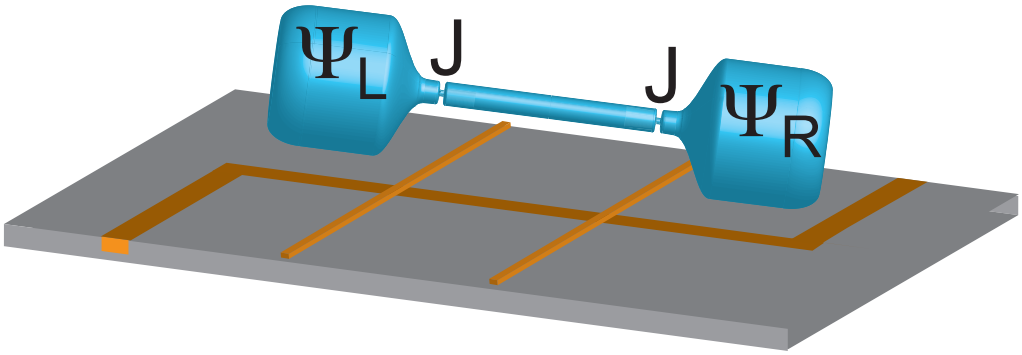


Figure 10.1: A schematic diagram showing the required geometry: 3D reservoirs linked by a 1D channel via Josephson junction couplings. Such a geometry may be implemented using an atom chip. Figure from Simpson, et al [30].

where $G = \frac{\mu_0 I}{2\pi z^2}$, $g = \frac{2\mu_0 I}{\pi L^2}$ and $z_0 = \frac{\mu_0 I}{2\pi B_0}$. The Z-shaped trap has a minimum with non-zero field located at $x = 0, y = 0, z = z_0 - \frac{G^2 z_0 + g B_I}{G^2 + g^2}$, slightly lower than for the simple wire in a homogeneous field considered above.

The advantage of this Z-shaped trap is that the confinement is harmonic and so theoretical treatment is much simpler, however it should be noted that this potential only provides a good harmonic approximation close to the field minimum while further away from the minimum the potential varies linearly. This means that at high temperatures atoms see a linear trapping potential but as they are cooled the confinement becomes harmonic. By varying both the current through the wire and the homogeneous external field, one can tune the axial and radial harmonic confinements independently so that a one-dimensional trap may be formed.

### 10.1.2 Experimental Realization of the Model

The model (described fully in chapter 6) is made up of three main parts which must be replicated in the experiment: the 3D reservoirs, the 1D channel and the

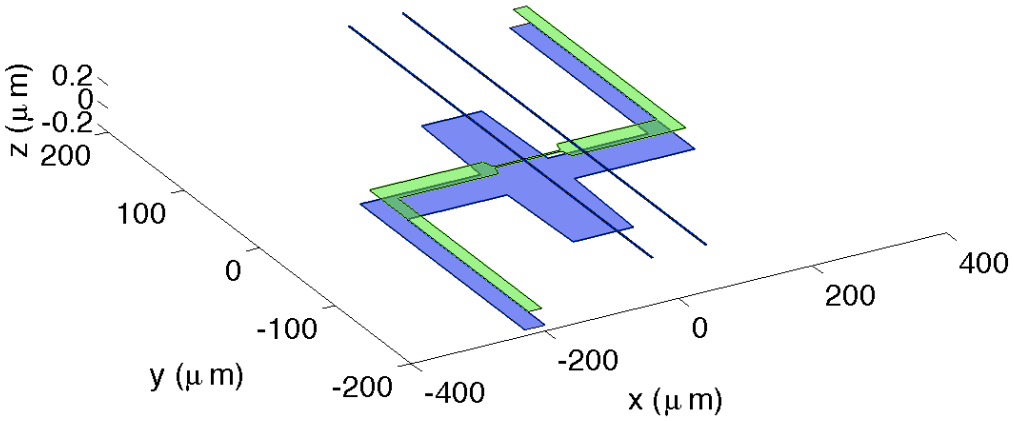


Figure 10.2: The wire layout for the atom chip. There are three vertically separated layers. The lower two layers contain Z-shaped wires with width varying along the length of the wire. The upper layer has two wires which form the Josephson barriers. Figure from Simpson, et al [30].

tunnelling barriers, as depicted in Fig. (10.1). It is also important that a phase difference between the reservoirs be established without introducing a chemical potential difference.

One possible scheme to produce this geometry on an atom chip has been designed in collaboration with Peter Krüger. Two parallel Z-shaped wires are embedded into different layers of an atom chip. The widths of the central section of the wires varies as a function of the length, x, with one of the wires becoming narrower in the central region while the other becomes wider, Fig. (10.2). This sets the harmonic confinement potentials in such a way that the trap is radially tighter along the central section, giving rise to 1d confinement in the central part of the wire only. The remainder of the wire forms the 3d reservoirs. The transition from the one-dimensional to the three-dimensional parts of the trap is illustrated for one barrier only in Fig. (10.3).

Initially, these wires carry co-propagating current, which has been chosen

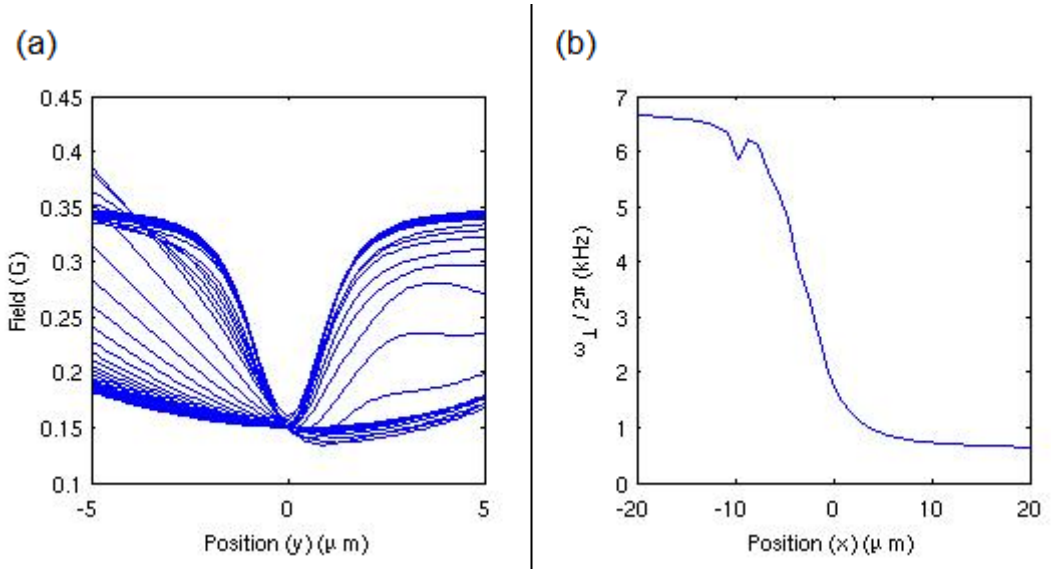


Figure 10.3: (a) The harmonic trapping potential in the y-direction taken at different values of x. It is clear that the trap goes from a broad shape in the reservoir, to a narrow shape in the channel. (b) The effective transverse oscillator frequency, $\omega_\perp$ at different points along the channel. This is small in the reservoirs ($x > 0$ in this graph) and large in the channel ($x < 0$ in this graph).

along with an external bias field $B_0$ parallel to the surface of the chip so that the trap height, $z_0$, is much larger than both the wire widths and the vertical distance between the wires ($z_0 \sim 100$microns). This means that the details arising from the widths of the wires are not resolved and the trap is essentially an elongated 3d reservoir. It is in this initial trap that the bosons may be cooled (see Chapter 1) to form a three-dimensional Bose-Einstein-Condensate.

Next, adiabatically decreasing the wire currents and increasing the homogeneous field $B_0$ will reduce the trap height, $z_0 \sim 1$micron , moving the condensate closer to the surface of the trap. As the condensate nears the chip surface, details concerning the widths of the wires are resolved so that the cloud will adiabatically split into two equal reservoirs and a one-dimensional channel, as defined by the Z-shaped wires.

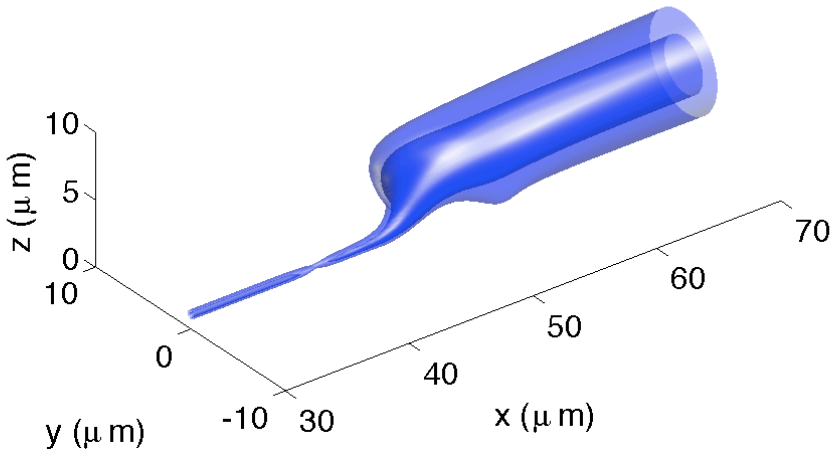


Figure 10.4: Graph showing typical equipotential surfaces of the trap near one end of the one-dimensional channel. It is possible to make out the large 3d reservoir, the narrow 1d channel and the Josephson barrier (in which the inner (lower) equipotential surface is cut, located at $x = 40\mu$m). Figure from Simpson, et al [30].

The Josephson barriers are introduced via a third layer of the atom chip. Two thin, parallel wires are positioned perpendicular to the central part of the Z-shaped wires and in line with the points at which the width of the Z-shaped wires change. This corresponds to producing additional potential at the ends of the one-dimensional channel. The barrier heights may be independently tuned by adjusting the current flowing through these wires.

This successfully gives rise to a potential trap with the correct geometry to observe the phenomena described in this thesis, as can be seen from the equipotential surface plot of Fig. (10.4). The next experimental challenge is to imprint a phase difference between the two reservoirs without introducing a chemical potential difference between them.

If the adjustable barriers are raised to prevent current from flowing then this

will maintain the chemical potential of the condensates. While the barriers are up, one may introduce a field gradient along $x$. This imbalance between the reservoirs will imprint a differential phase between the sub-clouds trapped in each reservoir whilst maintaining the chemical potential. One can then remove the field gradient to restore the balance between the reservoirs at the required phase difference. The adjustable barriers can then be lowered to observe the bosonic flow driven by the phase difference.

One problem arises from the uncertainty principle. If the barriers are raised so high that the particle numbers are completely fixed in the reservoirs and channel, then the phase cannot be known as suppressing the fluctuations in particle number enhances the fluctuations in phase. One can get round this problem in two ways. One possibility is to link the reservoirs 'round the back' through a channel much longer than the one-dimensional channel of interest. This means that the phase difference between the reservoirs remains a well defined variable, but the chemical potential is maintained by the fact that the phase is imprinted on a much quicker time-scale than it takes for the atoms to flow along this back channel. Imprinting the external phase difference in this way, before connecting the reservoirs, would allow to map out the the lowest (stable) energy state only but would be sufficient to observe changes in the direction of the flow for different external phase differences. Another possibility is to not raise the adjustable barriers so high that they completely prevent particles from flowing. Instead, the barriers are raised so that particles may slowly flow without significantly altering the chemical potential. The phase difference can then be imprinted *in vivo*, that is, as the current is flowing in the presence of the tunnelling barriers. Changing the phase difference in this way may allow exploration of the metastable branches of

the energy, which would show up in hysteretic behaviour of the flow.

## 10.2 Measurements

Having established how the model of Chapter 6 may be reproduced experimentally using an atom chip, in this section I will discuss possible measurements that could be made on the atoms in such a set-up to observe the features of the MF solution described in Chapters 8 and 9.

There are two main variables which may be experimentally probed. Firstly, the atomic density distribution gives information about the superflow, $I = dE/d\Phi$, as illustrated in Fig. (8.7). Secondly, the phase profile (see for example Fig. (8.5)) may be observed directly via an interference experiment.

The atomic density distribution along the channel may be probed using time-of-flight methods. All confining potentials are switched off and the atoms are allowed to fall freely. Because the atoms were tightly confined in the transverse dimensions, atoms travelling along the channel have relatively little transverse momentum and so the atomic density profile along the channel would remain almost unaffected during the time-of-flight as there would be a relatively small amount of spread of the atomic cloud in these transverse directions. Standard absorption imaging of these atoms would give the density profile up to a sensitivity of the order of 3 atoms/$\mu$m. Alternatively, a sheet of near-resonant light may be spread across the atom chip so as the atoms fall through it they are detected. Such fluorescence imaging has been shown to reach even single-atom sensitivity for low density systems.

Although such time-of-flight measurements are destructive, the advantage of

performing the experiment on an atom chip is that the experiment is very easily reproducible. This means that many repetitions can be carried out after waiting different lengths of time to build up an accurate, dynamic picture of the density distribution. Abrupt changes in direction of the observed superflow for different external phase differences would provide good experimental support for the MF solution.

The second type of measurement that can be made is using an interference experiment to observe the phase profile. In order to perform an interference experiment it is necessary to have an homogeneous reference phase with which the atoms in the one-dimensional channel may interfere. This may be achieved by taking the initial 3d cloud trapped far above the surface of the atom chip (see previous section) and splitting it in two. One way to do this would be by using radio-frequency dressed potential states to vertically split the trap into a double well [82]. The atomic cloud in one well can then be moved closer to the surface of the chip so that the channel-reservoir geometry is imposed on it, while the other cloud can be moved away from the surface of the chip, maintaining its 3D BEC nature. Once the two clouds are sufficiently separated, all coherence between the two condensates is lost so that the upper cloud provides an independent reference phase.

To observe the interference pattern, both clouds are released from their traps so that they expand and interfere with one another. This pattern may again be observed with either absorption or fluorescence imaging (similar to the observation of the density profile above). The phase profile, e.g. Fig. (8.5), would show up as an inhomogeneous phase pattern along the $x$-axis.

## 10.3 Estimate of Current

In this section I will make an approximation as to the order of magnitude of the current that could be obtained in such an experimental setup. Starting from the tunnelling Hamiltonian, the transmission coefficient across a single tunnel barrier can be written [see Appendix (D)] as

$$T = \frac{4\pi^2\Lambda^2}{N_{\rm res}LE_{\rm C}^2}, \tag{10.3.1}$$

where $E_{\rm C}$ is the condensate energy (the only relevant energy scale in the reservoir) and $\Lambda$ is the coefficient of the tunnelling Hamiltonian so that the tunnelling energy $J = \Lambda\sqrt{N_{\rm res}n}/\hbar$.

An alternate way to compute the transmission coefficient is to use (semi-classical) WKB theory. By integrating the energy between the classical turning points [see Appendix (D)], the transmission coefficient is given as

$$T = e^{-2\Delta x\sqrt{\frac{2m}{\hbar^2}\Delta U}}, \tag{10.3.2}$$

where $\Delta x$ is the length of the barrier and $\Delta U$ is the height of the barrier.

By equating these two expressions for the transmission coefficient (assuming that the barrier may adequately be described by the tunnelling Hamiltonian so that the overlap of wavefunctions is small, $J \ll \pi nc$), one can express the tunnelling energy in terms of the physical properties of the barrier,

$$J = \frac{N_{\rm res}\sqrt{N_{\rm ch}}E_{\rm C}}{2\pi\hbar}e^{-\Delta x\sqrt{\frac{2m}{\hbar^2}\Delta U}}. \tag{10.3.3}$$

In order to make an estimate for the order of magnitude of the current, there

are a number of physical values that I must utilize. I consider the experiment to be carried out on the atom chip as described in the previous section, with a condensate made up of $Rb^{87}$ atoms. The physical properties of $Rb^{87}$ necessary for making the estimate are outlined in the following table,

| Data for $Rb^{87}$ | | | |
|---|---|---|---|
| Mass | $m = 1.443 \times 10^{-25} kg$ | | |
| Scattering Length | $a_{\mathrm{s}} = 5.45nm$ [83] | | |
| Trappable States | F | $m_F$ | $g_F$ |
| | 1 | -1 | -1/2 |
| | 2 | 1 | 1/2 |
| | 2 | 2 | 1/2 |

where F = I + J is the angular momentum of the hyperfine state, $m_F$ is the magnetic quantum number and $g_F$ is the Landé g-factor. For $Rb^{87}$ atoms $J = 1/2$ from the single valence electron and $I = 3/2$. The physical properties of the atom trap are summarized in the following table,

| Physical Properties of the Atom Trap | |
|---|---|
| Transverse oscillator frequency in reservoir | $\omega_{\perp}^{\mathrm{res}} \sim 5,000\, rad\, s^{-1}$ |
| Transverse oscillator frequency in 1D channel | $\omega_{\perp}^{\mathrm{ch}} \sim 42,000\, rad\, s^{-1}$ |
| Number of atoms in reservoir | $N_{\mathrm{res}} = 10^4$ |
| Number of atoms in 1D channel | $N_{\mathrm{ch}} = 10^3$ |
| Length of 1D channel | $L = 100\mu m$ |

Here, $\omega_\perp^{\rm res}$ and $\omega_\perp^{\rm ch}$ have been read off of Fig. (10.3), while the atom numbers (which correspond to 10 particles per micron in the channel) are based on conservative estimates as to what is currently achievable for a condensate on an atom chip.

Using only the values stated in the above two tables, it is possible to compute a number of different physical properties of the system:

| | | |
|---|---|---|
| Critical Temperature | $k_B T_C = 0.94\hbar\omega_\perp^{\rm res} N^{1/3}$ | $T_C \approx 750nK$ |
| De Broglie Wavelength | $\Lambda = \frac{\sqrt{2\pi}\hbar}{\sqrt{m k_B T}}$ | $\Lambda \approx 600nm\,(at 100\text{nK})$ |
| Oscillator length in Reservoir | $a_\perp^{\rm res} = \sqrt{\hbar/m\omega_\perp^{\rm res}}$ | $a_\perp^{\rm res} \approx 380nm$ |
| Oscillator length in 1D Channel | $a_\perp^{\rm ch} = \sqrt{\hbar/m\omega_\perp^{\rm ch}}$ | $a_\perp^{\rm ch} \approx 130nm$ |
| Effective 3D density in Channel | $n_{3D}^{\rm ch} = \frac{N_{\rm ch}}{L(a_\perp^{\rm ch})^2}$ | $n_{3D}^{\rm ch} \approx 5.9 \times 10^{14}/\text{cm}^3$ |
| Effective 1D Coupling Constant in Channel | $g_{1D} = 2\hbar\omega_\perp^{\rm ch} a_s$ | $g_{1D} \approx 4.8 \times 10^{-38} Jm$ |
| Speed of Sound in 1D Channel | $c^2 = n_c h g_{1D}/m$ | $c \approx 2mm\,s^{-1}$ |
| Healing Length in 1D Channel | $\xi = \hbar/mc$ | $\xi \approx 400nm$ |
| Chemical Potential of 1D Channel | $\mu_{1D} = mc^2$ | $\mu_{1D} \approx 35nK$ |
| Thomas Fermi Chemical Potential of Reservoir | $E_C = \frac{15^{2/5}\hbar^2}{2m}\left(\frac{N_{\rm res} a_s}{(a_\perp^{\rm res})^6}\right)^{\frac{2}{5}}$ | $E_C \approx 400nK$ |
| Energy Level Spacing in Reservoir | $\Delta E_{\rm res} = \hbar\omega_\perp^{\rm res}$ | $\Delta E_{\rm res} \approx 40nK$ |
| Energy Level Spacing in 1D Channel | $\Delta E_{\rm ch} = \hbar\omega_\perp^{\rm ch}$ | $\Delta E_{\rm ch} \approx 320nK$ |
| Critical Current | $J_C = \frac{\hbar N_{\rm ch}}{mL^2}$ | $J_C \approx 100/\text{second}$ |

The energy of a tunnelling barrier of height $\Delta B$ in the magnetic field is given by the linear Zeeman energy $\Delta U = g_F m_F \mu_B \Delta B$. The superflow, $\mathcal{I} = \mp 2J \sin \phi_+$, is then proportional to

$$J = \frac{N_{res}\sqrt{N_{ch}}E_C}{2\pi\hbar} e^{-\Delta x\sqrt{\frac{2m}{\hbar^2}\Delta U}} \approx 3.3 \times 10^9 e^{-\Delta x\sqrt{\Delta B}\times 1.55\times 10^8}\mathrm{s}^{-1},$$

where $\Delta x$ is the barrier width in meters and $\Delta B$ is the barrier height in Gauss. A flow in which $\alpha = J/J_c = 1$ would correspond to a barrier satisfying $\Delta x\sqrt{\Delta B} \sim 1.115 \times 10^{-7}\mathrm{mG}^{1/2}$. In order for the tunnelling Hamiltonian to remain valid, the tunnelling energy must satisfy $J \ll \mu_{1D}/\hbar \approx 1000\mathrm{s}^{-1}$, which corresponds to a barrier satisfying $\Delta x\sqrt{\Delta B} \sim 0.967 \times 10^{-7}\mathrm{mG}^{1/2}$.

# Part IV

# DYNAMICS

Having demonstrated that there is no fluctuational mechanism that can bridge between the two branches of the MF solution, I now move on to investigate an alternative mechanism - the quantum quench. A quench is a sudden change in one of the parameters of the problem and as such it is a non-equilibrium situation.

To investigate the effects of the quench I will re-derive my action in real-time using the Keldysh formalism of chapter 5. This will allow me to derive the equations of motion for the system and study the dynamics following a quantum quench. I will focus only on a quench in the tunnelling strength $J$ at a fixed phase difference $2\Phi$. Such a quench may be experimentally accessed in the scheme outlined in chapter 10 by rapidly changing the strength of the lasers which form the tunnelling barriers.

The work in this section forms the basis of an article to be submitted for publication in which I am the first author in collaboration with I.V.Lerner and D.M.Gangardt [31].

# Chapter 11

# KELDYSH ACTION

The real time Luttinger action is defined as

$$S_{LL} = \frac{Kc}{2\pi}\int \mathrm{d}t \int\limits_{-L/2}^{L/2} \mathrm{d}x \left[\frac{1}{c^2}(\partial_t\varphi)^2 - (\partial_x\varphi)^2\right], \tag{11.0.1}$$

where $\varphi(x,t)$ is the phase field in the Luttinger channel.

I consider this action in a parallel way to the analysis given for the fluctuating action of chapter 9. There are independent phase jumps $\phi_{\mathrm{L,R}}$ at the boundaries and the phase in the left(right) reservoir is $\pm\Phi$ so that the boundary conditions on the field $\varphi$ are $\varphi(-L/2,t) = \Phi - \phi_{\mathrm{L}}$ and $\varphi(L/2,t) = -\Phi + \phi_{\mathrm{R}}$. Here, I assume that the phase difference, $2\Phi$ remains constant. I can use these boundary conditions to write the field as

$$\begin{aligned}\varphi(x,t) =& \Phi - \phi_{\mathrm{L}} - \frac{1}{L}\left(x + \frac{L}{2}\right)(2\Phi - \phi_{\mathrm{L}} - \phi_{\mathrm{R}}) \\ &+ \sum_{n\geq 1}\left[\varphi_{\mathrm{n,o}}\sin\left(\frac{2\pi n x}{L}\right) + \varphi_{\mathrm{n,e}}\cos\left(\frac{(2n-1)\pi x}{L}\right)\right].\end{aligned} \tag{11.0.2}$$

This means that

$$\begin{aligned}
\partial_x\varphi &= -\frac{2}{L}(\Phi-\phi_+)+\sum_{n\geq 1}\left[\frac{2\pi n}{L}\varphi_{\mathrm{n,o}}\cos\frac{2\pi nx}{L}-\frac{(2n-1)\pi}{L}\varphi_{\mathrm{n,e}}\sin\frac{(2n-1)\pi x}{L}\right],\\
\int_{-L/2}^{L/2}\mathrm{d}x\,(\partial_x\varphi)^2 &= \frac{4}{L}(\Phi-\phi_+)^2+\sum_{n\geq 1}\left[\frac{2\pi^2n^2}{L}\varphi_{\mathrm{n,o}}^2+\frac{(2n-1)^2\pi^2}{2L}\varphi_{\mathrm{n,e}}^2\right],\\
\partial_t\varphi &= -\dot{\phi}_-+\frac{2x}{L}\dot{\phi}_++\sum_{n\geq 1}\left[\dot{\varphi}_{\mathrm{n,o}}\sin\frac{2\pi nx}{L}+\dot{\varphi}_{\mathrm{n,e}}\cos\frac{(2n-1)\pi x}{L}\right],\\
\int_{-L/2}^{L/2}\mathrm{d}x\,(\partial_t\varphi)^2 &= L\dot{\phi}_-^2+\frac{L}{3}\dot{\phi}_+^2+\frac{L}{2}\sum_{n\geq 1}\left[\left(\dot{\varphi}_{\mathrm{n,o}}^2+\dot{\varphi}_{\mathrm{n,e}}^2\right)-\frac{4L(-1)^n}{\pi}\left(\frac{1}{2n}\dot{\varphi}_{\mathrm{n,o}}\dot{\phi}_+-\frac{1}{2n-1}\dot{\varphi}_{\mathrm{n,e}}\dot{\phi}_-\right)\right],
\end{aligned}\tag{11.0.3}$$

where $2\phi_\pm = \phi_{\mathrm{L}} \pm \phi_{\mathrm{R}}$. The Luttinger action may then be expressed along the Keldysh contour as

$$\begin{aligned}
S_{LL} =&\frac{Kc}{2\pi}\int_{C_K}\mathrm{d}t\left[-\frac{4}{L}(\Phi-\phi_+)^2+\frac{L}{c^2}\dot{\phi}_-^2+\frac{L}{3c^2}\dot{\phi}_+^2\right.\\
&+\sum_{n\geq 1}\left(\frac{L}{2c^2}\dot{\varphi}_{\mathrm{n,o}}^2-\frac{2\pi^2n^2}{L}\varphi_{\mathrm{n,o}}^2-\frac{2L(-1)^n}{\pi nc^2}\dot{\varphi}_{\mathrm{n,o}}\dot{\phi}_+\right)\\
&\left.+\sum_{n\geq 1}\left(\frac{L}{2c^2}\dot{\varphi}_{\mathrm{n,e}}^2-\frac{(2n-1)^2\pi^2}{2L}\varphi_{\mathrm{n,e}}^2+\frac{4L(-1)^n}{\pi(2n-1)c^2}\dot{\varphi}_{\mathrm{n,e}}\dot{\phi}_-\right)\right].
\end{aligned}\tag{11.0.4}$$

The fields on the upper(lower) part of the contour are given as e.g. $\phi^\pm = \phi^{\mathrm{cl}} \pm \phi^{\mathrm{q}}$, where 'cl' and 'q' indicate the classical and quantum part of the field respectively. Making these substitutions, the action is written as

$$\begin{aligned}
S_{LL} =&\frac{Kc}{2\pi}\int_{-\infty}^{\infty}\mathrm{d}t\left[-\frac{16}{L}(\phi_+^{\mathrm{cl}}\phi_+^{\mathrm{q}}-\Phi\phi_+^{\mathrm{q}})+\frac{4L}{c^2}\dot{\phi}_-^{\mathrm{cl}}\dot{\phi}_-^{\mathrm{q}}+\frac{4L}{3c^2}\dot{\phi}_+^{\mathrm{cl}}\dot{\phi}_+^{\mathrm{q}}\right.\\
&\left.+\sum_{n\geq 1}\left(\frac{2L}{c^2}\dot{\varphi}_{\mathrm{n,o}}^{\mathrm{cl}}\dot{\varphi}_{\mathrm{n,o}}^{\mathrm{q}}-\frac{8\pi^2n^2}{L}\varphi_{\mathrm{n,o}}^{\mathrm{cl}}\varphi_{\mathrm{n,o}}^{\mathrm{q}}-\frac{4L(-1)^n}{\pi nc^2}(\dot{\varphi}_{\mathrm{n,o}}^{\mathrm{cl}}\dot{\phi}_+^{q}+\dot{\varphi}_{\mathrm{n,o}}^{\mathrm{q}}\dot{\phi}_+^{\mathrm{cl}})\right)\right.
\end{aligned}$$

$$+\sum_{n\geq 1}\left(\frac{2L}{c^2}\dot{\varphi}^{\rm cl}_{\rm n,e}\dot{\varphi}^{\rm q}_{\rm n,e}-\frac{2\pi^2(2n-1)^2}{L}\varphi^{\rm cl}_{\rm n,e}\varphi^{\rm q}_{\rm n,e}+\frac{8L(-1)^n}{\pi(2n-1)c^2}(\dot{\varphi}^{\rm cl}_{\rm n,e}\dot{\phi}^{\rm q}_{-}+\dot{\varphi}^{\rm q}_{\rm n,e}\dot{\phi}^{\rm cl}_{-})\right)\Bigg]. \tag{11.0.5}$$

The $\varphi_{\rm n,o}$ and $\varphi_{\rm n,e}$ fields may then be integrated out by Fourier transforming to frequency-space and completing the square in the action: $\bar{\phi}_n T^{-1}\phi_n \pm \bar{\phi}_n A\eta \pm \bar{\eta}A\phi_n = (\bar{\phi}_n \pm \bar{\eta}AT)T^{-1}(\phi_n \pm TA\eta) - \bar{\eta}ATA\eta$, similar to the fluctuation calculation above.

The Luttinger action is then written as

$$\begin{aligned}S_{LL} = &\sum_{\eta=\pm}\int\frac{{\rm d}\omega}{2\pi}\Big(\phi^{\rm cl}_\eta(-\omega),\quad \phi^{\rm q}_\eta(-\omega)\Big)\begin{pmatrix}0 & [G^{-1}_\eta]^{A}(\omega)\\ [G^{-1}_\eta]^{\rm R}(\omega) & [G^{-1}_\eta]^{\rm K}(\omega)\end{pmatrix}\begin{pmatrix}\phi^{\rm cl}_\eta(\omega)\\ \phi^{\rm q}_\eta(\omega)\end{pmatrix}\\ &+\int{\rm d}t\,8J_{\rm C}\Phi\phi^{\rm q}_+(t),\end{aligned} \tag{11.0.6}$$

where

$$\begin{aligned}[G^{-1}_+]^{\rm R(A)}(\omega) &= \frac{Kc}{2\pi}\left[-\frac{8}{L}+\frac{2L}{3c^2}\omega_\pm^2+\frac{L^3\omega_\pm^4}{\pi^4c^4}\sum_{n\geq 1}\frac{1}{n^2\left(n^2-\frac{L^2\omega_\pm^2}{4\pi^2c^2}\right)}\right],\\ [G^{-1}_-]^{\rm R(A)}(\omega) &= \frac{Kc}{2\pi}\left[\frac{2L}{c^2}\omega_\pm^2+\frac{16L^3\omega_\pm^4}{\pi^4c^4}\sum_{n\geq 1}\frac{1}{(2n-1)^2\left((2n-1)^2-\frac{L^2\omega_\pm^2}{\pi^2c^2}\right)}\right].\end{aligned} \tag{11.0.7}$$

Here I let $\omega_\pm = \omega \pm i\delta$ and the limit $\delta\to 0$ is taken at the end of the calculation.

Consider first $[G^{-1}_+]^{\rm R(A)}(\omega)$; the sum can be written as

$$\sum_{n\geq 1}\frac{1}{n^2\left(n^2-\frac{L^2\omega_\pm^2}{4\pi^2c^2}\right)} = \frac{4\pi^2c^2}{L^2\omega_\pm^2}\sum_{n\geq 1}\left[\frac{1}{n^2-\frac{L^2\omega_\pm^2}{4\pi^2c^2}}-\frac{1}{n^2}\right]. \tag{11.0.8}$$

By definition, $\sum_{n\geq 1}\frac{1}{n^2}=\frac{\pi^2}{6}$,so that the Green's functions may be written as

$$\begin{aligned}[G_+^{-1}]^{\mathrm{R(A)}}(\omega) &= \frac{Kc}{2\pi}\left[-\frac{8}{L}+\frac{2L}{3c^2}\omega_\pm^2+\frac{L^3\omega_\pm^4}{\pi^4c^4}\frac{4\pi^2c^2}{L^2\omega_\pm^2}\left(\sum_{n\geq 1}\frac{1}{n^2-\frac{\omega_\pm^2L^2}{4\pi^2c^2}}-\frac{\pi^2}{6}\right)\right]\\ &= \frac{Kc}{2\pi}\left[-\frac{8}{L}+\frac{2L\omega_\pm^2}{3c^2}+\frac{4L\omega_\pm^2}{\pi^2c^2}\sum_{n\geq 1}\frac{1}{n^2-\frac{L^2\omega_\pm^2}{4\pi^2c^2}}-\frac{2L}{3c^2}\omega_\pm^2\right]\\ &= \frac{Kc}{2\pi}\left[-\frac{8}{L}+\frac{16}{L}\omega_\pm^2\sum_{n\geq 1}\frac{1}{\omega_n^2-\omega_\pm^2}\right], \end{aligned} \tag{11.0.9}$$

where $\omega_n=\frac{2\pi nc}{L}\equiv\pi\omega_0 n$ are the energy modes of the phonons in the channel. Note that evaluating this sum gives the Green's function to be

$$[G_+^{-1}]^{\mathrm{R(A)}}(\omega)=-\frac{2K}{\pi}\omega_\pm\cot\left(\frac{\omega_\pm}{\omega_0}\right), \tag{11.0.10}$$

which is clearly the analytic continuation of the $\coth$ function obtained in the fluctuating action of chapter 9. In what follows, it is easier to work with the sum of Eq. (11.0.9) rather than the $\cot$ of Eq. (11.0.10).

All essential information for the dynamics is given by the asymptotes of the Green's function, i.e. the short and long time limits ($\omega\gg\omega_0$ and $\omega\ll\omega_0$ respectively). The first term of Eq. (11.0.9) gives the zero mode (long time) contribution to the Green's function. On taking the limit $\omega\gg\omega_0$, the sum in the second term of Eq.(11.0.9) becomes an integral which can be evaluated using $\omega_n=x$, so $\mathrm{d}x=2\pi c/L$ to get

$$\begin{aligned}\frac{8Kc}{\pi L}\omega_\pm^2\sum_{n\geq 1}\frac{1}{\omega_n^2-\omega_\pm^2} &= \frac{8Kc}{\pi}\omega_\pm^2\int_0^\infty\frac{\mathrm{d}x}{2\pi c}\frac{1}{x^2-\omega_\pm^2}\\ &= \frac{K\omega_\pm}{\pi^2}(\pm 2\pi i). \end{aligned} \tag{11.0.11}$$

On taking $\delta \to 0$, the Green's functions are then written as

$$[G_+^{-1}]^{\mathrm{R(A)}}(\omega) = -\frac{4Kc}{\pi L} \pm i\frac{2K\omega}{\pi}. \tag{11.0.12}$$

The Keldysh component is given by the fluctuation-dissipation theorem

$$[G_+^{-1}]^{\mathrm{K}}(\omega) = \Big[[G^{-1}]^{\mathrm{R}} - [G^{-1}]^{A}\Big] \coth\frac{\omega}{2T} = i\frac{4K}{\pi}\omega \coth\frac{\omega}{2T}. \tag{11.0.13}$$

I then Fourier transform these expressions back into t-space (see Appendix C) so that

$$\begin{aligned}
[G_+^{-1}]^{\mathrm{R(A)}}(t-t') &= -\frac{4Kc}{\pi L}\delta(t-t') \mp \frac{2K}{\pi}\partial_t\delta(t-t'), \\
[G_+^{-1}]^{\mathrm{K}}(t-t') &= \frac{4iK}{\pi}\left[2T\delta(t-t') - \frac{\pi T^2}{\sinh^2\pi T(t-t')}\right].
\end{aligned} \tag{11.0.14}$$

These expressions bare a close resemblance to the Keldysh equations for dissipative tunnelling [64] as should be expected. Now I consider $[G_-^{-1}]^{\mathrm{R(A)}}(\omega)$ in a similar fashion; the sum can be written as

$$\sum_{n\geq 1}\frac{1}{(2n-1)^2\left((2n-1)^2 - \frac{L^2\omega_\pm^2}{\pi^2c^2}\right)} = \frac{\pi^2c^2}{L^2\omega_\pm^2}\sum_{n\geq 1}\left[\frac{1}{(2n-1)^2 - \frac{L^2\omega_\pm^2}{\pi^2c^2}} - \frac{1}{(2n-1)^2}\right]. \tag{11.0.15}$$

By definition, $\sum\limits_{n\geq 1}\frac{1}{(2n-1)^2} = \frac{\pi^2}{8}$ so that the Green's functions can then be written as

$$\begin{aligned}
[G_-^{-1}]^{\mathrm{R(A)}}(\omega) &= \frac{Kc}{2\pi}\left[\frac{2L}{c^2}\omega_\pm^2 + \frac{16L^3\omega_\pm^4}{\pi^4c^4}\frac{\pi^2c^2}{L^2\omega_\pm^2}\left(\sum_{n\geq 1}\frac{1}{(2n-1)^2 - \frac{L^2\omega_\pm^2}{\pi^2c^2}} - \frac{\pi^2}{8}\right)\right] \\
&= \frac{Kc}{2\pi}\left[\frac{2L}{c^2}\omega_\pm^2 + \frac{16L\omega_\pm^2}{\pi^2c^2}\sum_{n\geq 1}\frac{1}{(2n-1)^2 - \frac{L^2\omega_\pm^2}{\pi^2c^2}} - \frac{2L}{c^2}\omega_\pm^2\right]
\end{aligned}$$

$$= \frac{8Kc}{\pi L}\sum_{n\geq 1}\frac{\omega_{\pm}^2}{\omega_n^2-\omega_{\pm}^2}, \tag{11.0.16}$$

where $\omega_n = (2n-1)\pi c/L$. Again, this can be expressed as

$$[G_-^{-1}]^{\mathrm{R(A)}}(\omega) = \frac{2K}{\pi}\omega_{\pm}\tan\left(\frac{\omega_{\pm}}{\omega_0}\right), \tag{11.0.17}$$

which is the analytical continuation of the $\tanh$ term from the fluctuating action but it is simpler in what follows to retain the summation expression. In the limit that $\omega \gg \omega_0$, the sum is approximated as an integral: let $(2n-1)\pi c/L = x$ and the resulting integral is identical to the previous case so we have (after completing the corresponding calculations)

$$\begin{aligned}
[G_-^{-1}]^{\mathrm{R(A)}}(t-t') &= \mp\frac{2K}{\pi}\delta(t-t')\partial_t, \\
[G_-^{-1}]^{\mathrm{K}}(t-t') &= \frac{4iK}{\pi}\left[2T\delta(t-t') - \frac{\pi T^2}{\sinh^2\pi T(t-t')}\right].
\end{aligned} \tag{11.0.18}$$

The tunnelling action is given by

$$S_{\mathrm{Tun}} = \int_{C_K}\mathrm{d}t\,[2J\cos\phi_{\mathrm{L}} + 2J\cos\phi_{\mathrm{R}}]. \tag{11.0.19}$$

As above, on the upper(lower) contour the fields are given by e.g. $z^{\pm} = z^{\mathrm{cl}} \pm z^{\mathrm{q}}$, and the action becomes

$$\begin{aligned}
S_{Tun} &= 2J\int_{-\infty}^{\infty}\mathrm{d}t\left[\cos(\phi_{\mathrm{L}}^{\mathrm{cl}}+\phi_{\mathrm{L}}^{\mathrm{q}}) - \cos(\phi_{\mathrm{L}}^{\mathrm{cl}}-\phi_{\mathrm{L}}^{\mathrm{q}}) + \cos(\phi_{\mathrm{R}}^{\mathrm{cl}}+\phi_{\mathrm{R}}^{\mathrm{q}}) - \cos(\phi_{\mathrm{R}}^{\mathrm{cl}}-\phi_{\mathrm{R}}^{\mathrm{q}})\right] \\
&= -4J\int_{-\infty}^{\infty}\mathrm{d}t\left[\sin\phi_{\mathrm{L}}^{\mathrm{cl}}\sin\phi_{\mathrm{L}}^{\mathrm{q}} + \sin\phi_{\mathrm{R}}^{\mathrm{cl}}\sin\phi_{\mathrm{R}}^{\mathrm{q}}\right].
\end{aligned} \tag{11.0.20}$$

The total action for the channel connected to the reservoirs is then:

$$S = \int \mathrm{d}t \left[ 8J_{\mathrm{C}}\Phi\phi_{+}^{\mathrm{q}}(t) - 4J\sin\phi_{\mathrm{L}}^{\mathrm{cl}}(t)\sin\phi_{\mathrm{L}}^{\mathrm{q}}(t) - 4J\sin\phi_{\mathrm{R}}^{\mathrm{cl}}(t)\sin\phi_{\mathrm{R}}^{\mathrm{q}}(t) \right.$$
$$- \frac{4K}{\pi}\left(\dot{\phi}_{+}^{\mathrm{cl}}(t)\phi_{+}^{\mathrm{q}}(t) + \dot{\phi}_{-}^{\mathrm{cl}}(t)\phi_{-}^{\mathrm{q}}(t)\right) + \frac{8iKT}{\pi}\left([\phi_{+}^{\mathrm{q}}(t)]^2 + [\phi_{-}^{\mathrm{q}}(t)]^2\right)$$
$$\left. + iKT^2\int \mathrm{d}t' \frac{(\phi_{+}^{\mathrm{q}}(t) - \phi_{+}^{\mathrm{q}}(t'))^2}{\sinh^2\pi T(t-t')} + iKT^2\int \mathrm{d}t' \frac{(\phi_{-}^{\mathrm{q}}(t) - \phi_{-}^{\mathrm{q}}(t'))^2}{\sinh^2\pi T(t-t')} \right]. \tag{11.0.21}$$

# Chapter 12

# QUENCH DYNAMICS

## 12.1 Equations of Motion

The semi-classical equations of motion are obtained by expanding the action of Eq. (11.0.21) to first order in quantum components and minimizing according to $\delta S[\phi^{\mathrm{q}}]/\delta\phi^{\mathrm{q}} = 0$. Performing the functional derivative gives

$$\begin{aligned}\dot{\phi}_+ &= \omega_0(\Phi - \phi_+) - \frac{2\pi J}{K}\sin\phi_+\cos\phi_-,\\ \dot{\phi}_- &= -\frac{2\pi J}{K}\sin\phi_-\cos\phi_+,\end{aligned} \tag{12.1.1}$$

where $\omega_0 = 2c/L$ as above. Note that the *steady state* solutions (i.e. $\dot{\phi}_\pm \to 0$) are the MF equations of chapter 8 as expected.

These equations of motion are non-linear and cannot be solved exactly. Instead, I have used a computer to numerically solve these equations for initial conditions as outlined fully below. I have verified my numerics by repeating the calculations using a number of different ODE solving packages on both MatLab and Mathematica. The phase portrait is depicted in Fig. (12.1) for $\Phi = 0$ and $\omega_0 = \alpha = 1$.

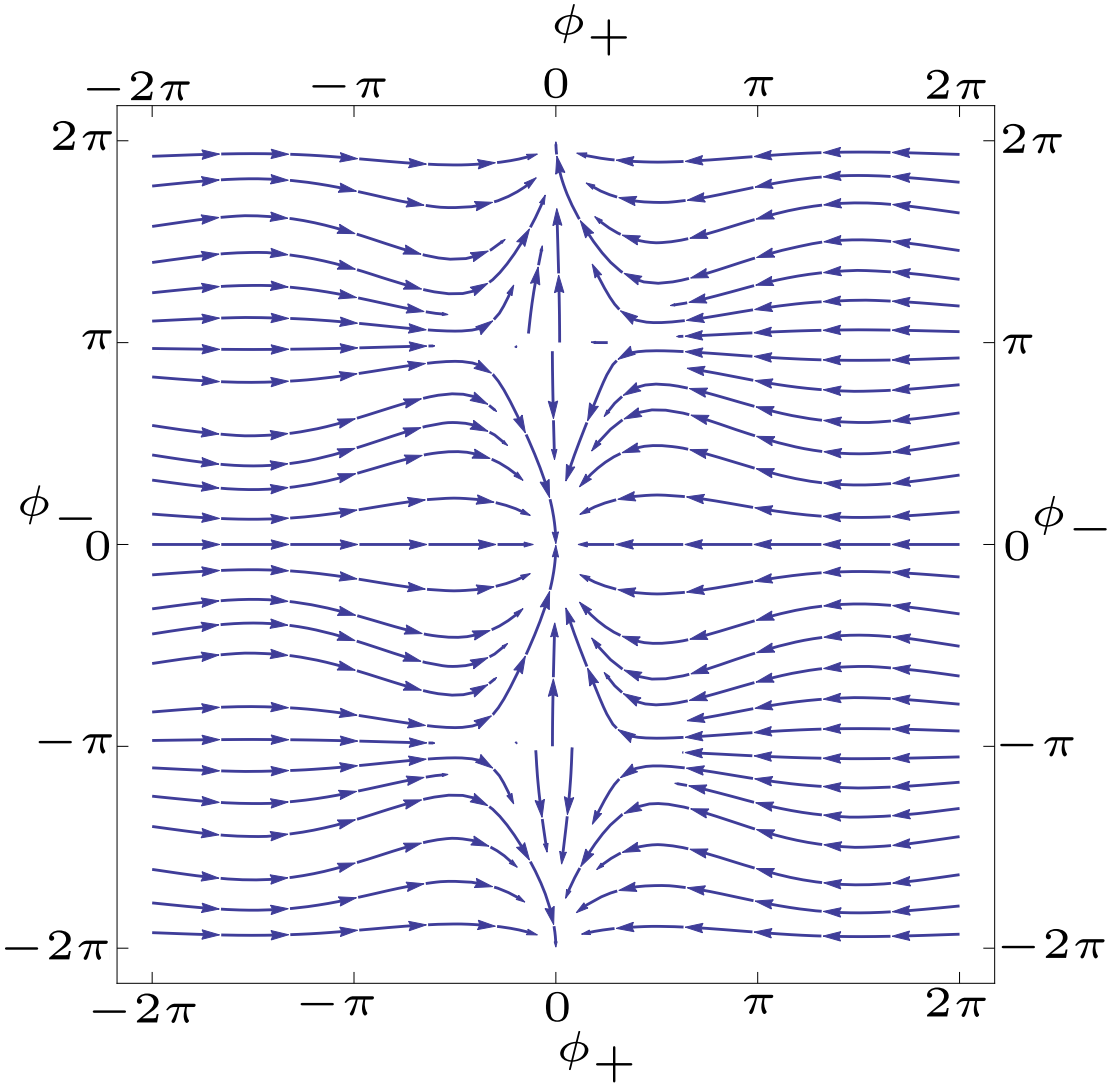


Figure 12.1: The phase portrait for $\phi_+$ and $\phi_-$ with $\Phi = 0$ and $\omega_0 = \alpha = 1$. Streamlines head towards the stable (symmetric) minima with $\phi_- = 0, \pm 2\pi$.

## 12.2 Quench in Tunnelling

As I have been treating the tunnel barriers at the ends of the channel as weak links, it is natural to first consider a situation in which the barriers are initially infinitely high so no current flows and are suddenly dropped to a finite value. Such a quench demonstrates how the MF solution of part III is established. Mathematically, this corresponds to introducing a time dependence on the tunnelling energy, $J(t) = J\Theta(t - t_0)$.

One problem which arises is that because the channel is completely cut, the density fluctuations are suppressed and so by the uncertainty principle, the phase fluctuations are enhanced. This means that the initial condition for the fields $\phi_\pm$ are unknown.

The standard tool for dealing with such a scenario is the Wigner function - see e.g. [84] for a clear review of quantum mechanics in phase space. Treating the initial condition as a random variable, this variable must be distributed according to the Wigner quasi-probability distribution function [85, 86]. This distribution is the quantum analogue to the classical phase-space probability density (Liouville density), where in the quantum case the uncertainty principle prohibits exact knowledge of the phase-space co-ordinates. By computing the current for a given initial condition and averaging over many such realisations one may obtain a physical picture of the current.

To compute the Wigner distribution function, consider the Luttinger Hamiltonian expressed in terms of the conjugate variables $\varphi(x,t)$ and $\Pi(x,t) = -\frac{1}{\pi}\partial_x\theta(x,t)$,

$$H = \frac{c}{2}\int_0^L \mathrm{d}x\Big[\frac{K}{\pi}(\partial_x\varphi)^2 + \frac{\pi}{K}(\Pi)^2\Big]$$

$$= \frac{c}{2}\sum_q \Big[q^2\frac{K}{\pi}|\varphi(q)|^2 + \frac{\pi}{K}|\Pi(q)|^2\Big]. \tag{12.2.1}$$

By completing the square, this may be expressed

$$\begin{aligned} H &= \sum_q \frac{Kcq^2}{2\pi}\Bigg[\bigg(\varphi(-q) - \frac{\pi i}{Kq}\Pi(-q)\bigg)\bigg(\varphi(q) + \frac{\pi i}{Kq}\Pi(q)\bigg) + \frac{\pi i}{Kq}\Pi(-q)\varphi(q) - \frac{\pi i}{Kq}\varphi(-q)\Pi(q)\Bigg], \\ &= \sum_q \omega(q)\Big(b^\dagger(q)b(q) + \frac{1}{2}\Big), \end{aligned} \tag{12.2.2}$$

where $\omega(q) = cq$ is the linear dispersion, $b(q) = \sqrt{\frac{Kq}{2\pi}}\big(\varphi(q) + \frac{\pi i}{Kq}\Pi(q)\big)$ and I have made use of the commutation relation $[\Pi(x), \varphi(x')] = i\delta(x - x')$, see Eq. (2.2.4).

This explicitly reveals the analogy to a quantum harmonic oscillator $H = \omega(\psi^\dagger\psi + 1/2)$ with $\psi = \sqrt{\frac{m\omega}{2}}(x + \frac{i}{m\omega}p)$. The ground state of the harmonic oscillator is $\psi_0(x) = (2\pi a_0^2)^{-1/4}e^{-(x/2a_0)^2}$, with the oscillator length $a_0 = (2m\omega)^{-1/2}$. The Wigner function is then given as

$$\begin{aligned} W(x,p) &= \int \mathrm{d}y \psi^\dagger(x + y/2)\psi(x - y/2)e^{ipy} \\ &= \frac{1}{a_0\sqrt{2\pi}}\int \mathrm{d}y e^{-\frac{(x+y/2)^2}{4a_0^2}} e^{-\frac{(x-y/2)^2}{4a_0^2}} e^{ipy} \\ &= 2e^{-\frac{x^2}{2a_0^2} - 2p^2a_0^2}. \end{aligned} \tag{12.2.3}$$

By analogy, the Wigner distribution function for the Luttinger channel is

$$W(\varphi(q), \theta(q)) \sim \prod_q e^{-\frac{Kq}{\pi}|\varphi(q)|^2 - \frac{\pi}{Kq}|\Pi(q)|^2}. \tag{12.2.4}$$

The initial state has $K \gg 1$ so the second term in the exponential may be ignored. The phase in the Luttinger channel is $\varphi(x) = \frac{1}{\sqrt{L}}\sum_q e^{-iqx}\varphi(q)$, where $q = 2\pi n/L$.

The phase at the end-points of the Luttinger channel is then given as

$$\varphi(\pm L/2) = \sum_n (-1)^n \varphi(n), \tag{12.2.5}$$

where $\varphi(n)$ is chosen randomly from the Wigner distribution - a normal distribution with mean 0 and variance $\sqrt{L/(4nK)}$ as per Eq. (12.2.4). The initial conditions for $\phi_\pm$ are then given by

$$\begin{aligned}\phi_+ &= \frac{1}{2}(\phi_\mathrm{L} + \phi_\mathrm{R}) = \frac{1}{2}(2\Phi + \varphi(L/2) - \varphi(-L/2)),\\ \phi_- &= \frac{1}{2}(\phi_\mathrm{L} - \phi_\mathrm{R}) = -\frac{1}{2}(\varphi(L/2) + \varphi(-L/2)),\end{aligned} \tag{12.2.6}$$

where $\varphi(\pm L/2)$ are given by Eq. (12.2.5).

I have numerically analysed the equations of motion to give plots of $\phi_\pm(t)$ averaged over many such realisations. The graphs Figs. (12.2)-(12.4) show the results of the simulations with $K = 1000$, $\alpha = 1$, $L = 1$and $\omega = 1$. It can be shown that changing the values of these parameters does not fundamentally alter the structure of the solution. The axis scaling is the same in all of the graphs for ease of comparison and in each case the average is taken over $10^4$ realisations.

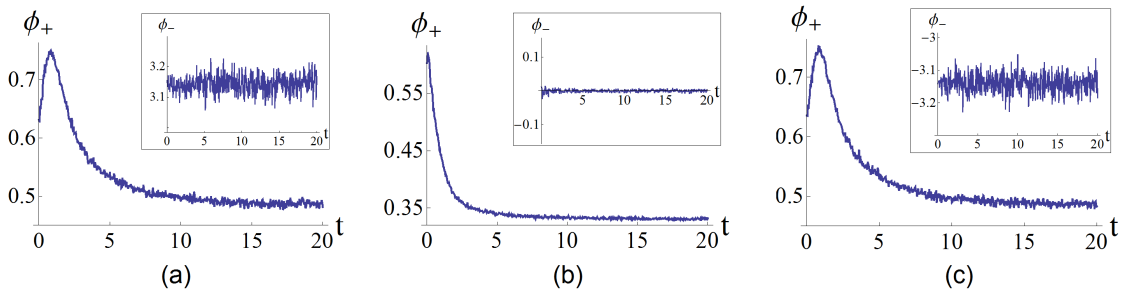


Figure 12.2: Phase dynamics for $\Phi = 0.2\pi$. (a) Initial conditions $\varphi(\pm L/2, 0) \in [-2\pi, 0]$ (b) Initial conditions $\varphi(\pm L/2, 0) \in [-\pi, \pi]$ (c) Initial conditions $\varphi(\pm L/2, 0) \in [0, 2\pi]$.

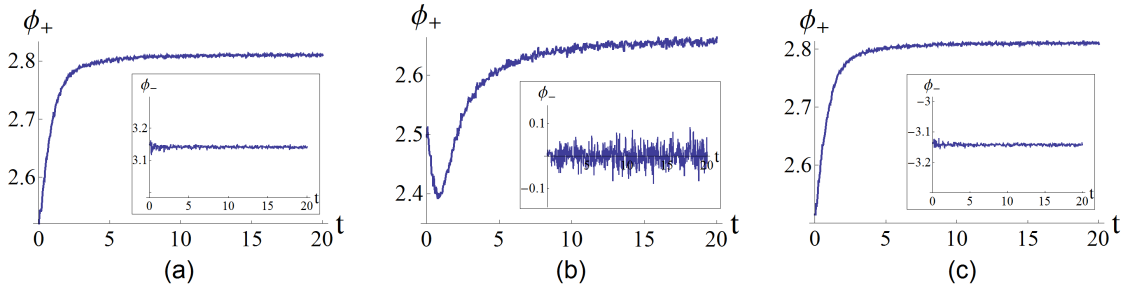


Figure 12.3: Phase dynamics for $\Phi = 0.8\pi$. (a) Initial conditions $\varphi(\pm L/2, 0) \in [-2\pi, 0]$ (b) Initial conditions $\varphi(\pm L/2, 0) \in [-\pi, \pi]$ (c) Initial conditions $\varphi(\pm L/2, 0) \in [0, 2\pi]$.

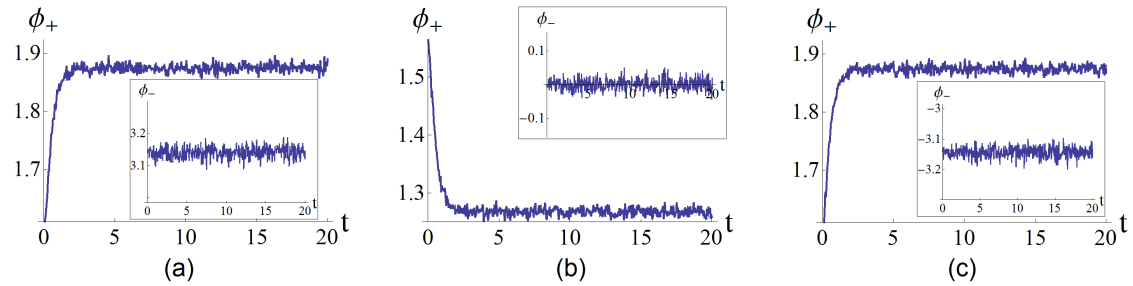


Figure 12.4: Phase dynamics for $\Phi = 0.5\pi$. (a) Initial conditions $\varphi(\pm L/2, 0) \in [-2\pi, 0]$ (b) Initial conditions $\varphi(\pm L/2, 0) \in [-\pi, \pi]$ (c) Initial conditions $\varphi(\pm L/2, 0) \in [0, 2\pi]$.

Fig. (12.2) shows the phase dynamics for $\Phi = 0.2\pi$, where the low energy stable solution is on the symmetric branch. When the initial condition for $\varphi(\pm L/2)$ is set between $-\pi$ and $\pi$, the only possible energy minimum on the symmetric branch is at $\phi_- = 0$. The majority of initial configurations will thus flow to this minima as is depicted in graph (b) where the fluctuations about the average are small. The noise in the average comes from realisations in which the initial conditions lie close enough to the asymmetric minima with $\phi_- = \pm\pi$. For the situations in which the initial conditions on $\varphi(\pm L/2)$ are chosen between $-2\pi$ and $0$

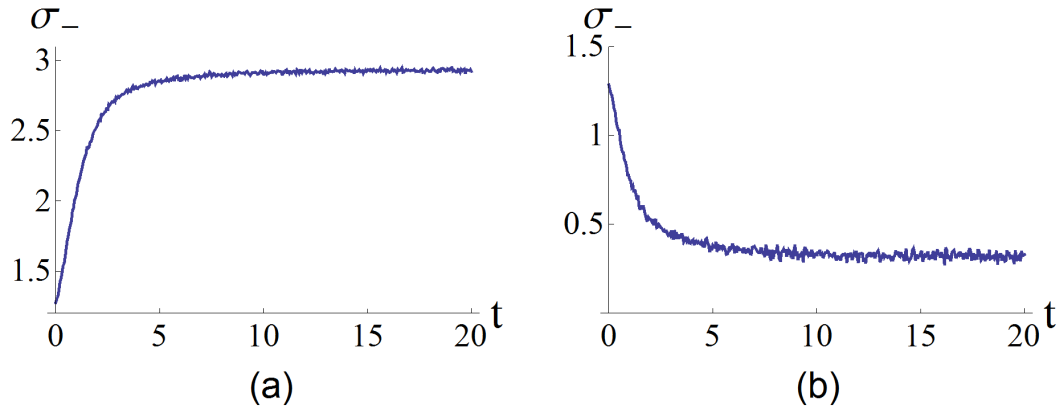


Figure 12.5: The standard deviation $\sigma_-$ in the data used to compute the average $\phi_-$ for $\Phi = 0.2\pi$ above. (a) Initial conditions $\phi_0(x) \in [-2\pi, 0]$ (b) Initial conditions $\phi_0(x) \in [-\pi, \pi]$.

or between $0$ and $2\pi$ - graphs (a) and (c) - the average value of $\phi_-$ appears to be $\pm\pi$ with large fluctuations. These large fluctuations are indicative of an average which beats between two different values. For example, in graph (a) around half of the time the initial condition $\phi(\pm L/2, 0)$ will be between $-2\pi$ and $-\pi$ so that the phase evolves to the minimum at $\phi_- = 2\pi$, while the rest of the time the initial condition $\phi(\pm L/2, 0)$ will be between $-\pi$ and $0$ so that the phase evolves to the minimum at $\phi_- = 0$.

This theory is backed up by computing the standard deviation across the $10^4$ realisations used to calculate each point. Fig. (12.5) illustrates the standard deviation in the data used to compute the the average of $\phi_-$ above. It shows that for (a), initial $\varphi(\pm L/2)$ chosen between $-2\pi$ and $0$, the standard deviation increases to a large value ($\approx \pi$), indicating that the data is widely spread as would be expected if the data predominantly splits between two separate energy minima. This is in contrast to (b), initial $\varphi(\pm L/2)$ chosen between $-\pi$ and $\pi$, where the standard deviation decreases to a smaller value ($\approx 0.5$), indicating that the data is more

compact as would be expected if the data predominantly lies in a single energy minima. It does not vanish at long times due to the existence of a small number of configurations which may evolve to the asymmetric minimum (as mentioned above).

This pattern of evolving to the closest energy minimum is also seen in Figs. (12.3) and (12.4) for $\Phi = 0.8\pi$ and $\Phi = 0.5\pi$ respectively . In Fig. (12.3) the majority of the realisations will fall into the lowest energy minimum, which now corresponds to the asymmetric branch of the MF solution and similar 'beating' of the average between two possible minima is observed. The picture in Fig. (12.4) is slightly more complex - at this point, the minima corresponding to the symmetric and asymmetric branches are degenerate. This means that initial $\phi_-$ close to $-\pi$ will flow to $-\pi$, initial $\phi_-$ close to $0$ will flow to $0$ and so on for integer $\pi$. The average phases are thus beating between three possible minima *in all cases* (a)-(c).

In summary, the picture emerging from these simulations is that wherever the initial conditions lie in the energy profile, the system will simply evolve to the phase configuration corresponding to the closest energy minimum. This is consistent with the phase portrait Fig. (12.1) and suggests the possibility of manipulating the minima of the energy profile in order to achieve switching between different branches of the MF solution.

It was established in chapter 8 that the MF solution with energy minimum at $\Phi = j\pi$ is stable in the region $[j\pi - (\pi/2 + \alpha), j\pi + (\pi/2 + \alpha)]$, dependent on the dimensionless tunnelling parameter $\alpha \equiv J/J_{\mathrm{C}}$. One can easily imagine a scenario in which a quench to a smaller value of $\alpha$ decreases the range of stability so that a MF solution which was previously stable becomes unstable and evolves into the new closest stable minimum, which may correspond to a different branch of the

MF solution.

As a concrete example, I shall consider a quench $\frac{\alpha(t)}{\alpha_0} = 0.55 - 0.45 \tanh \frac{t-t_0}{\delta}$, where at time $t = t_0$ the tunnelling is smoothly quenched to a tenth of its initial value (in the following simulations I will use $\alpha_0 = 1$) over a time-scale set by $\delta$. The limit $\delta \to 0$ represents the limit of a (sudden) quantum quench, although in realistic experimental situations the quench is never instantaneous. The equations of motion can then be written as

$$\begin{aligned}\dot{\phi}_+ &= \omega_0 \Big[\Phi - \phi_+ - \Big(0.55 - 0.45 \tanh \frac{t-t_0}{\delta}\Big) \sin\phi_+ \cos\phi_-\Big], \\ \dot{\phi}_- &= -\omega_0 \Big(0.55 - 0.45 \tanh \frac{t-t_0}{\delta}\Big) \sin\phi_- \cos\phi_+. \end{aligned} \tag{12.2.7}$$

These equations may then be solved numerically. I have used MatLab where it is possible to verify results by using a selection of different solvers. The graphs below all use the 'ode113' solver, with $\omega_0 = 1$. I have chosen $t_0 = 50$, which gives the system sufficient time to reach a steady state corresponding to the energy minimum closest to the initial conditions before the quench is initiated.

Fig. (12.6) shows the phase dynamics after the quench described above with $\delta = 1$ for three different values of $\Phi$. The initial conditions have been chosen as $\phi_+(0) = 1$, $\phi_-(0) = 0.1$. For $\Phi = \pi/2 + 0.05$ the phase initially evolves to the (metastable) symmetric minimum corresponding to $\phi_- = 0$, as depicted in graph (a). After the quench, this solution remains stable and so $\phi_-$ remains unchanged, while $\phi_+$ evolves to a new value satisfying the symmetric MF equation Eq. (8.0.4a) for $\alpha = 0.1$. Graph (c) depicts the phase dynamics for $\Phi = \pi/2 + 2$ - at this point the symmetric branch is unstable for both values of $\alpha$ so the phase evolves to the stable asymmetric minimum at $\phi_- = \pi$ with a similar change in $\phi_+$ after the

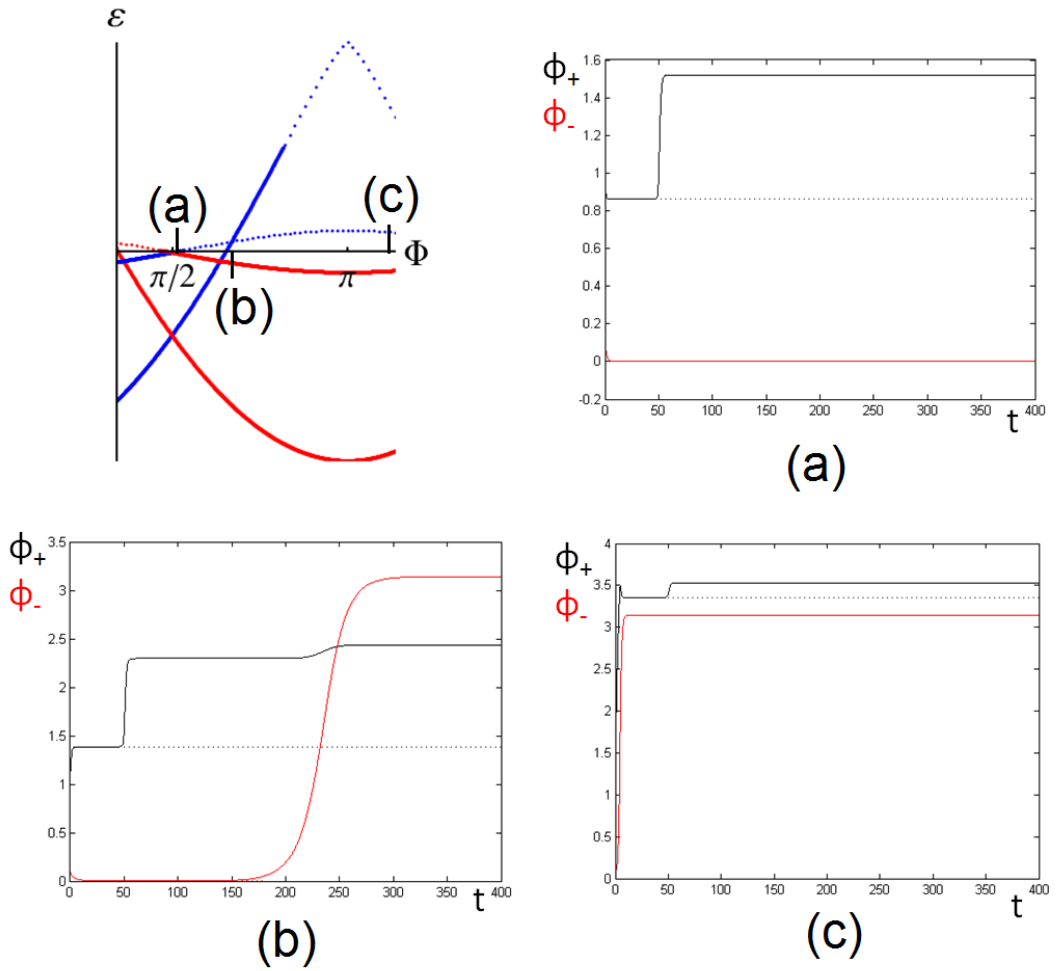


Figure 12.6: Quench in tunnelling strength. The energy profile for $\alpha = 1$ and $\alpha = 0.1$ is shown near $\Phi = \pi/2$ - the blue(red) solid lines represent stable (a)symmetric solutions, while dotted lines are unstable solutions. (a) Quench at $\Phi = \pi/2 + 0.05$ - symmetric solution is stable for both $\alpha = 1$ and $\alpha = 0.1$. (b) Quench at $\Phi = \pi/2 + 0.5$ - symmetric solution is stable for $\alpha = 1$ and unstable for $\alpha = 0.1$. (c) Quench at $\Phi = \pi/2+2$ - symmetric solution is unstable for both $\alpha = 1$ and $\alpha = 0.1$.

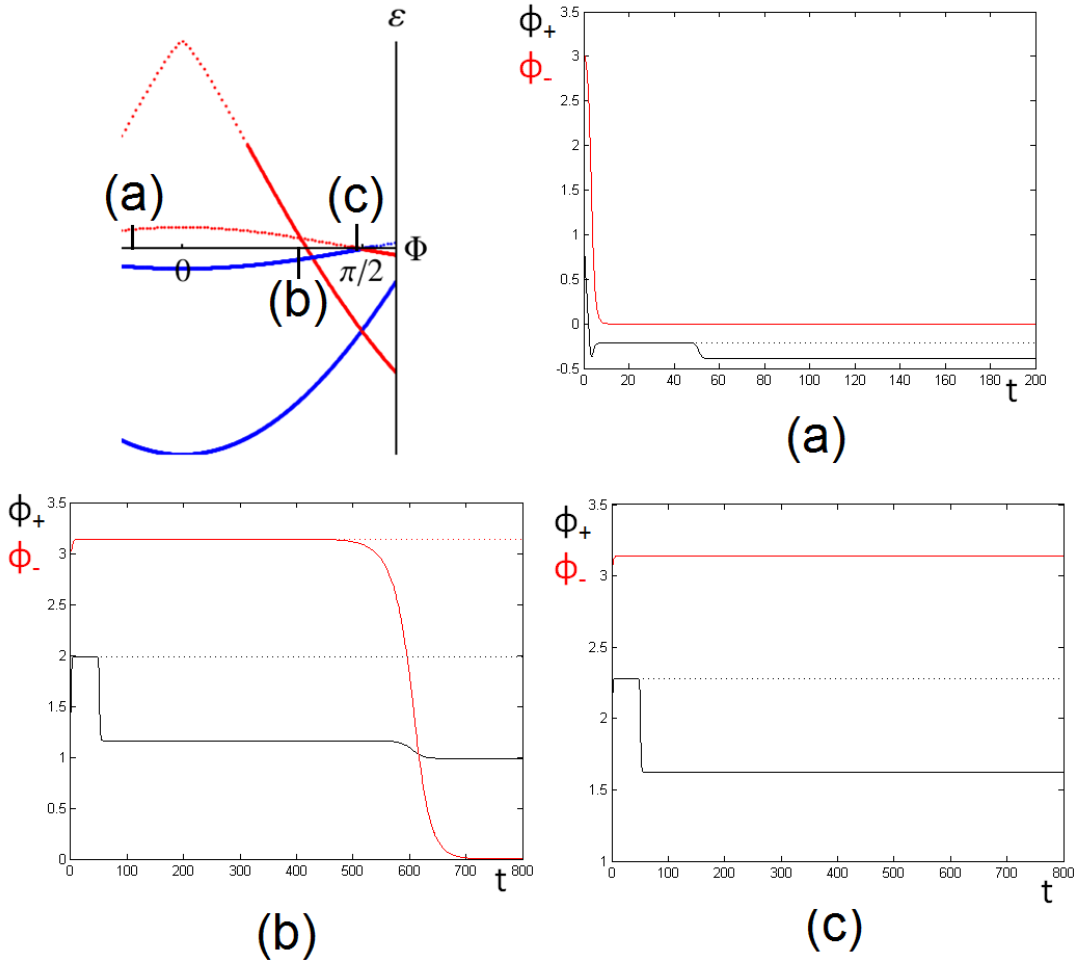


Figure 12.7: Quench in tunnelling strength. The energy profile for $\alpha = 1$ and $\alpha = 0.1$ is shown near $\Phi = \pi/2$ - the blue(red) solid lines represent stable (a)symmetric solutions, while dotted lines are unstable solutions. (a) Quench at $\Phi = \pi/2 - 2$ - asymmetric solution is unstable for both $\alpha = 1$ and $\alpha = 0.1$. (b) Quench at $\Phi = \pi/2 - 0.5$ - asymmetric solution is stable for $\alpha = 1$ and unstable for $\alpha = 0.1$. (c) Quench at $\Phi = \pi/2 - 0.05$ - asymmetric solution is stable for both $\alpha = 1$ and $\alpha = 0.1$.

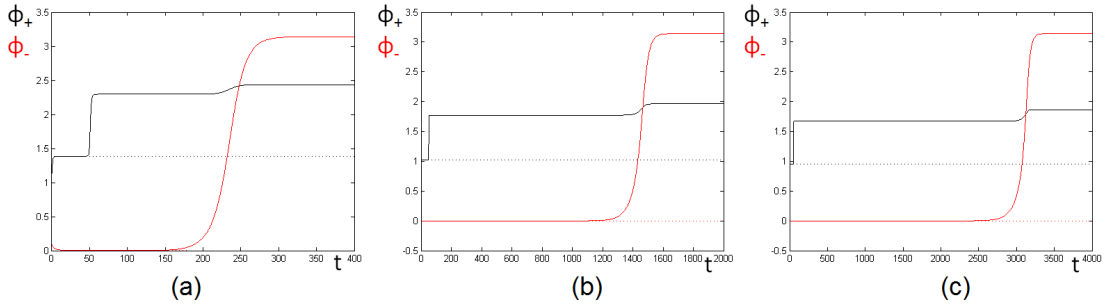


Figure 12.8: The quench for (a) : $\Phi = \pi/2 + 0.5$, (b) : $\Phi = \pi/2 + 0.3$ and (c) : $\Phi = \pi/2 + 0.2$. The closer the phase is to being stable after the quench, the longer the time-scale of switching between the branches.

quench to satisfy the new value of $\alpha$.

More significantly, graph (b) depicts the phase dynamics for $\Phi = \pi/2 + 0.5$. Here, the initial conditions above were chosen so that the phase initially evolves into the (metastable) symmetric minimum. After the quench there is an immediate change in $\phi_+$ as it adjusts to the new value of $\alpha$ as before, but on a much longer time-scale the solution switches from the symmetric ($\phi_- = 0$) to the asymmetric ($\phi_- = \pi$) branch. This is because the symmetric branch is no longer stable at the new value of $\alpha$. This phenomenon can also be observed for values of $\Phi$ smaller than $\pi/2$ if the initial conditions are chosen sufficiently close to the (metastable) asymmetric minimum. This is depicted in Fig. (12.7) for $\phi_+(0) = 1$ and $\phi_-(0) = \pi - 0.1$. In fact, as long as the initial conditions are such that one initially evolves on to a metastable branch, any change in tunnelling which leads to the metastable branch becoming unstable will give rise to switching between different branches of the solution.

One can (numerically) show that the time-scale of the switching between the different branches of the solution is dependent on the external phase difference $\Phi$. If this is chosen close to the end point of the region of stability, $\Phi \approx j\pi \pm (\pi/2 + \alpha)$

the switching happens on a much longer time-scale than if $\Phi$ is chosen away from the (post-quench) stable region. This is illustrated in Fig. (12.8) where the phase dynamics after the quench are shown for three different values of $\Phi$ progressively closer to the critical point $\Phi = \pi/2 + 0.1$.

In order to quantify this discussion, I linearise the equations of motion Eqs. (12.1.1) and solve for $\Phi$ close to the end point of stability after the quench, $\Phi = \pi/2 + \alpha + \epsilon$ where $\alpha_0 - \alpha = \Delta\alpha \gg \epsilon$. For simplicity I consider the sudden quench

$$\alpha(t) = \begin{cases} \alpha_0 & t < t_0, \\ \alpha & t > t_0. \end{cases} \tag{12.2.8}$$

Assuming initial conditions $\phi_+ \simeq \pi/2$, $\phi_- \simeq 0$, one can solve the first of Eqs. (12.1.1) using $\sin\phi_+ \cos\phi_- \simeq 1$ to obtain

$$\phi_+(t) = \phi_+^{(0)} e^{-\omega_0 t} + \left(\frac{\pi}{2} + \epsilon - \Delta\alpha\right)\left(1 - e^{-\omega_0 t}\right), \tag{12.2.9}$$

which converges to the long-time equilibrium value $\phi_+ \to \pi/2 + \epsilon - \Delta\alpha$. Substituting this result into the second of Eqs. (12.1.1) gives $\dot{\phi}_- = -\omega_0\alpha_0\Delta\alpha\phi_-$. Solving this equation gives an exponentially small value of $\phi_-$ at the quench time,

$$\phi_-(t_0) \sim e^{-\omega_0\alpha_0\Delta\alpha t_0}. \tag{12.2.10}$$

Similarly, after the quench, $\phi_+ \to \pi/2 + \epsilon$, so that $\dot{\phi}_- \simeq \omega_0\alpha\epsilon\phi_-$ and

$$\phi_-(t) = \phi_-(t_0) e^{\alpha\omega_0\epsilon(t-t_0)}. \tag{12.2.11}$$

Comparing Eq. (12.2.10) with Eq. (12.2.11), the typical time-scale for the dynamics

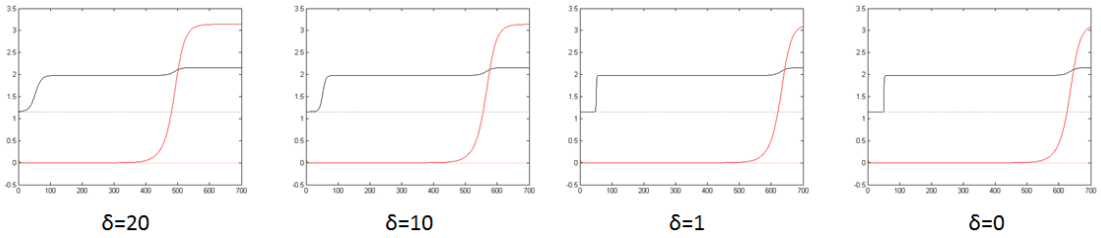


Figure 12.9: Quantum quench at $\Phi = \pi/2 + 0.5$ for different values of switching time $\delta$.

of $\phi_-$ is given by

$$t^* - t_0 \simeq \frac{\alpha_0 \Delta\alpha t_0}{\alpha\epsilon} \tag{12.2.12}$$

which shows an inverse dependence on the distance $\epsilon$ from the equilibrium solution after the quench.

One can also (numerically) show that the time-scale of switching is dependent on the quench time, $\delta$. The sudden quench ($\delta = 0$) results in a later switching than the smooth quench ($\delta \gg 0$) as illustrated in Fig. (12.9). It is interesting to note that $\delta$ alters the smoothness of the transition of $\phi_+$ from one value of $\alpha$ to the other, but that the shape of the switching in $\phi_-$ appears unaltered.

In conclusion, I have numerically investigated the phase dynamics after a shift in tunnelling energy. I have shown that such a mechanism can give rise to a shift between the symmetric and asymmetric branches of the MF solution. Finally, I have described the dependence of this switching on different parameters that one may investigate experimentally.

# Chapter 13

# CONCLUSIONS

This thesis is the result of my own work and is based on material published in Physical Review Letters [30] for which I am the first author. I began by providing a targeted overview of the different fields of physics and techniques that I have learnt about during my PhD study and have used in my original research, which forms the bulk of this work.

I have theoretically investigated the bosonic flow along a one-dimensional channel between two three-dimensional BEC reservoirs linked to the ends of the channel via weak tunnel junctions. The BEC reservoirs are considered identical except for a constant phase difference $2\Phi$ which drives the particle current along the channel. I have demonstrated that a perturbative approach, pertinent to parallel superconducting problems, completely fails in the bosonic case as the theory diverges at leading order. Instead, I have developed a non-perturbative mean field solution which has striking non-trivial behaviour.

The structure of the mean field solution is that the total phase difference between the reservoirs is comprised of two parts: a (linear) superflow along the channel and phase drops located at the tunnel junctions. I have demonstrated that there are two distinct branches to this solution - a symmetric branch in which

the phase jumps at the left/right tunnel junctions are identical and an asymmetric branch in which the phase jumps at the left/right tunnel junctions differ by $2\pi$. The symmetric branch is stable in the interval $\Phi \in [2j\pi-(\pi/2+\alpha), 2j\pi+(\pi/2+\alpha)]$ while the asymmetric branch is stable for $\Phi \in [(2j-1)\pi-(\pi/2+\alpha), (2j-1)\pi+(\pi/2+\alpha)]$ where $j$ is any integer and $\alpha = J/J_c = JmL/n$ is the dimensionless tunnelling parameter. Remarkably, these intervals *always* overlap in the region $\Phi \in [(2j-1)\pi/2-\alpha, (2j-1)\pi/2+\alpha]$. The $2\pi-$periodicity of the solution with respect to the external phase difference is maintained by discontinuous jumps between the different branches of the solution which may occur anywhere in the overlapping region. These discontinuities are reflected in the superflow, which behaves as a piece-wise sinusoid for $\alpha < \pi/2$ and a sawtooth function for $\alpha > \pi/2$.

I have demonstrated both from an RG and an instantonic perspective that this mean field solution is robust against phase fluctuations for values of the Luttinger parameter $K > 1/2$. In particular this means that for the bosonic flow, fluctuations are unable to bridge the gap between different branches of the mean field solution and do not lead to 'avoided crossings' in which the fluctuations smear out the cusps in the energy profile.

As an alternative scheme for switching between different branches of the mean field solution I have explored the phase dynamics following a quench in the dimensionless tunnelling energy. Having evaluated the semi-classical equations of motion for the phase, I have numerically shown that a quench from the 'infinite barrier' limit results in a phase profile corresponding to the closest minimum (MF solution) to the initial conditions. I have also shown that it is possible to initiate a jump between different branches of the solution by changing $\alpha$ such that a previously (meta)stable solution becomes unstable.

It would be interesting to test these predictions experimentally and I have outlined one possible realisation using the potential shaping abilities of an atom chip. Such an experiment would give access to measurements of the mean field phase profile and superflow along the channel. Further theoretical treatment of the problem is also required to inform future experiments. For instance, it would be interesting to study the effects of making the external phase difference a dynamic parameter, as experimentally an additional laser can be used to change the phase in one or both of the reservoirs in real time. I would expect adiabatic changes of the phase difference to follow a metastable branch of the solution until the end-point of stability at which point the solution would jump to a new stable configuration which may or may not be on the same branch of the mean field solution. It would also be interesting to investigate a quench in external phase difference as another possible mechanism of switching between different branches of the mean field solution.

# Part V

# APPENDICES

# Appendix A

# DUAL REPRESENTATION

For the case of a weak impurity, the mean field solution can be built using the duality between the $\theta$ and $\phi$ representations of the Luttinger channel. If there were no tunnel junctions, the whole of the phase difference between the reservoirs would be taken by the linear superflow along the channel, $\partial_x\varphi = -2\Phi/L$. Then, by the continuity equation

$$\dot{n} = -\partial_x \frac{n}{m}\partial_x\varphi = \frac{2\Phi}{mL}\partial_x n. \tag{A.0.1}$$

Integrating this across the channel length gives

$$\begin{aligned}\frac{\mathrm{d}}{\mathrm{d}t}\int_{-L/2}^{L/2} n(x)\,\mathrm{d}x &= \frac{2\Phi}{mL}\int_{-L/2}^{L/2}\partial_x n\,\mathrm{d}x \\ \dot{N}_{\mathrm{LL}} &= \frac{2\Phi}{mL}[n(L/2) - n(-L/2)].\end{aligned} \tag{A.0.2}$$

At the mean field level (ignoring fluctuations), there is no accumulation of particles along the channel so that $\dot{N}_{\mathrm{LL}} = 0$ meaning the density is the same at each edge of the channel, $n(L/2) = n(-L/2)$. Substituting this into the definition for density $n(x) = n_0 - \frac{1}{\pi}\partial_x\theta$ gives the condition $\partial_x\theta(L/2) = \partial_x\theta(-L/2)$. At $x = \pm L/2$,

the particle current is $I = \dot{N}_{\rm L} = -\frac{2\Phi n}{mL} = -\dot{N}_{\rm R}$ so that

$$\partial_x \theta(L/2) = \pi n_0 + \frac{mL}{2\Phi}\dot{N}_{\rm L} = \pi n_0 - \frac{mL}{2\Phi}\dot{N}_{\rm R} = \partial_x \theta(-L/2). \tag{A.0.3}$$

In the steady state, $\dot{n} = 0$ so that by the continuity equation $\partial_x n = 0$ implying that $\partial_x \theta$ is constant along the channel. Up to a constant, the mean field solution may then be written as

$$\theta_0(x) = \left[\pi n_0 + \frac{mL}{2\Phi}\dot{N}_{\rm L}\right] x = \alpha x, \tag{A.0.4}$$

where the constant pre factor has been written as $\alpha = \pi n_0 + \frac{mL}{2\Phi}\dot{N}_{\rm L}$ for simplicity.

Introducing tunnel barriers will cause a density depletion at the ends of the channel. To account for this as well as fluctuations about the mean field solution above, I write

$$\begin{aligned}\theta(x,\tau) &= \theta_{\rm L}(\tau) + \frac{1}{L}\left(x + \frac{L}{2}\right)(\theta_{\rm R}(\tau) - \theta_{\rm L}(\tau)) + \sum_{n=1}^{\infty}\left[\theta_n^{\rm o}(\tau)\sin\frac{2\pi n x}{L} + \theta_n^{\rm e}(\tau)\cos\frac{(2n-1)\pi x}{L}\right] \\ &= \theta_+(\tau) + \frac{2x}{L}\theta_-(\tau) + \sum_{n=1}^{\infty}\left[\theta_n^{\rm o}(\tau)\sin\frac{2\pi n x}{L} + \theta_n^{\rm e}(\tau)\cos\frac{(2n-1)\pi x}{L}\right]\end{aligned} \tag{A.0.5}$$

where $\theta_{\rm L}(\tau) = \theta_0(-L/2) + \delta\theta_{\rm L}(\tau)$, $\theta_{\rm R}(\tau) = \theta_0(L/2) + \delta\theta_{\rm R}(\tau)$ and $2\theta_\pm(\tau) = \theta_{\rm R}(\tau) \pm \theta_{\rm L}(\tau)$. The Luttinger action is then given by substituting this expression into

$$S_{\rm LL} = \frac{c}{2\pi K}\int_{-L/2}^{L/2}{\rm d}x\int{\rm d}\tau\left[(\partial_x\theta)^2 + \frac{1}{c^2}(\partial_\tau\theta)^2\right]. \tag{A.0.6}$$

The calculation is identical to that for the phase variables $\phi_\pm$ in chapter 9 and

results in the action

$$S = \frac{1}{4\pi^2 K}\int |\omega| \mathrm{d}\omega \left[|\delta\theta_{\mathrm{L}}(\omega)|^2 + |\delta\theta_{\mathrm{R}}|^2\right] + \frac{cL}{2\pi K}\int \mathrm{d}\tau \Big[\alpha^2 + \frac{2\alpha}{L}(\delta\theta_{\mathrm{R}}(\tau) - \delta\theta_{\mathrm{L}}(\tau))\Big]. \tag{A.0.7}$$

Then, following the prescription for a single impurity (see chapter 4) the impurity potential is described by the action

$$\begin{aligned} S_{\mathrm{imp}} &= V_0 \int \mathrm{d}\tau \left[\cos(2\theta_{\mathrm{L}}(\tau) + \pi N) + \cos(2\theta_{\mathrm{R}}(\tau) - \pi N)\right] \\ &= V_0 \int \mathrm{d}\tau \left[\cos\left(2\delta\theta_{\mathrm{L}}(\tau) - \frac{mL^2}{2\Phi}\dot{N}_{\mathrm{L}}\right) + \cos\left(2\delta\theta_{\mathrm{R}}(\tau) + \frac{mL^2}{2\Phi}\dot{N}_{\mathrm{L}}\right)\right]. \end{aligned} \tag{A.0.8}$$

Performing the RG analysis is parallel to chapter 9 so that the resulting RG equation is

$$\frac{\mathrm{d}\log V_0}{\mathrm{d}\log b} = 1 - 2K. \tag{A.0.9}$$

This shows that for $K > 1/2$, the tunnel junctions are an irrelevant perturbation and the end-point of the RG is the (linear) free flow described above. For $K < 1/2$ the tunnel junctions are a relevant perturbation so that at low energies the flow is cut. These results are in agreement with the fluctuational calculations for the dual variables $\phi_{\pm}$ in chapter 9 of the main text.

# Appendix B

# ASYMMETRIC TUNNELLING ENERGIES

I this appendix I consider the effect of asymmetric tunnelling energies and show that all features of the mean field solution remain in the asymmetric case, justifying a posteriori why I have chosen to consider only the simpler symmetric case in detail. Such a change in tunnelling energies corresponds to considering the tunnelling action

$$S_{\mathrm{T}} = 2\int_0^\beta \mathrm{d}\tau\Big[J_{\mathrm{R}}\cos\phi_{\mathrm{R}} + J_{\mathrm{L}}\cos\phi_{\mathrm{L}}\Big], \tag{B.0.1}$$

where $J_{\mathrm{L}} \neq J_{\mathrm{R}}$. Following exactly the same procedure as used to calculate the symmetric MF solution in chapter 8, one can obtain the asymmetric MF energy

$$\varepsilon = \quad 2(\Phi-\phi_+)^2 - 2\Big[\alpha_{\mathrm{R}}\cos\phi_{\mathrm{R}} + \alpha_{\mathrm{L}}\cos\phi_{\mathrm{L}}\Big]. \tag{B.0.2}$$

Then, the equations minimizing the asymmetric MF energy with respect to $\phi_+$ and $\phi_-$ (parallel to Eqs. (8.0.4)) are

$$\Phi - \phi_+ = \frac{2\alpha_{\mathrm{L}}\alpha_{\mathrm{R}}}{\alpha_{\mathrm{L}}+\alpha_{\mathrm{R}}}\sin\phi_+\cos\phi_-\,, \tag{B.0.3a}$$

$$\cos\phi_+\sin\phi_- = \frac{\alpha_{\mathrm{R}}-\alpha_{\mathrm{L}}}{\alpha_{\mathrm{R}}+\alpha_{\mathrm{L}}}\sin\phi_+\cos\phi_-\,. \tag{B.0.3b}$$

A direct comparison of Eqs. (B.0.3) with Eqs. (8.0.4) reveals that the symmetric $\alpha$ of Eq. (8.0.4a) is simply replaced in the asymmetric case by the harmonic average of $\alpha_{\rm L}$ and $\alpha_{\rm R}$ in Eq. (B.0.3a). It is also evident that Eq. (B.0.3b) has two solutions in the interval $\phi_- \in [0, 2\pi)$, which I shall call $\phi_{-,1}$ and $\phi_{-,2}$. These solutions are shifted away from the (symmetric) solutions, $\phi_- = 0, \pi$ of Eq. (8.0.4b) for $J_{\rm R} = J_{\rm L}$, although they have the property that $\phi_{-,2} - \phi_{-,1} = \pi$ so that $\cos\phi_{-,1} = -\cos\phi_{-,2}$. This means that the field $\phi_-$ acts as a label for solutions with $\pm\alpha_{\rm L(R)}$ in Eq. (B.0.3a), parallel to the symmetric case. Thus I have shown that all essential features of the symmetric MF solution of chapter 8 are retained for the case of asymmetric tunnelling energies, with only a simple change of parameters.

Note also that the fluctuational part of the action arising from the Luttinger channel, Eq. (9.1.16) can be written not in terms of symmetric and asymmetric fluctuations, but rather the fluctuations on the left (right) barrier

$$S_{\rm fl} = \int \frac{{\rm d}\omega}{4\pi} \frac{K}{\pi} |\omega| \Big[ |\widetilde{\phi}_{\rm L}(\omega)|^2 + |\widetilde{\phi}_{\rm R}(\omega)|^2 \Big]. \tag{B.0.4}$$

This separation means that the parts of the action corresponding to the left (right) barriers may be renormalized independently. As the co-efficient in action (B.0.4) is the same for the left and right parts, it is clear that $\alpha_{\rm L}$ and $\alpha_{\rm R}$ will be renormalized in an equivalent way so that the difference in tunnelling energies $\alpha_{\rm L} - \alpha_{\rm R}$ is a marginal parameter of the RG - neither increasing or decreasing as the scale is changed. Consequently, it is again apparent that introducing different tunnelling energies for the two barriers will not wipe out any of the main features of the symmetric solution, justifying the detailed study of only the symmetric situation.

# Appendix C

# A SMORGASBORD OF MATHEMATICS

In this appendix I provide some further mathematical derivations that have been used in some of the calculations in the main part of this thesis. For convenience, the calculations are provided in the order of the chapters in which the results are used.

- **Chapter 9.1**

  I have used the result that

$$\sum_{n=1}^{\infty} \frac{1}{n^2(a^2+n^2)} = \frac{1}{a^2}\sum_{n=1}^{\infty}\Big[\frac{1}{n^2} - \frac{1}{a^2+n^2}\Big] = \frac{1}{2a^4} + \frac{\pi^2}{6a^2} - \frac{\pi\coth[\pi a]}{2a^3}. \quad \text{(C.0.1)}$$

  The first part of the sum can be shown by writing Parseval's theorem for the function $f(x) = x$:

$$\sum_{n=-\infty}^{\infty} |a_n|^2 = \frac{1}{2\pi}\int_{-\pi}^{\pi} x^2 \mathrm{d}x, \quad \text{(C.0.2)}$$

  where

$$a_n = \frac{1}{2\pi}\int_{-\pi}^{\pi} \mathrm{d}x\, x e^{-inx} = \frac{-i}{2\pi}\int_{-\pi}^{\pi} \mathrm{d}x\, x \sin[nx] = \frac{i}{n}(-1)^n, \quad \text{(C.0.3)}$$

for $n \neq 0$ and $a_n = 0$ for $n = 0$. This gives $|a_n|^2 = \frac{1}{n^2}$ so that

$$\sum_{n=1}^{\infty} \frac{1}{n^2} = \frac{1}{4\pi} \int_{-\pi}^{\pi} x^2 \, \mathrm{d}x \; = \frac{\pi^2}{6}. \tag{C.0.4}$$

The second sum may be simplified to

$$\sum_{n=1}^{\infty} \frac{1}{a^2 + n^2} = \frac{1}{2} \left[ \sum_{n=-\infty}^{\infty} \frac{1}{a^2 + n^2} - \frac{1}{a^2} \right]. \tag{C.0.5}$$

The infinite sum is then computed (parallel to the Matsubara technique) with the help of the function $\coth[\pi z]$ which has poles at $z = ni$ with residue $1/\pi$. In this way, the integral

$$I = \int \frac{\mathrm{d}z}{2\pi i} \frac{\coth[\pi z]}{a^2 - z^2} \tag{C.0.6}$$

may be computed by closing the contour *either* around the poles up the imaginary axis *or* the poles at $z = \pm a$. The equivalence of these results gives

$$\frac{1}{\pi} \sum_{n=-\infty}^{\infty} \frac{1}{a^2 - (in)^2} = \frac{1}{2a} \coth[\pi a] - \frac{1}{2a} \coth[-\pi a] = \frac{1}{a} \coth[\pi a]. \tag{C.0.7}$$

Combining the results of Eqs. (C.0.4),(C.0.5) and (C.0.7) gives the desired identity Eq. (C.0.1).

Using these results along with the fact that $\sum\limits_{n=1}^{\infty} f(2n-1) = \sum\limits_{n=1}^{\infty} f(n) - \sum\limits_{n=1}^{\infty} f(2n)$ gives rise to the identity

$$\sum_{n=1}^{\infty} \frac{1}{(2n-1)^2((2n-1)^2 + a^2)} = \frac{\pi^2}{8a^2} - \frac{\pi \tanh[\pi a/2]}{4a^3}. \tag{C.0.8}$$

- **Chapter 9.3**

  Here I compute the integral

$$I = \int_{-\infty}^{\infty} \mathrm{d}t\, e^{-4K\ln[it]+i\varepsilon t} = \varepsilon^{4K-1} e^{-2\pi i K} \int_{-\infty}^{\infty} \mathrm{d}x\, e^{-4K\ln x + ix}, \tag{C.0.9}$$

  where $x = \varepsilon t$. Using complex analysis, for $\varepsilon > 0$ this integral may be closed in the upper-half plane and collapsed around the branch cut along the negative x-axis. The logarithm takes a different phase above and below the branch-cut.

$$\begin{aligned} I &= \Theta[\varepsilon]\varepsilon^{4K-1} e^{-2\pi i K}\left[\int_{-\infty}^{0} \mathrm{d}x e^{-4K\ln x + ix} + \int_{0}^{-\infty} \mathrm{d}x e^{-4K(\ln x + 2\pi i) + ix}\right] \\ &= \Theta[\varepsilon]\varepsilon^{4K-1} e^{-2\pi i K}\left[\int_{0}^{\infty} \mathrm{d}x\, (-x)^{-4K} e^{-x}\right](1 - e^{-8\pi i K}) \\ &= \Theta[\varepsilon]\varepsilon^{4K-1} e^{-2\pi i K} 2i \sin[4\pi K] \int_{0}^{\infty} x^{-4K} e^{-ix}. \end{aligned} \tag{C.0.10}$$

  Using the definition of the gamma function $\frac{\Gamma(1+b)}{a^{1+b}} = \int_0^\infty x^b e^{-ax}$, this can be written

$$I = \Theta[\varepsilon]\varepsilon^{4K-1} e^{-2\pi i K} 2i \sin[4\pi K] \frac{\Gamma(1-4K)}{i e^{-2\pi i K}} = \Theta[\varepsilon]\varepsilon^{4K-1} 2 \sin[4\pi K]\Gamma(1-4K). \tag{C.0.11}$$

  Finally, using the property of the gamma function $\Gamma(z)\Gamma(1-z) = \frac{\pi}{\sin[\pi z]}$ one obtains the result quoted in the main text,

$$I = \int_{-\infty}^{\infty} \mathrm{d}t\, e^{-4K\ln[it]+i\varepsilon t} = \frac{2\pi}{\Gamma(4K)} \Theta(\varepsilon)\varepsilon^{4K-1}. \tag{C.0.12}$$

- **Chapter 11**

  Here, I will compute the (temporal) Fourier transform of the Keldysh Green's function. Using the series definition of the $\coth$ function (above), one has

$$\omega \coth \frac{\omega}{2T} = 2T + 4T \sum_{n=1}^{\infty} \frac{\omega^2}{\omega_n^2 + \omega^2}, \tag{C.0.13}$$

  where $\omega_n = 2\pi n T$. The Fourier transform of the Green's function $[G^{-1}]^{\mathrm{K}}(\omega) \propto \omega \coth \frac{\omega}{2T}$ is then given by

$$\begin{aligned}[G^{-1}]^{\mathrm{K}}(t-t') &\propto \int \frac{\mathrm{d}\omega}{2\pi} e^{-i\omega(t-t')} \left[ 2T + 4T \sum_{n=1}^{\infty} \frac{\omega^2}{\omega_n^2 + \omega^2} \right] \\ &= 2T\delta(t-t') + 4T \sum_{n=1}^{\infty} \int \frac{\mathrm{d}\omega}{2\pi} e^{-i\omega(t-t')} \frac{\omega^2}{(\omega + i\omega_n)(\omega - i\omega_n)}.\end{aligned} \tag{C.0.14}$$

  Performing the integral

$$\int \frac{\mathrm{d}\omega}{2\pi} \frac{\omega e^{-i\omega(t-t')}}{\omega \pm i\omega_n} = -\omega_n \Theta(\pm(t-t')) e^{\mp\omega_n(t-t')}, \tag{C.0.15}$$

  means that the sum in the second term of the Green's function may be simplified (using $\omega_n = 2\pi n T$) to

$$-\pi T \sum_{n=1}^{\infty} n e^{-2\pi n T|t-t'|} = -\pi T \frac{e^{-2\pi T|t-t'|}}{\left(1 - e^{-2\pi T|t-t'|}\right)^2} = -\frac{\pi T}{4} \mathrm{cosech}^{\,2}[\pi T(t-t')]. \tag{C.0.16}$$

  Combining these results gives the Fourier transform

$$[G^{-1}]^{\mathrm{K}}(t-t') \propto 2T\delta(t-t') - \pi T^2 \mathrm{cosech}^{\,2}[\pi T(t-t')]. \tag{C.0.17}$$

# Appendix D

# CALCULATION OF TRANSMISSION COEFFICIENT

In this appendix I calculate the transmission coefficient for a tunnel junction. I first use a Green's function approach to calculate the transmission coefficient for the tunnelling Hamiltonian and then perform a parallel calculation using a (semi-classical) WKB approach.

## D.1 Tunnelling Hamiltonian

I begin with the standard Hamiltonian describing tunnelling between two reservoirs,

$$H = \sum_{p,\eta=\mathrm{L,R}} \frac{1}{L_\eta} \varepsilon_{\eta,p} \Psi^\dagger_{\eta,p} \Psi_{\eta,p} - \frac{\Lambda}{\sqrt{L_\mathrm{L} L_\mathrm{R}}} \sum_{p,q} \Big[ \Psi^\dagger_{\mathrm{L},p} \Psi_{\mathrm{R},q} + \Psi^\dagger_{\mathrm{R},q} \Psi_{\mathrm{L},p} \Big], \tag{D.1.1}$$

where the field operator $\Psi(x) = \frac{1}{\sqrt{L}} \sum\limits_p \Psi_p e^{ipx}$ and $\Lambda$ is a phenomenological tunnelling parameter. Here, the first term describes the energy of the left(right) reservoir while the second term describes the tunnelling between them. The current is

defined as $I = \langle \dot{N}_{\rm L} \rangle = -\langle \dot{N}_{\rm R} \rangle = \frac{i}{\hbar}\langle [H_T, N] \rangle$. Calculating these commutators for bosonic particles gives:

$$\frac{1}{L_{\rm L}\sqrt{L_{\rm L}L_{\rm R}}} \sum_{p,q,n} \Big[ \Psi^\dagger_{{\rm L},p}\Psi_{{\rm R},q}, \Psi^\dagger_{{\rm L},n}\Psi_{{\rm L},n} \Big] = -\frac{1}{\sqrt{L_{\rm L}L_{\rm R}}} \sum_{p,q} \Psi^\dagger_{{\rm L},p}\Psi_{{\rm R},q}, \tag{D.1.2}$$

$$\frac{1}{L_{\rm L}\sqrt{L_{\rm L}L_{\rm R}}} \sum_{p,q,n} \Big[ \Psi^\dagger_{{\rm R},q}\Psi_{{\rm L},p}, \Psi^\dagger_{{\rm L},n}\Psi_{{\rm L},n} \Big] = \frac{1}{\sqrt{L_{\rm L}L_{\rm R}}} \sum_{p,q} \Psi^\dagger_{{\rm R},q}\Psi_{{\rm L},p}. \tag{D.1.3}$$

This means the current is defined as

$$I = \frac{-i\Lambda}{\hbar}\frac{1}{\sqrt{L_{\rm L}L_{\rm R}}} \sum_{p,q} \Big( \langle \Psi^\dagger_{{\rm R},q}\Psi_{{\rm L},p} \rangle - \langle \Psi^\dagger_{{\rm L},p}\Psi_{{\rm R},q} \rangle \Big). \tag{D.1.4}$$

To compute these averages I use perturbation theory assuming $\Lambda$ is small.

$$\begin{aligned}
\langle \Psi^\dagger_{{\rm R},q}\Psi_{{\rm L},p} \rangle &= \int {\rm D}\Psi_{\rm R}{\rm D}\Psi_{\rm L}\, \Psi^\dagger_{{\rm R},q}(t)\Psi_{{\rm L},p}(t) e^{iS_0 + iS_T} \\
&= \langle \Psi^\dagger_{{\rm R},q}(t)\Psi_{{\rm L},p}(t) \rangle_0 + \frac{i\Lambda}{\sqrt{L_{\rm L}L_{\rm R}}} \sum_{n,m} \int {\rm d}t' \Bigg( \langle \Psi^\dagger_{{\rm R},q}(t)\Psi_{{\rm L},p}(t)\Psi^\dagger_{{\rm L},n}(t')\Psi_{{\rm R},m}(t') \rangle_0 \\
&\qquad + \langle \Psi^\dagger_{{\rm R},q}(t)\Psi_{{\rm L},p}(t)\Psi^\dagger_{{\rm R},m}(t')\Psi_{{\rm L},n}(t') \rangle_0 \Bigg) + \ldots
\end{aligned} \tag{D.1.5}$$

Terms mixing L and R do not appear in the action $S_0$ obtained from the first term of Eq. (D.1.1) so that the first term in the perturbative expansion is $0$. Also, the only terms appearing in $S_0$ are of the form $\Psi^\dagger_n \Psi_n$ so that the second term can be simplified using Wick's theorem:

$$\langle \Psi^\dagger_{{\rm R},q}\Psi_{{\rm L},p} \rangle = \frac{i\Lambda}{\sqrt{L_{\rm L}L_{\rm R}}} \sum_{n,m} \int {\rm d}t' \langle \Psi^\dagger_{{\rm R},q}(t)\Psi_{{\rm R},m}(t') \rangle_0 \langle \Psi_{{\rm L},p}(t)\Psi^\dagger_{{\rm L},n}(t') \rangle_0 \delta_{q,m}\delta_{p,n}, \tag{D.1.6}$$

$$\langle \Psi^\dagger_{{\rm L},p}\Psi_{{\rm R},q} \rangle = \frac{i\Lambda}{\sqrt{L_{\rm L}L_{\rm R}}} \sum_{n,m} \int {\rm d}t' \langle \Psi^\dagger_{{\rm L},p}(t)\Psi_{{\rm L},n}(t') \rangle_0 \langle \Psi_{{\rm R},q}(t)\Psi^\dagger_{{\rm R},m}(t') \rangle_0 \delta_{q,m}\delta_{p,n}. \tag{D.1.7}$$

The Lesser and Greater Green's functions are defined as

$$\begin{aligned} g^{<}_{p,q}(t-t') &= -i\langle \Psi^{\dagger}_{q}(t')\Psi_{p}(t)\rangle \delta_{p,q}, \\ g^{>}_{p,q}(t-t') &= -i\langle \Psi_{p}(t)\Psi^{\dagger}_{q}(t')\rangle \delta_{p,q}. \end{aligned} \tag{D.1.8}$$

This means that the current can be written as

$$I = \frac{\Lambda^2}{\hbar L_{\mathrm{L}} L_{\mathrm{R}}} \sum_{p,q} \int \mathrm{d}t \Big( -g^{<}_{\mathrm{R},q}(-t) g^{>}_{\mathrm{L},p}(t) - g^{<}_{\mathrm{L},p}(-t) g^{>}_{\mathrm{R},q}(t) \Big). \tag{D.1.9}$$

For non-interacting, equilibrium bosons, the lesser Green's function in energy representation is the same as the Bose-Distribution function, $ig^{<}(\omega) = \langle \Psi^{\dagger}(q,\omega)\Psi(q,\omega)\rangle = n_{\mathrm{B}}(\omega) = 1/(e^{\beta(\omega-\mu)}-1)$ so that

$$\begin{aligned} ig^{<}_{p}(t) &= n_{\mathrm{B}}(p) e^{-i\omega_p t}, \\ ig^{>}_{p}(t) &= (1+n_{\mathrm{B}}(p)) e^{-i\omega_p t}, \end{aligned} \tag{D.1.10}$$

where the second equation follows from the commutation relation. Using $\sum_{p} \to \frac{L}{2\pi}\int \mathrm{d}p$, the current is given as

$$\begin{aligned} I &= \frac{\Lambda^2}{\hbar} \int \mathrm{d}t \int \frac{\mathrm{d}k \mathrm{d}k'}{4\pi^2} \Big[ n^{\mathrm{R}}_{\mathrm{B}}(k)(1+n^{\mathrm{L}}_{\mathrm{B}}(k')) e^{-it(\omega_{k'}-\omega_k)} - n^{\mathrm{L}}_{\mathrm{B}}(k')(1+n^{\mathrm{R}}_{\mathrm{B}}(k)) e^{-it(\omega_k-\omega_{k'})} \Big] \\ &= \frac{\Lambda^2}{\hbar} \int \mathrm{d}t \int \mathrm{d}\omega \mathrm{d}\omega' \rho_R(\omega)\rho_L(\omega') \Big[ n^{\mathrm{R}}_{\mathrm{B}}(\omega)(1+n^{\mathrm{L}}_{\mathrm{B}}(\omega')) e^{-it(\omega'-\omega)} - n^{\mathrm{L}}_{\mathrm{B}}(\omega')(1+n^{\mathrm{R}}_{\mathrm{B}}(\omega)) e^{-it(\omega-\omega')} \Big], \end{aligned} \tag{D.1.11}$$

where $\rho(\omega) = \frac{1}{2\pi}\frac{\mathrm{d}k}{\mathrm{d}\omega}$ is the one dimensional density of states in the left/right lead. Performing the time integral gives a delta function, leaving

$$I = \frac{2\pi\Lambda^2}{\hbar}\int \mathrm{d}\omega \rho_R(\omega)\rho_L(\omega)[n_{\mathrm{B}}^{\mathrm{R}}(\omega) - n_{\mathrm{B}}^{\mathrm{L}}(\omega)]. \tag{D.1.12}$$

The density of states is defined as $\rho(\omega) = \frac{1}{L}\sum_n \delta(\omega - \omega_n)$ so that the final result is given by

$$I = \frac{1}{h}\int \mathrm{d}\omega [n_{\mathrm{B}}^{\mathrm{R}}(\omega) - n_{\mathrm{B}}^{\mathrm{L}}(\omega)]T(\omega), \tag{D.1.13}$$

$$T(\omega) = \frac{4\pi^2}{L_{\mathrm{L}}L_{\mathrm{R}}}\sum_{p,q}\Lambda^2\delta(\omega - \omega_p)\delta(\omega - \omega_q), \tag{D.1.14}$$

where $\omega_p$ are the energy levels in the left lead, $\omega_q$ are the energy levels in the right lead, and $T(\omega)$ is the transmission coefficient for the tunnelling Hamiltonian. Here I have utilized Landauer's idea of conductance as transmission to express the current in the form of a 'Landauer-Buttiker' formula.

## D.2 WKB Theory

The WKB theory is a semi-classical method of solving the Schrödinger equation,

$$i\hbar\partial_t\Psi(x,t) = -\frac{\hbar^2}{2m}\partial_x^2\Psi(x,t) + V(x)\Psi(x,t). \tag{D.2.1}$$

The continuity equation is given as

$$0 = \partial_t\rho + \partial_x j, \tag{D.2.2}$$

where $\rho = |\Psi(x,t)|^2$ and $j = \frac{\hbar}{2mi}\Big(\Psi^\dagger(x,t)\partial_x\Psi(x,t) - \Psi(x,t)\partial_x\Psi^\dagger(x,t)\Big)$. The wavefunction is then written as $\Psi(x,t) = \sqrt{\rho}e^{\frac{i}{\hbar}\phi}$, where $j = \frac{\rho}{m}\partial_x\phi$. This form of the wavefunction is then substituted back into the Schrödinger equation giving

$$-\partial_t\phi = \frac{1}{2m}(\partial_x\phi)^2 + V(x) - \frac{\hbar^2}{4m\rho}\partial_x^2\rho + \frac{\hbar^2}{8m\rho^2}(\partial_x\rho)^2, \tag{D.2.3}$$

where I have substituted the continuity equation in order to show that the terms linear in $\hbar$ cancel.

A stationary solution to the Schrödinger equation has the form $\Psi(x,t) = \Psi(x)e^{-iEt/\hbar}$, so that $\rho(x,t) = \rho(x)$ and $\phi(x,t) = \phi(x) - Et$. The WKB approximation is to expand the phase in powers of $\hbar$ so that $\phi(x) = \phi_0(x) + \hbar\phi_1(x) + \hbar^2\phi_2(x) + ...$ and solve the equation order by order as $\hbar \to 0$. The semi-classical result is the zeroth order term of this expansion, where Eq. (D.2.3) is the classical (Hamilton's) equation of motion. At zeroth order, one has

$$\begin{aligned} E =& \frac{1}{2m}(\partial_x\phi_0(x))^2 + V(x), \\ \phi_0(x) =& \pm\int \mathrm{d}x'\sqrt{2m(E - V(x'))}. \end{aligned} \tag{D.2.4}$$

The continuity equation gives $j = \frac{\rho}{m}\partial_x\phi(x) = \frac{\rho}{m}\sqrt{2m(E-V(x))}$. This must be a constant as the density $\rho$ is time-independent. This means that $\rho = c/\sqrt{2m(E-V)}$, where $c$ is a constant. Combining all of this information gives the stationary WKB wavefunction

$$\Psi(x) = \frac{c}{\left(2m(E-V(x))\right)^{1/4}}\, e^{\pm\frac{i}{\hbar}\int \mathrm{d}x'\sqrt{2m(E-V(x'))}}. \tag{D.2.5}$$

The WKB approximation breaks down when the momentum $k = \sqrt{2m(E-V(x))} \to$

$0$, i.e. near the classical turning points of the potential. At these points, the potential can be expanded $V(x) = V(x_0) + (x - x_0)V'(x_0)$, which at linear order in the Schrödinger equation gives rise to an Airy function, but this is beyond the scope of the approximation required here.

The transmission coefficient is given (to leading order) by the probability of a particle travelling from $x = x_-$ to $x = x_+$, where $x_\pm$ are the classical turning points of the barrier potential,

$$T = \frac{|\Psi(x_-)|^2}{|\Psi(x_+)|^2} \approx e^{-\frac{2}{\hbar}\int_{x_-}^{x_+} \mathrm{d}x\sqrt{2m(V(x)-E)}}. \tag{D.2.6}$$

# Appendix E

# CONTRAST FUNCTION

The contrast function $C_{\rm L}(t) = \langle \cos \phi_{\rm L}^{\rm cl}(t) \rangle$ is another possible observable of the system. This can be computed from the action Eq. (11.0.21) following e.g. [87,88]. The retarded and advanced Green's functions are

$$
\begin{aligned}
[G_+^{-1}]^{\rm R(A)}(\omega) &= -4J_{\rm c} \pm \frac{2Ki\omega}{\pi}, \\
G_+^{\rm R(A)}(t,t') &= \int \frac{{\rm d}\omega}{2\pi} \frac{e^{-i\omega(t-t')}}{-4J_{\rm c} \pm 2Ki\omega/\pi} = -\frac{\pi}{2K}\Theta(\pm(t-t')). \qquad \text{(E.0.1)} \\
[G_-^{-1}]^{\rm R(A)}(\omega) &= \pm\frac{2Ki\omega}{\pi}, \\
G_-^{\rm R(A)}(t,t') &= \pm \int \frac{{\rm d}\omega}{2\pi} \frac{\pi e^{-i\omega(t-t')}}{2Ki\omega} = -\frac{\pi}{2K}\Theta(\pm(t-t')). \qquad \text{(E.0.2)}
\end{aligned}
$$

Using the Keldysh Green's function at zero temperature $[G_\pm^{-1}]^{\rm K}(\omega) = 4iK|\omega|/\pi$, it is useful to compute the correlation function

$$
\begin{aligned}
\langle (\phi_\pm^{\rm cl}(t) - \phi_\pm^{\rm cl}(t'))^2 \rangle_\pm &= \int \frac{{\rm d}\omega}{2\pi} \langle \phi_\pm^{\rm cl}(\omega)\phi_\pm^{\rm cl}(\omega)\rangle_\pm (2 - 2\cos\omega(t-t')) \\
&= \int \frac{{\rm d}\omega}{2\pi} i G_\pm^{\rm K} (2 - 2\cos\omega(t-t')) \\
&= \frac{1}{2K}\int_0^\infty {\rm d}\omega \frac{1-\cos\omega(t-t')}{\omega} = \frac{1}{2K}\log\Lambda(t-t'), \qquad \text{(E.0.3)}
\end{aligned}
$$

for an appropriate cut-off parameter $\Lambda$. Also, $\langle(\phi^{\rm cl}_{\pm}(t)+\phi^{\rm cl}_{\pm}(t'))^2\rangle_{\pm}=0$ following from chapter 3. Then, expanding the action in terms of the tunnelling energy $J$ gives, to first order,

$$\begin{aligned}\left\langle e^{i\phi^{\rm cl}_{\rm L}}\right\rangle &= \left\langle e^{i\phi^{\rm cl}_{\rm L}+8iJ_{\rm c}\Phi\int {\rm d}t'\phi^{\rm q}_{+}(t')-4iJ\int {\rm d}t'\left[\sin\phi^{\rm cl}_{\rm L}(t')\sin\phi^{\rm q}_{\rm L}(t')+\sin\phi^{\rm cl}_{\rm R}(t')\sin\phi^{\rm q}_{\rm R}(t')\right]}\right\rangle_{\pm}\\ &= 2J\int {\rm d}t'\left\langle e^{i\left(\phi^{\rm cl}_{+}(t)+\phi^{\rm cl}_{-}(t')+8J_{\rm c}\Phi\int {\rm d}\bar{t}\phi^{\rm q}_{+}(\bar{t})-\phi^{\rm cl}_{+}(t')-\phi^{\rm cl}_{-}(t')\right)}\sin(\phi^{\rm q}_{+}(t')+\phi^{\rm q}_{-}(t'))\right\rangle_{\pm}.\end{aligned} \tag{E.0.4}$$

This average can be computed using the identity $\left\langle e^{iA}\right\rangle = e^{-\frac{1}{2}\left\langle A^2\right\rangle}$, the Green's functions above and the fact that $\langle\phi^{\rm q}\phi^{\rm q}\rangle=0$ due to the causality structure (see chapter 5). The exponent then becomes

$$\begin{aligned}-\frac{1}{2}\Bigg[&\langle(\phi^{\rm cl}_{+}(t)-\phi^{\rm cl}_{+}(t'))^2\rangle_{+}+\langle(\phi^{\rm cl}_{-}(t)-\phi^{\rm cl}_{-}(t'))^2\rangle_{-}+8J_{\rm c}\int {\rm d}\bar{t}\Big\langle\Big[\phi^{\rm q}_{+}(\bar{t})\Big(\phi^{\rm cl}_{+}(t)-\phi^{\rm cl}_{+}(t')\Big)\\ &+\Big(\phi^{\rm cl}_{+}(t)-\phi^{\rm cl}_{+}(t')\Big)\phi^{\rm q}_{+}(\bar{t})\Big]\Big\rangle_{+}\mp\Big\langle\phi^{\rm q}_{+}(t')\Big(\phi^{\rm cl}_{+}(t)-\phi^{\rm cl}_{+}(t')\Big)+\Big(\phi^{\rm cl}_{+}(t)-\phi^{\rm cl}_{+}(t')\Big)\phi^{\rm q}_{+}(t')\Big\rangle_{+}\\ &\mp\Big\langle\phi^{\rm q}_{-}(t')\Big(\phi^{\rm cl}_{-}(t)-\phi^{\rm cl}_{-}(t')\Big)+\Big(\phi^{\rm cl}_{-}(t)-\phi^{\rm cl}_{-}(t')\Big)\phi^{\rm q}_{-}(t')\Big\rangle_{-}\Bigg].\end{aligned} \tag{E.0.5}$$

Using the property of Green's functions $G^{\rm R}(t,t)+G^{\rm A}(t,t)=0$ and the identities given above, this average may be expressed as

$$\begin{aligned}-\frac{1}{2}\Bigg[&\frac{1}{2K}\log\Lambda(t-t')+\frac{1}{2K}\log\Lambda(t-t')+16J_{\rm c}\Phi i\int {\rm d}\bar{t}\Big(G^{\rm R}_{+}(t,\bar{t})-G^{\rm R}_{+}(\bar{t},t')\Big)\\ &\mp 2i\Big(G^{\rm R}_{+}(t,t')+G^{\rm R}_{-}(t,t')\Big)\Bigg]=-\frac{1}{2K}\log\Lambda(t-t')+\frac{4\pi iJ_{\rm c}\Phi}{K}(t-t')\mp\frac{\pi i}{K}\Theta(t-t').\end{aligned} \tag{E.0.6}$$

Assuming the tunnelling is switched abruptly, $J(t) = J\Theta(t - t_0)$ one then has

$$\left\langle e^{i\phi_{\mathrm{L}}^{\mathrm{cl}}} \right\rangle = 2J \sin\frac{\pi}{K} \int_{t_0}^{t} \mathrm{d}t' \left[\Lambda(t - t')\right]^{-\frac{1}{2K}} e^{i2\Phi\omega_0(t-t')}, \tag{E.0.7}$$

where $\omega_0 = 2c/L$. Taking the real part of this, the contrast function is given by

$$\begin{aligned} C_{\mathrm{L}}(t) &= 2J\Lambda^{-\frac{1}{2K}} \sin\frac{\pi}{K} \int_0^{t-t_0} \mathrm{d}x \, \frac{\cos(2\Phi\omega_0 x)}{x^{\frac{1}{2K}}} \\ &= 2J\Lambda^{-\frac{1}{2K}} \sin\frac{\pi}{K} \frac{(t-t_0)^{1-\frac{1}{2K}}}{1-\frac{1}{2K}} \, {}_1F_2\left[\frac{1}{2} - \frac{1}{4K}; \frac{1}{2}, \frac{3}{2} - \frac{1}{4K}; -\Phi^2\omega_0^2(t-t_0)^2\right], \end{aligned} \tag{E.0.8}$$

where ${}_1F_2$ is an hyper-geometric function and the result of the integral is only valid for $K > 1/2$ giving the same critical $K$ as the main text. A parallel calculation may also be performed for the right end of the channel. In the limit $\Phi \to 0$ the function is given as

$$C_{\mathrm{L}}(t) = 2J\Lambda^{-\frac{1}{2K}} \sin\frac{\pi}{K} \frac{(t-t_0)^{1-\frac{1}{2K}}}{1-\frac{1}{2K}}, \tag{E.0.9}$$

while in the limit $(t - t_0) \gg 1/(\Phi\omega)$ one has

$$C_{\mathrm{L}}(t) = 2\frac{J}{\omega_0}\left(\frac{\omega_0}{\Lambda}\right)^{\frac{1}{2K}} \sin\frac{\pi}{K} \sin\frac{\pi}{4K} \Gamma\left(1 - \frac{1}{2K}\right) |2\Phi|^{\frac{1}{2K}-1}. \tag{E.0.10}$$

# Bibliography


[1] J. Billy, V. Josse, Z. Zuo, A. Bernard, B. Hambrecht, P. Lugan, D. Clement, L. Sanchez-Palencia, P. Bouyer, and A. Aspect, Direct observation of Anderson localization of matter waves in a controlled disorder, Nature **453**, 891 (2008).

[2] G. Roati, C. D'Errico, L. Fallani, M. Fattori, C. Fort, M. Zaccanti, G. Modugno, M. Modugno, and M. Inguscio, Anderson localization of a non-interacting Bose-Einstein condensate, Nature **453**, 895 (2008).

[3] S. Levy, E. Lahoud, I. Shomroni, and J. Steinhauer, The a.c. and d.c. Josephson effects in a Bose-Einstein condensate, Nature **449**, 579 (2007).

[4] S. Palzer, C. Zipkes, C. Sias, and M. Köhl, Quantum transport through a Tonks-Girardeau gas, Phys. Rev. Lett. **103**, 150601 (2009).

[5] J. Catani, G. Lamporesi, D. Naik, M. Gring, M. Inguscio, F. Minardi, A. Kantian, and T. Giamarchi, Quantum dynamics of impurities in a one-dimensional Bose gas, Phys. Rev. A **85**, 023623 (2012).

[6] A. Ramanathan, K. C. Wright, S. R. Muniz, M. Zelan, W. T. Hill, C. J. Lobb, K. Helmerson, W. D. Phillips, and G. K. Campbell, Superflow in a Toroidal Bose-Einstein Condensate: An Atom Circuit with a Tunable Weak Link, Phys. Rev. Lett. **106**, 130401 (2011).

[7] L. Tanzi, E. Lucioni, S. Chaudhuri, L. Gori, A. Kumar, C. D'Errico, M. Inguscio, and G. Modugno, Transport of a Bose Gas in 1D Disordered Lattices at the Fluid-Insulator Transition, Phys. Rev. Lett. **111**, 115301 (2013).

[8] C. L. Kane and M. P. A. Fisher, Transport in a One-Channel Luttinger Liquid, Phys. Rev. Lett. **68**, 1220 (1992).

[9] C. L. Kane and M. P. A. Fisher, Transmission through barriers and resonant tunneling in an interacting one-dimensional electron gas, Phys. Rev. B **46**, 15233 (1992).

[10] K. A. Matveev, D. Yue, and L. I. Glazman, Tunnelling in One-Dimensional Non-Luttinger Electron Liquid, Phys. Rev. Lett. **71**, 3351 (1993).

[11] A. Furusaki and N. Nagaosa, Single-barrier problem and Anderson localization in a one-dimensional interacting electron system, Phys. Rev. B **47**, 4631 (1993).

[12] M. Fabrizio and A. O. Gogolin, Interacting one-dimensional electron gas with open boundaries, Phys. Rev. B **51**, 17827 (1995).

[13] A. Furusaki and K. A. Matveev, Occupation of a Resonant Level Coupled to a Chiral Luttinger Liquid, Phys. Rev. Lett. **88**, 226404 (2002).

[14] D. G. Polyakov and I. V. Gornyi, Transport of interacting electrons through a double barrier in quantum wires, Phys. Rev. B **68**, 035421 (2003).

[15] Y. V. Nazarov and L. I. Glazman, Resonant Tunneling of Interacting Electrons in a One-Dimensional Wire, Phys. Rev. Lett. **91**, 126804 (2003).

[16] I. V. Lerner, V. I. Yudson, and I. V. Yurkevich, Quantum wire hybridized with a single-level impurity, Phys. Rev. Lett. **100**, 256805 (2008).

[17] M. Goldstein and R. Berkovits, Duality between Different Geometries of a Resonant Level in a Luttinger Liquid, Phys. Rev. Lett. **104**, 106403 (2010).

[18] M. Bockrath, D. H. Cobden, J. Lu, A. G. Rinzler, R. E. Smalley, L. Balents, and P. L. McEuen, Luttinger-liquid behaviour in carbon nanotubes, Nature **397**, 598 (1999).

[19] M. Bockrath, W. J. Liang, D. Bozovic, J. H. Hafner, C. M. Lieber, M. Tinkham, and H. K. Park, Resonant electron scattering by defects in single-walled carbon nanotubes, Science **291**, 283 (2001).

[20] Z. Yao, H. W. C. Postma, L. Balents, and C. Dekker, Carbon nanotube intramolecular junctions, Nature **402**, 273 (1999).

[21] O. M. Auslaender, A. Yacoby, R. de Picciotto, K. W. Baldwin, L. N. Pfeiffer, and K. W. West, Tunneling spectroscopy of them elementary excitations in a one-dimensional wire, Science **295**, 825 (2002).

[22] L. Venkataraman, Y. S. Hong, and P. Kim, Electron Transport in a Multichannel One-Dimensional Conductor: Molybdenum Selenide Nanowires, Phys. Rev. Lett. **96**, 076601 (2006).

[23] E. Levy, A. Tsukernik, M. Karpovski, A. Palevski, B. Dwir, E. Pelucchi, A. Rudra, E. Kapon, and Y. Oreg, Luttinger-Liquid Behavior in Weakly Disordered Quantum Wires, Phys. Rev. Lett. **97**, 196802 (2006).

[24] E. Levy, I. Sternfeld, M. Eshkol, M. Karpovski, B. Dwir, A. Rudra, E. Kapon, Y. Oreg, and A. Palevski, Experimental evidence for Luttinger liquid behavior in sufficiently long GaAs V-groove quantum wires, Phys. Rev. B **85**, 045315 (2012).

[25] J.-P. Brantut, J. Meineke, D. Stadler, S. Krinner, and T. Esslinger, Conduction of Ultracold Fermions Through a Mesoscopic Channel, Science **337**, 1069 (2012).

[26] D. Stadler, S. Krinner, J. Meineke, J.-P. Brantut, and T. Esslinger, Observing the drop of resistance in the flow of a superfluid Fermi gas, Nature **491**, 736 (2012).

[27] L. H. Kristinsdóttir, O. Karlström, J. Bjerlin, J. C. Cremon, P. Schlagheck, A. Wacker, and S. M. Reimann, Total Current Blockade in an Ultracold Dipolar Quantum Wire, Phys. Rev. Lett. **110**, 085303 (2013).

[28] T. Paul, M. Hartung, K. Richter, and P. Schlagheck, Nonlinear transport of Bose-Einstein condensates through mesoscopic waveguides, Phys. Rev. A **76**, 063605 (2007).

[29] D. B. Gutman, Y. Gefen, and A. D. Mirlin, Cold bosons in the Landauer setup, Phys. Rev. B **85**, 125102 (2012).

[30] D.P.Simpson, D.M.Gangardt, I.V.Lerner, and P.Krüger, One-Dimensional Transport of Bosons between Weakly Linked Reservoirs, Phys. Rev. Lett. **112**, 100601 (2014).

[31] D.P.Simpson, D.M.Gangardt, and I.V.Lerner, Mean Field Dynamics of Ultracold Bosons in a One-Dimensional Channel, unpublished .

[32] S. Bose, Plancks Law and Light Quantum Hypothesis, Z. Phys **26**, 178 (1924).

[33] A. Einstein, Quantentheorie des einatomigen idealen Gases, Sitzber. Kgl. Preuss. Akad. Wiss **3** (1925).

[34] F. London, The $\lambda-$Phenomenon of Liquid Helium and the Bose-Einstein Degeneracy, Nature **141**, 643 (1938).

[35] N. Bogoliubov, On the theory of superfluidity, J. Phys. (USSR) **11**, 23 (1947).

[36] L. Landau and E. Lifshitz, Statisticheskai Fizika, Fizmatgiz, Moscow (1951).

[37] O. Penrose and L. Onsager, Bose-Einstein condensation and liquid helium, Phys. Rev. **104**, 576 (1956).

[38] C. Hecht, The possible superfluid behaviour of hydrogen atom gases and liquids, Physica **25**, 1159 (1951).

[39] M. H. Anderson, J. R. Ensher, M. R. Matthews, C. E. Wieman, and E. A. Cornell, Observation of Bose-Einstein condensation in a dilute atomic vapor, Science **269**, 198 (1995).

[40] M. A. Cazalilla, R. Citro, T. Giamarchi, E. Orignac, and M. Rigol, One dimensional bosons: From condensed matter systems to ultracold gases, Rev. Mod. Phys. **83**, 1405 (2011).

[41] F. Dalfovo, S. Giorgini, L. P. Pitaevskii, and S. Stringari, Theory of Bose-Einstein condensation in trapped gases, Rev. Mod. Phys. **71**, 463 (1999).

[42] I. Bloch, J. Dalibard, and W. Zwerger, Many-body physics with ultracold gases, Rev. Mod. Phys. **80**, 885 (2008).

[43] L. Pitaevskii and S. Stringari, *Bose Einstein Condensation*, Oxford University Press, Oxford, 2003.

[44] C.J.Pethick and H.Smith, *Bose-Einstein Condensation in Dilute Gases*, Cambridge University Press, 2002.

[45] A. J. Leggett, Bose-Einstein condensation in the alkali gases: Some fundamental concepts, Rev. Mod. Phys. **73**, 307 (2001).

[46] A. Imambekov, T. L. Schmidt, and L. I. Glazman, One-dimensional quantum liquids: Beyond the Luttinger liquid paradigm, Rev. Mod. Phys. **84**, 1253 (2012).

[47] C. M.Inguscio, S.Stringari, editor, *Bose-Einstein Condensation in Atomic Gases*, IOS Press, 1999.

[48] M. C.M.Savage, *Bose-Einstein Condensation: From Atomic Physics to Quantum Fluids*, World Scientific Publishing, 2000.

[49] B. Josephson, Possible new effects in superconductive tunnelling, Phys. Lett. **1**, 251 (1962).

[50] M. Tinkham, *Introduction to Superconductivity*, Dover, New York, 1996, p.226.

[51] P. L. Richards, Analog of the ac Josephson Effect in Superfluid Helium, Phys. Rev. A **2**, 1532–1541 (Oct 1970).

[52] M. Abbarchi, A. Amo, V. Sala, D. Solnyshkov, H. Flayac, L. Ferrier, I. Sagnes, E. Galopin, A. Lemaître, G. Malpuech, et al., Macroscopic quantum self-trapping and Josephson oscillations of exciton polaritons, Nature Physics **9**(5), 275–279 (2013).

[53] S. Tomonaga, Remarks on Bloch's Method of Sound Waves applied to Many-Fermion Problems, Prog. Theor. Phys. **5**, 544 (1950).

[54] J. M. Luttinger, An Exactly Soluble Model of a Many Fermion System, J. Math. Phys. **4**, 1154 (1963).

[55] D. C. Mattis and E. H. Lieb, Exact Solution of a Many Fermion System and Its Associated Boson Field, J. Math. Phys. **6**, 304 (1965).

[56] F. D. M. Haldane, 'Luttinger liquid theory' of one-dimensional quantum fluids. I. Properties of the Luttinger model and their extension to the general 1D interacting spinless Fermi gas, J. Phys. C **14**, 2585 (1981).

[57] F. D. M. Haldane, Effective Harmonic-Fluid Approach to Low-Energy Properties of One-Dimensional Quantum Fluids, Phys. Rev. Lett. **47**, 1840 (Dec 1981).

[58] M. A. Cazalilla, Bosonizing one-dimensional cold atomic gases, Journal of Physics B: Atomic, Molecular and Optical Physics **37**, S1 (2004).

[59] T. Giamarchi, *Quantum Physics in One Dimension*, Clarendon Press, London, 2004.

[60] A. Altland and B. Simons, *Condensed Matter Field Theory*, Cambridge University Press, 2010.

[61] M. E. Fisher, Renormalization group theory: Its basis and formulation in statistical physics, Rev. Mod. Phys. **70**, 653 (1998).

[62] K. G. Wilson, The renormalization group: Critical phenomena and the Kondo problem, Rev. Mod. Phys. **47**, 773 (1975).

[63] L. Kadanoff, Scaling laws for Ising models near T(c), Physics **2**, 263 (1966).

[64] A. Kamanev, *Field Theory of Non-Equilibrium Systems*, Cambridge University Press, Cambridge, 2011.

[65] G.Stefanucci and R. van Leeuwen, *Nonequilibrium Many-Body Theory of Quantum Systems*, Cambridge University Press, Cambridge, 2013.

[66] L. Landau and E. Lifshitz, *Statistical Physics Part I*, Pergamon Press, Oxford, 1986.

[67] J. Schwinger, Brownian Motion of a Quantum Oscillator, Journal of Mathematical Physics **2**, 407 (1961).

[68] L. Keldysh, Diagram Technique for Nonequilibrium Processes, Sov. Phys. JETP **20**, 1018 (1965).

[69] R. Fazio, F. W. J. Hekking, and A. A. Odintsov, dc and ac Josephson effect in a superconductor˘Luttinger-liquid˘superconductor system, Phys. Rev. B **53**, 6653 (1996).

[70] R. Fazio, F. W. J. Hekking, and A. A. Odintsov, Josephson Current through a Luttinger Liquid, Phys. Rev. Lett. **74**, 1843 (1995).

[71] D. L. Maslov, M. Stone, P. M. Goldbart, and D. Loss, Josephson current and proximity effect in Luttinger liquids, Phys. Rev. B **53**, 1548 (1996).

[72] I. Affleck, J.-S. Caux, and A. M. Zagoskin, Andreev scattering and Josephson current in a one-dimensional electron liquid, Phys. Rev. B **62**, 1433 (2000).

[73] H. P. Büchler, V. B. Geshkenbein, and G. Blatter, Superfluidity versus Bloch Oscillations in Confined Atomic Gases, Phys. Rev. Lett. **87**, 100403 (2001).

[74] M. Schecter, A. Kamenev, D. M. Gangardt, and A. Lamacraft, Critical Velocity of a Mobile Impurity in One-Dimensional Quantum Liquids, Phys. Rev. Lett. **108**, 207001 (2012).

[75] M. Schecter, D. Gangardt, and A. Kamenev, Dynamics and Bloch oscillations of mobile impurities in one-dimensional quantum liquids, Ann. Phys. (N.Y.) **327**, 639 (2012).

[76] D. L. Maslov, M. Stone, P. M. Goldbart, and D. Loss, Josephson current and proximity effect in Luttinger liquids, Phys. Rev. B **53**, 1548 (1996).

[77] J. von Delft and H. Schoeller, Bosonization for beginners refermionization for experts, Annalen der Physik **7**, 225 (1998).

[78] J.-S. Caux, H. Saleur, and F. Siano, Josephson Current in Luttinger Liquid-Superconductor Junctions, Phys. Rev. Lett. **88**, 106402 (2002).

[79] J.-S. Caux, H. Saleur, and F. Siano, The two-boundary sine-Gordon model, Nucl. Phys. B **672**, 411 (2003).

[80] R. Folman, P. Krüger, D. Cassettari, B. Hessmo, T. Maier, and J. Schmiedmayer, Controlling Cold Atoms using Nanofabricated Surfaces: Atom Chips, Phys. Rev. Lett. **84**, 4749 (2000).

[81] R. Folman, P. Krüger, J. Schmiedmayer, J. Denschlag, and C. Henkel, Microscopic atom optics: From wires to an atom chip, Advances In Atomic, Molecular, and Optical Physics **48**, 263356 (2002).

[82] S. Hofferberth, I. Lesanovsky, B. Fischer, J. Verdu, and J. Schmiedmayer, Radiofrequency-dressed-state potentials for neutral atoms, Nature Physics **2**, 710 (2006).

[83] P. S. Julienne, F. H. Mies, E. Tiesinga, and C. J. Williams, Collisional Stability of Double Bose Condensates, Phys. Rev. Lett. **78**, 1880 (1997).

[84] C. Zachos, D. Fairlie, and T. Curtright, *Quantum mechanics in phase space: an overview with selected papers*, volume 34, World Scientific, 2005.

[85] W. B. Case, Wigner functions and Weyl transforms for pedestrians, American Journal of Physics **76**, 937 (2008).

[86] A. Polkovnikov, Phase space representation of quantum dynamics, Annals of Physics **325**, 1790 (2010).

[87] E. G. Dalla Torre, E. Demler, and A. Polkovnikov, Universal Rephasing Dynamics after a Quantum Quench via Sudden Coupling of Two Initially Independent Condensates, Phys. Rev. Lett. **110**, 090404 (2013).

[88] M. J. Salvay, H. A. Aita, and C. M. Naón, Transient effects in the backscattered current of a Luttinger liquid, Phys. Rev. B **81**, 125406 (2010).